Stony Brook University

Intercellular transfer of functional RNA through extracellular vesicles is a medium of communication between cells.

A Dissertation Presented

by

Sudipto Kumar Chakrabortty

to

The Graduate School

in Partial Fulfillment of the

Requirements

for the Degree of

Doctor of Philosophy

in

Genetics

Stony Brook University

August 2015

Stony Brook University

The Graduate School

Sudipto Kumar Chakrabortty

We, the dissertation committee for the above candidate for the

Doctor of Philosophy degree, hereby recommend

acceptance of this dissertation.

Dr. Thomas Gingeras – Dissertation Advisor
Professor, Cold Spring Harbor Laboratory

Dr. David Jackson- Chairperson of Defense
Professor, Cold Spring Harbor Laboratory

Dr. Linda VanAelst
Professor, Cold Spring Harbor Laboratory

Dr. Gerald Thomsen
Professor, Department of Biochemistry and Cell Biology, Stony Brook University

Dr. Douglas Taylor
Chief Scientific Officer, Exosome Sciences

This dissertation is accepted by the Graduate School

Charles Taber
Dean of the Graduate School

Abstract of the Dissertation

Intercellular transfer of functional RNA through extracellular vesicles is a medium of communication between cells

by

Sudipto Kumar Chakrabortty

Doctor of Philosophy

In

Genetics

Stony Brook University

2015

Proper functioning of a multi-cellular organism requires well-coordinated intra- and inter-cellular communication among its cells. Mammalian cells have well established modes of inter-cellular communication, which include cell-cell contact via gap junctions, synaptic transmission, and paracrine and endocrine communication through secreted molecules. Extracellular vesicles (EV) serve as a vehicle for transfer of biomolecules between cells. This study aims to establish if EV mediated transfer of encapsulated RNA represents a novel mode of intercellular communication.

At the outset, we developed and validated a novel, relatively cost effective and efficient approach of isolation of EVs. Comprehensive characterization of EV RNA derived from several cell types revealed the diversity of small RNA cargo, and suggested non-random and cell type specific sorting of RNA molecules into EVs. Further analysis revealed gene family specific fragmentation patterns of non-coding RNAs detected within EVs. We also explored the temporal

dynamics, spatial localization, and integrity of EV RNA upon transfer into another cell. We further demonstrate dynamic sorting of small RNA molecules into EVs by cells with different environmental stimulus, as well as cell type specific molecular responses, when different cells were exposed to the same EV stimuli, underscoring the context dependent interpretation of the complex EV messages. Finally, as a specific example of EV RNA functionality, we report the possible involvement of a 31 nucleotide processed fragment of RNY5, one of the most abundant and enriched RNA components of cancer cell derived EVs, in selectively inducing cell death in primary cells of diverse developmental origins and identified an eight nucleotide motif crucial for its functionality. The transfer of processed, functional RNY5 fragments through EVs hints at the under-appreciated role of EV RNA in cancer cell microenvironment.

Thus, our study supports the hypothesis that EV mediated transfer of RNA represents a novel mode of intercellular communication, through which cells may influence the transcriptional landscape of another cell in their microenvironment.

Dedication Page

This work is dedicated to my parents, Shri Arun kumar Chakrabortty and Mrs. Sikha Chakrabortty, and my sister Ms. Sharmistha Chakrabortty, who has supported me all my life and encouraged me to chase my dreams, no matter how far-fetched they may seem. I would like to dedicate this work to all my teachers in the past who have inspired me and ignited my mind with curiosity and thirst for knowledge. Finally, I dedicate my work to the unsung heroes of science, standing on whose shoulders, I have attempted to peek into the vast darkness of the unknown.

Table of Contents

List of Tables

List of Figures

List of Abbreviations

Extracellular vesicles	EVs
Cerebrospinal fluid	CSF
Multi-vesicular bodies	MVBs
Intraluminal vesicles	ILVs
Transmission electron microscopy	TEM
Sialic acid binding immunoglobulin lectins	SIGLEC
Syncytial membrane released microvesicles	STBM
Syncytiotrophoblast	STB
Natural killer	NK
Bone morphogenetic protein	BMP
Vascular endothelial growth factor	VEGF
Bone sialoprotein	BSP
Transforming growth factor beta	TGFβ
Tumor necrosis factor related apoptosis inducing ligand	TRAIL
Fas ligand	FasL
Delta-like 4	Dll4
Epidermal growth factor receptor	EGFR

Hypoxia inducing factor-1	HIF-1
Tyrosine-kinase	KIT
Matrix metalloproteinase	MMP1
Outer membrane vesicles	OMVs
Endosomal sorting complex required for transport	ESCRT
Transferrin receptor	TfR
Mitogen activated protein kinase	MAPK
Natural killer group 2D	NKG2D
Interleukin	IL
Migration inhibitory factor	MIF
Vascular endothelial growth factor	VEGF
Toll like receptors	TLR
High mobility group Box1	HMGB1
Intercellular adhesion molecule-1	ICAM-1
Heat shock proteins	HSPs
Lysobisphosphatidic acid	LBPA
Untranslated regions	UTR

Heterogeneous ribonucleprotein A2B1	hnRNPA2B1
Next generation sequencing	NGS
Messenger RNA	mRNA
Long non-coding RNA	lincRNA
Transfer RNA	tRNA
Ribosomal RNA	rRNA
Miscellaneous RNA	MiscRNA
Human Y RNA	hY RNA
Reads per million	RPM
High density lipoprotein	HDL
Nominal molecular weight limit	NMWL
Phosphate buffer saline	PBS
Nanoparticle Tracking Analysis	NTA
Tobacco acid pyrophosphatase	TAP
Short RNA	sRNA
Human umbilical vein endothelial cells	HUVEC
Human fetal foreskin fibroblasts	HFFF

Acknowledgments

First and foremost, I would like to acknowledge the immense contribution of my parents Shri Arun Kumar Chakrabortty and Mrs. Sikha Chakrabortty towards successful completion of my research, for it is they who ignited the spark of curiosity in my mind as a child, inspired me to chase my dreams and instilled in me the strength of character to walk the extra mile towards achieving my goal. They sacrificed their present to secure my future. Without their unwavering support and continuous encouragement from my sister Sharmistha Chakrabortty, this work would have never seen the light of the day.

Next, I would like to express my deepest gratitude towards my dissertation advisor, Dr. Thomas Gingeras, for without his support, this work is simply unimaginable to me. Tom accepted me in his lab when I had nothing more than curiosity and the will to learn. Instead of defining a project for me, he set my imagination free by asking me to come up with my own scientific question and provided me complete independence to pursue research on my area of interest in his lab. Over the last six years, he held my hands with immense patience as I took my baby and often faltering steps towards my scientific goals. As the principal investigator, he managed the projects described in 2nd, 3rd and 4th chapters of this manuscript.

Over the last six years, I have learnt many of the skills necessary for a career in life science research from my colleagues and friends at Cold Spring Harbor Laboratory and Stony Brook University. I am grateful to Jorg Drenkow, Research Associate in Gingeras lab, who initiated me in molecular biology techniques. Jorg also performed long RNASeq cDNA libraries construction as described in Chapter 3 of this manuscript. I am also grateful to Alex Dobin, Computational manager in Gingeras lab, who taught me the basics of RNASeq analysis and helped me with mapping of RNASeq results to combined human and mouse genome as

described in chapter3 and chapter4 of this manuscript. Acknowledgements are due to Stephen Hearn and Zsolt Lazar from Microscopy shared resources at CSHL who taught me the basics of microscopy. Stephen Hearn performed the transmission electron microscopy and Immuno-electron microscopy experiments as described in 2nd, 3rd and 4th chapters of this manuscript. I am particularly grateful to Pamela Moody from Flow cytometry facility for teaching me flow cytometry. I would also like to thank the sequencing facility at CSHL under Dr. Richard McCombie for their continuous support. Special thanks are due to Dr. Ashish Saxena at Memorial Sloan Kettering Cancer Center, NY for graciously permitting me to perform Nanoparticle Tracking Analysis in his lab.

Over the last two years, I have worked in close collaboration with Dr. Ashwin Prakash, computer scientist, Dr. Gal Nechooshtan, Post-Doctoral fellow and Alexandra Scavelli, Research Technician in Gingeras lab. I am grateful to Alexandra for helping me out with cell culture and in constructing some of the small RNA-Seq libraries described in 2nd and 3rd chapters of this manuscript. Acknowledgements are due to Gal Nechooshtan for performing the Norther Blotting and RNA processing assays reported in chapter 4 of this manuscript. But by far, the greatest contribution to this work was made by Dr. Ashwin Prakash, who helped me immensely with advanced computational analysis of the RNASeq data, without which this work would never have been complete. Ashwin has performed all the RNASeq analysis as described in 2nd, 3rd and 4th chapters of this manuscript. I am most grateful to all my colleagues in Gingeras lab for their questions, suggestions and never-ending discussions over endless cups of coffee on my research.

Finally, this journey would have been more arduous if not for the support I have received from my friends at CSHL and Stony Brook University. I am thankful to Stony Brook Genetics Program for providing me this wonderful opportunity to pursue research in life sciences. A

special vote of thanks to Kathryn Bell, Genetics Program Co-coordinator (affectionately called the ‘Mommy’ of Stony Brook Genetics students for being a pillar of support for all these years).

Chapter 1

Introduction

The ability of a cell to perceive signal/stimuli and initiate an appropriate response forms the basis of all cellular activity, growth and development. In any complex multi-cellular organism, this is established through complex signal transduction pathways and coordination among various specialized cell populations through intercellular communication. Established modes of inter-cellular communication in multi-cellular organisms include direct cell to cell and cell-extracellular matrix contacts via junctions, receptor-ligand interactions, hormones and synaptic transmissions [1-4]. Recently, extracellular vesicles (EVs) have emerged as a key component of the extracellular environment and a medium of intercellular communication [5-7].

1.1. Historical context of EV research

The earliest observations of EVs were made by Chargaff and West in 1946 [8] as platelet derived pro-coagulant particles in the plasma and was subsequently referred as platelet dust in 1967 [9]. Subsequently, multiple independent observations of EVs have been made in various biological systems, including cell culture medium [10, 11] and body fluids such as such blood plasma [12], urine [13, 14], saliva [13], cerebrospinal fluid (CSF) [15, 16], amniotic fluid [13, 17], synovial fluid [18, 19], etc. Today, release of vesicles into extracellular environment appears to be a universal property of eukaryotic as well as prokaryotic life investigated.

1.2 Classes of extracellular vesicles

Extracellular vesicles have been broadly classified into three categories, namely, apoptotic bodies, microvesicles and exosomes [20]. Apoptotic bodies are large membrane

blebs/vesicles released by cells undergoing apoptosis. Their size varies between 1-5 microns and is largest in size among EVs. Microvesicles are membrane vesicles that are released from the plasma membrane of cells. The size of microvesicles usually varies between 200nm-1microns [7]. The third and perhaps the most well studied class of EVs are called exosomes. Exosomes are EVs of endosomal origin which range in size between 30-200nm [7, 21, 22].

Ultrastructural studies by Johnstone et.al on sheep reticulocytes revealed that the biogenesis of exosomes occurs in late endosomal structures in the cytoplasm, known as multi-vesicular bodies (MVBs)[23-25]. The membrane of the MVBs, upon undergoing an inward invagination leads to the formation of smaller vesicles within themselves called intraluminal vesicles (ILV). The MVBs at this point have two fates; it could either fuse with the lysosomes and destroy its cargo or fuse with the plasma membrane. While the factors that determine the fate of MVBs still remain unknown, when the MVBs fuse with the plasma membrane, the ILVs are released into the extracellular environment. These ILVs, once released outside the cell, are called exosomes [7, 21, 22]. Exosomes have been reported to carry proteins, RNA, DNA and lipids as part of their molecular cargo and composition. Under transmission electron microscopy (TEM), exosomes display a typical cup shaped morphology and is believed to be result of negative staining. In sucrose density gradient centrifugations, exosomes display a density of 1.13-1.19 gm/ml [7, 21, 22].

While emerging studies focused on the specific and in-depth characterization of EV classes indicated differences in protein and RNA cargo of these EV classes [26-30], identification of EV class specific markers have been lacking due to crude and non-standardized isolation procedures leading to heterogeneity in EV isolates and lack of consensus in classification parameters and nomenclature [31, 32]. Hence, even though this study is intended to

focus on the class of EVs traditionally described as ‘exosomes’, the all-encompassing terminology of ‘EV’ has been used for the rest of the study.

1.3 Uptake and bio-distribution of EVs

Although detailed molecular mechanisms that govern interactions between EV and its target cell are poorly understood and are currently an area of active investigation, at least three different mechanisms of EV uptake has been reported. First, EVs interact with cells through surface exposed ligand and receptor binding interactions. Such membrane interactions target EVs to particular cells and trigger downstream intracellular signaling pathways in the cell [33-35]. Specific adhesion molecules on EV surface, such as galectin-5 and sialic acid binding immunoglobulin lectins (Siglec) are involved in targeting of EVs [36, 37]. Second, EVs may interact with the recipient cell by direct fusion of the EV membrane with the plasma membrane, a process known as macro-pinocytosis. Such an interaction might result in transfer of functionally active cell-surface receptors to the plasma membrane and a consequent emptying of its internal cargo in the cell [21, 38, 39]. Third, uptake of entire EVs by cells occurs through phagocytosis, resulting in intracellular delivery of its membrane enclosed molecular cargo [40, 41]. This later mechanism is believed to be the major route of EV uptake by cells *in-vitro* and may be the underlying reason for the lack of cell type specificity in uptake often observed in *in-vitro* studies [42].

Bio-distribution of EVs *in-vivo* however is variable, depending on the source cells from which EVs were derived [43]. For example, while EVs from multiple cell types injected in circulation possess a very short half-life, with 90% clearance observed in typically less than 30 minutes [36, 44, 45], EVs from platelets demonstrate a significantly higher half-life of 5.5 hours

[46]. The *in-vivo* bio-distribution of EVs may be further influenced by differential uptake of EVs from different sources by the various organs in the body. For example, while EVs from red blood cells were shown to be taken up by liver (44.9%), bone (22.5%), skin (9.7%), spleen (3.4%), kidney (2.7%) and lung (1.8%), melanoma derived EVs were primarily detected in lung and spleen [45, 46]. Site of injection and normal or diseased conditions of source cells may represent other criteria governing the *in-vivo* distribution of EVs.

1.4 Composition and sorting of proteins in EV

Extensive characterization of the proteome cargo of EVs has revealed enrichment of specific classes of proteins in EVs. For example, membrane bound tetraspanin family of proteins such as CD9, CD63 and CD81, 14-3-3 and major histocompatibility complex (MHC) molecules, cytosolic proteins such as heat shock protein family (HSP70, HSP90), proteins involved in vesicle biogenesis and trafficking such as Rab family (Rab27A, Rab27B, Rab11, Rab35), Tsg101, Alix and cytoskeletal proteins such as actin and tubulins are abundant in EVs [10, 11, 43, 47-52]. Interestingly, proteins enriched in EVs have been reported to be enriched in certain post-translational modifications. Unique glycosylation and lectin binding patterns such as N-acetyl lactosamine, complex N-glycan as well as sialylated and fucosylated epitopes have been reported on EV proteins [53, 54]. These surface glycosylation patterns mediate uptake of EVs by recipient cells [37, 54, 55].

Several mechanisms have been reported to be involved in sorting of proteins to EVs. For example, endosomal sorting complex required for transport (ESCRT) proteins are involved in sorting of ubiquitinated proteins to EVs [56-59]. Involvement of membrane components such as lectins and tetraspanin-enriched micro-domains in protein sorting has been reported [54, 60, 61].

More recently, a membrane curvature-based mechanism of protein sorting has been suggested [62, 63]. This non-EV specific process occurs at the membrane budding step, when various membrane components redistribute to different regions with fitting membrane curvature to minimize the membrane free energy. ESCRT complex is believed to occupy the neck region of the budding membrane where it mediates fission of the membrane bud, and disintegrates upon vesicle pinch off. This redistribution of membrane bound components is later reflected in pinched off vesicles resulting in enrichment of specific proteins and lipids in EVs [56-60].

1.5 Lipid composition of EVs

Multiple studies focused on the lipid composition of EVs have reported the enrichment of certain lipids molecules in EVs such as sphingomyelin, cholesterol, phosphatidylserine and glycosphingolipids [64-66]. The characteristic lipid composition of EVs plays an important role in its formation, functionality and exceptional stability in extracellular environment [67, 68]. For example, while ceramide regulates the biogenesis of ILVs within MVBs [69], cholesterol regulate the release of EVs by cells [70-72]. Lysobisphosphatidic acid (LBPA) and phosphatidic acid represent other lipid moieties implicated in EV biogenesis [66, 73]. Abundance of cholesterol and sphingomyelin in EV membranes suggests specific sorting of membrane domains enriched with these molecules into EVs [70, 74, 75].

1.6 DNA composition of EVs

Initial studies on nucleic acids composition of EVs reported little to no presence of DNA in EVs [76], recent studies have brought forth contradictory evidence demonstrating the presence of single-stranded, double stranded and mitochondrial DNA in EVs [77-81]. Although uptake of EV DNA, esp. mitochondrial DNA, has been reported by recipient cells, the physiological

significance of EV DNA transfer remains unknown [78]. Differential sorting of DNA cargo to different EV categories has been reported recently, suggesting the involvement of underlying sorting mechanisms that are not yet understood [28]. Interestingly, abundance of retrotransposon elements and oncogenic DNA in tumor derived EVs have been reported [77]. Moreover, genomic DNA carried by tumor derived EVs were shown to recapitulate the mutational status of the source tumor cells, and may represent a novel and translational approach of non-invasive diagnosis of tumor through EV DNA profiling from body fluids [28, 79, 81].

1.7 Composition and sorting of RNA in EVs

Although various studies have explored the repertoire of EV RNA cargo, the true nature and extent of annotated RNA molecules in EVs still remains unclear. First evidence of the presence of messenger RNA (mRNA) came in 2006 when Ratajczak et.al reported the presence of *Oct4* and other pluripotency factor mRNAs in murine stem cell derived EVs [82]. This report was followed by Valadi et.al in 2007 reporting the presence of 1300 mRNA and 121 microRNAs in EVs from human and mouse mast cell lines [83]. Another independent study by Skog et.al in 2008 also showed the presence of messenger RNA in EVs [84]. Bioanalyzer RNA profiles from these and other studies showed an enrichment of small RNA (<200 nucleotides) molecules in EVs, with majority of RNA less than 700 nucleotides [85, 86]. Thus, evidence for full length mRNAs or intact annotated RNAs over several hundred nucleotides is sparse,

Subsequently, over the last few years, numerous studies have confirmed the presence of encapsulated RNA in EVs from various body fluids and cell culture medium [10, 11].While early studies on EV RNA focused primarily on microRNAs [87-89]and messenger RNAs [90-92], subsequent next-generation-sequencing (NGS) based studies on EV RNA reported the

presence of mRNA fragments [86], long non-coding RNA (lincRNA) [93, 94], piwi-interacting *RNA* [94] and fragments of various non-coding RNAs such as ribosomal RNA (rRNA) [94, 95], transfer RNA (t-RNA), Vault and Y-RNAs in EVs [96-99].While most early studies reported the presence of little or no 18S and 28S ribosomal RNA in EVs, recent studies have presented contradictory reports demonstrating the abundance of ribosomal RNA fragments in EVs [95]. While most studies have reported the presence of processed microRNAs within EVs, unexpectedly, a study by Chen et.al reported the enrichment of unprocessed pre-microRNA within EVs [85].

Interestingly, some of the RNA molecules detected in EV, such as specific micro-RNAs and Y-RNAs, were reported to be present several fold higher in EVs than the secreting cell independent of the level of expression of the RNA in the cell, while other microRNAs were observed to be excluded from EVs [88, 89, 98, 100, 101]. Enrichment of specific RNA molecules in EVs suggests the involvement of specific EV RNA sorting mechanism(s) present in the cell. At least four different mechanisms have been suggested. For example, computational motif analysis of transcripts enriched in glioblastoma EVs by Batagov et.al identified three 8nt long motifs (ACCAGCCU, CAGUGAGC and UAAUCCCA) in the 3'end of mRNA transcripts enriched in EVs and interestingly, predicted shorter half-life of EV enriched transcripts compared with cytoplasmic transcripts [102]. However, the motifs predicted by Batagov et.al remains to be validated. Another study by Bolukbasi et.al identified 25 nucleotide long zip-code like sequences in the 3'untranslated regions (UTR) of messenger RNA transcripts enriched in EVs [103]. Most importantly, incorporation of this motif into reporter genes led to the enrichment of reporter transcripts in EVs. Enrichment of transcripts with non-templated additions of uridine at the 3'end of microRNA were proposed by Pegtel et.al as another

mechanism which distinguishes EV RNA from cellular RNA and were suggested as a mechanism of enrichment of microRNAs in EVs [104]. However, further experiments are required to validate the suggested mechanism. More recently, an elegant study by Villaroyya-Beltri et.al reported the involvement of the protein heterogeneous ribonucleoprotein A2B1 (hnRNPA2B1), a member of the hnRNP family, in specific loading of a subset of microRNA into EVs [105]. In this study, a 4 nucleotide 'GGAG' motif was identified in a subset of microRNAs enriched in EVs and binding of sumoylated hnRNPA2B1 to 'GGAG motif' in these microRNAs was demonstrated to be necessary for their sorting into EVs [105]. Although the last study represents the most comprehensive investigation so far towards sorting of a subset of micro-RNAs in EVs, mechanisms that regulate the specific sorting of all other RNA molecules enriched in EVs, such a s Y RNA and t-RNA remain unknown to date.

1.8 Biological roles of EVs

Role of EVs in physiological systems

The biological functionality of EVs has been explored in various physiological systems. For example, during embryonic development, EVs play an important role in the regulation of cell fate, positioning and migration through the formation of Wnt and Hedgehog morphogen gradients [106-112]. During pregnancy, EVs mediate immunological communication between fetus and mother during pregnancy [113, 114]. While syncytial membrane released microvesicles (STBMs) possess immune-activating, pro-coagulant and anti-angiogenic properties [115], on the other hand, syncytiotrophoblast [STB] derived EVs demonstrate immunosuppressive properties and are suggested to play a role in maintenance of successful pregnancy via down regulation of T-cell or natural killer (NK) cell mediated cytotoxicity [116-118]. In the nervous system, EVs

have been reported to mediate intercellular communication between neurons and between neuron and glia. For example, neuron derived EVs has been suggested to regulate synaptic plasticity through transfer of Wnt protein and Synaptogamin-4 across synapse [119, 120]. Glia derived EVs have been implicated in the modulation of neuro-transmission [121-123], propagation of inflammation in central nervous system [124], enhance stress resistance [125] and mediate axonal regeneration after nerve damage [126].While EVs released by innate immune cells have been reported to contribute in both pro-inflammatory [127-134] and anti-inflammatory signaling [135, 136], one of the best understood functions of EVs in the adaptive immune system is its role in antigen presentation by dendritic cells [137-140], B cells [141, 142], macrophages [143] and mast cells [144], indicating the presence of infection, inflammation or malfunctioning of that tissue and inducing downstream immunogenic or tolerogenic response [145-150]. Matrix vesicles have been shown to mediate the delivery of Bone morphogenetic protein (BMP), Vascular endothelial growth factor (VEGF) and Bone sialoprotein (BSP) at the site of mineralization and play a crucial role in bone calcification [151, 152]. Prostate derived EVs in the seminal fluid have been suggested to interact with sperm cells and stimulate its capacitation [153-155], improve chances of fertilization by protecting the sperm cell from the immune system in the female genital tract [156-158]. Importance of EV mediated intercellular communication in tissue regeneration and repair [91, 159-163] has been reported recently.

Role of EVs in body fluids

Various functional roles of the EVs present in body fluids have been suggested. For example, EVs present in blood plasma have been reported to be involved in various physiological functions such as coagulation [164, 165], reticulocyte maturation [24, 166, 167] and modulation of vasculature [92, 168-171]. EVs in (CSF) may play a protective role against

amyloid beta accumulation through sequestration of amyloid beta oligomers via surface proteins such as prion PrP^C [172]. EVs present in uterine fluid has been suggested to be mediate endometrial-embryo cross talk and has been associated with sperm capacitation, fertilization and embryo implantation [173-177]. EVs in amniotic fluid may induce immuno-modulatory effects to maximize fetal survival during pregnancy [178-180]. EVs detected in Broncho-alveolar lavage fluid may act as signal conveyors for nanoparticles, pathogens, allergens and induce systemic immune response [43, 181-185]. EVs present in breast milk are enriched with immune-related micro-RNAs, and possible transfer of EVs from mother's milk to the infant may participate in the development of infant's immune system [186-191]. Salivary EVs have been shown to carry tissue factor which may be involved in coagulation and wound healing [192, 193]. Cell-to-cell communication between nephrons mediated by urinary EVs has been suggested to be involved in various roles related to kidney physiology, including possible contribution in host defense by boosting coagulation and hemostasis [194-197]. Biliary EVs have been suggested to mediate cholangiocyte regulation and proliferation through interaction with primary cilia [198, 199]. Feces contain bacterial EVs from the gut microbiota and have recently been shown to induce systemic inflammation response when injected in mice [200].

Role of EVs in cancer

The role of EVs in mediating interactions between tumor and other normal cells in its microenvironment is currently a subject of intense investigation. For example, cancer cell derived EVs have been reported to induce both immune-stimulating and immune-suppressive effects. For example, antigen delivery by tumor derived EVs are capable of eliciting anti-tumor immune response through activation of T cells or dendritic cells [201-205]. On the other hand, tumor cells of various lineages release EVs carrying death ligands such as Fas ligand (FasL) and

Tumor necrosis factor (TNF) related apoptosis inducing ligand (TRAIL) which induces cell death in primary leucocytes but not tumor cells themselves, a process that has been suggested to be a mechanism of immune evasion of tumor cells [206-209]. Tumor cells also release regulatory cytokines such as Transforming growth factor-beta1 (TGF-β1) through EVs to suppress proliferation of CD8+ T cells and elevate the number of regulatory T cells [210-214], and induce differentiation of myeloid cells into myeloid derived suppressor cells through TGF-β1 and Prostaglandin-E2 carrying EVs [215-217].

The ability of tumor derived EVs to modulate vasculature to suit its own growth and proliferation has been reported in multiple studies. For example, transfer of pancreatic cancer cell derived EVs carrying Tspan8 protein to endothelial cells reportedly enhanced vessel branching [61, 218]. Colorectal cancer and glioma derived EVs containing Delta-like 4 (Dll4) protein were shown to promote angiogenic sprouting and increased vessel density via modulation of Notch signaling [170, 219]. Hypoxia cued EVs from multiple myeloma were reported to accelerate angiogenesis by targeting the *Hypoxia inducing factor -1 (HIF-1)* signaling pathway via *miR-135b* [220]. Transfer of mutant epidermal growth factor receptor (EGF-R) protein by lung cancer EVs to endothelial cells has also been suggested to induce pro-angiogenic response [34].

EVs have been suggested to mediate tumor's interactions with its stroma in its microenvironment. Tumor EVs carrying TGF-beta on its surface were reported to trigger differentiation of normal mesenchymal stromal cells into a myo-fibroblastic phenotype via *SMAD* dependent pathway [221-223]. Transfer of oncogenic protein Tyrosine kinase-(KIT) from gastrointestinal stromal tumor derived EVs to adjacent progenitor smooth muscle cells altered

them to tumor supporting stromal cells and activated signaling pathways downstream of *KIT* resulting in enhanced secretion of Matrix metalloproteinase 1 (MMP1) and tumor invasion [224].

Tumor derived EVs have been suggested to play an important role in the formation of pre-metastatic niche. For example, melanoma derived EVs were demonstrated to prime lymph nodes by causing micro-anatomical changes, seeding the site for subsequent migration of melanoma cells and establishment of metastatic site [225]. Transfer of MET protein through melanoma derived EVs to bone marrow progenitors has been reported to be another important mechanism for metastatic progression [35, 226].

Role of EVs in lower organisms

EV mediated intercellular communication is not a unique characteristic of mammalian cells alone, and various functional roles of EV transfer by lower organisms, including bacteria and parasites have been reported as well. For example, intra and inter species transfer of proteins and signaling molecules through bacterial outer membranous vesicles (OMVs) has been suggested to facilitate quorum sensing [227, 228], transfer antibiotic resistance [229, 230], spread pathogenicity [231], mediate interactions between host and its microbiome [43, 232], aid bacterial survival during stressful conditions through sequestration and discarding of misfolded proteins [233] and in formation and maintenance of biofilms [234-238]. EVs released by parasitic organisms, such as Trypanosoma *Cruzi* [239-241], Leishmania *Donovani* [242-246] and Plasmodium *Falciparum* [247-250] transfer proteins and RNA to its hosts and have been suggested to be involved with immune-modulatory functions, spreading of pathogenesis and provide an immune evasion route for parasites.

In spite of such a diverse array of functional roles mediated by EVs, most of these studies have failed to identify the encapsulated molecules within EVs involved in the function. Among all the studies which did identify the responsible functional molecule within EVs, an overwhelming majority of them has implicated proteins as the responsible functional molecule within EVs. Relatively fewer studies have reported the functional roles played by lipids and RNA through EVs.

1.9 Evidence of the involvement of proteins in EV functionality

Functionality of both EV membrane bound proteins as well as soluble proteins in EV cargo has been investigated extensively. Surface proteins present on the EV membrane are capable of triggering downstream signaling in the target cell through receptor ligands interactions. Several EV membrane proteins, such as transferrin receptor (TfR) [251], MHC I and II [252-257] and tetraspanins [60, 61] have been reported to trigger downstream signaling pathways in the recipient cell such as integrin and calcium signaling pathways [258], mitogen activated protein kinase pathways (MAPK) [251], natural killer group 2D signaling pathways (NKG2D) [210, 259], etc. Multiple studies have also reported EV mediated secretion of leaderless cytokines such as Interleukin-1 beta (IL-1β) [260], IL-18 [261], IL-32 [262], IL-6 [263] as well as Macrophage migration inhibitory factor (MIF) [264], Vascular endothelial growth factor (VEGF) [265] and TNF [266] in the extracellular space. Macrophages cause inflammation induced programmed cell death in smooth muscle cells through EV mediated transfer of functional pyroptic caspase-1 [267]. Mast cell derived EVs containing immune-modulatory proteins such as MHC-II, Intercellular adhesion molecule-1 (ICAM-1), Heat shock proteins (HSPs) etc. target other Mast cells, induce DC maturation and deliver antigens for cross presentation and induce B and T cell activation [76, 144]. Activated T-cells release immune –

regulatory EVs carrying MHC, T-cell receptor, Apo2, FasL and NKG2D ligand [268] and have been reported to inhibit NK cell cytotoxicity [269], block T-cell stimulation [270], promote T-cell apoptosis [271], and down-modulate T-cell stimulatory capacity of antigen presenting cells [272].

1.10 Evidence for functionality of EV lipids

Evidence of EV lipid functionality is relatively scarce. Apart from the role of lipids in the biogenesis of EVs, transfer of bioactive lipids such as cholesterol and eicosanoids between cells by EVs has been reported and various functional roles have been attributed [66]. For example, EV bound prostaglandins were shown to trigger prostaglandin dependent intracellular pathways upon uptake in the recipient cells [273]. Sphingomyelin in pancreatic tumor derived EV stimulates angiogenesis through activation of *Notch* signaling pathway [274, 275]. Transfer of cholesterol to sperm cells by EVs present in seminal fluid has been suggested to play an important role in reproduction [276, 277].

1.11 Evidence for functionality of EV RNA

mRNA mediated functional studies

While several studies have reported the ability of EVs to transfer full length and functional messenger RNAs between cells, many of these studies have lacked crucial controls experiments, leaving the evidence of functionality ambiguous. First evidence of functional messenger RNA transfer was obtained when Ratajczak et.al reported transfer of *Oct4* mRNA from embryonic stem cells through EVs increased the levels of Oct-4 protein in recipient bone marrow mononuclear cells [82]. However, pre-treating the EVs with RNase abrogated the enhancement of Oct-4 protein expression, suggesting the *Oct4* mRNA was present outside the

EVs and not encapsulated within EVs. Another study by Valadi et.al demonstrated that murine mast cell derived EVs transfer messenger RNA to human mast cells and murine mRNAs were subsequently translated to murine proteins [101]. However, the presence of the respective protein counterparts of these mRNAs in EVs was not verified in this study, leaving a possibility that the detected proteins may have been present in the EVs themselves as well. Moreover, RNase treatment of EVs to confirm the mRNA was encapsulated within EVs was also not performed, leaving the possibility that the detected RNA was outside EVs. Another study by Bruno et.al reported transfer of human mesenchymal stem cell derived EVs containing 239 mRNAs to murine kidney epithelial cells *in-vitro* and *in-vivo*, of which two were found to be internalized and translated into full length proteins [91, 278]. However, this study also did not investigate the protein content of EVs and in fact, reported loss of the messenger RNA level upon RNase treatment of EVs, again suggesting mRNA was present outside EVs. Yet another study by Deregibus et.al claimed transfer of messenger RNAs from endothelial progenitor cells to microvascular endothelial cells triggered neo-angiogenesis and showed transfer and subsequent translation of GFP mRNA to recipient cells while GFP protein was not detected in EVs [92]. However, RNase treatment of the EVs resulted in loss of GFP protein signal in recipient cell as well as purported mRNA functionality, suggesting yet again the observed phenotype didn't arise from EV encapsulated messenger RNA.

Further contradictory evidence regarding the presence and transfer of functional messenger RNAs in EVs has been reported recently. Recent studies by Batagov et.al [86] have reported the enrichment of 3'UTR fragments of messenger RNAs in EVs, not full length messenger RNAs. Multiple deep profiling studies of EV RNA by RNA-Seq have corroborated the presence of mRNA fragments in EVs rather than full length transcripts [94, 98, 99].

Moreover, a recent study by Kanada et.al [279] reported little to no transfer and subsequent translation of functional messenger RNAs by EVs, further contradicting the initial studies of functional messenger RNA transfer.

MicroRNA based functional studies

EVs mediated transfer and functionality of microRNAs has been reported to play a functional role in several physiological roles such as neuron-to-astrocyte communication in central nervous system [280], muscle cell differentiation [281], osteogenic differentiation [282], follicular maturation [283], etc. Pegtel et.al was among the first to demonstrate that EBV infected B cells transfer mature EBV microRNA through EVs to uninfected B cells, causing a dose dependent repression of its targets, suggesting a functional delivery of microRNA through EVs [284]. Subsequently, multiple studies have reported the transfer of microRNAs between cells by EVs and subsequent modulation of target gene expression as well as reporter luciferase assay in the recipient cells [48, 88, 285, 286]. For example, CD63+ EVs derived from T cells were reported to transfer mir-355 microRNA and downregulate the expression of Sox4 in antigen-presenting cells [88, 287, 288]. Transfer of pro-angiogenic microRNAs like *mir-126* and *mir-296* by EVs from endothelial progenitor cells were reported to induce angiogenesis in endothelial cells [289]. However, in this study, the phenotype was attenuated upon RNAse treatment of EVs, suggesting the observed function was at least partially mediated by vesicle-free microRNAs. Another study by Zhang et.al reported the transfer of *mir-150* by blood cell derived EVs downregulate *c-Myc* expression in human mammary epithelial cells (HMEC-1 cells) [290]. Transfer of *mir-143* and *mir-145* by endothelial cell derived EVs to smooth muscle cells induced downregulation of its targets resulting in an athero-protective phenotype [291]. Thus, taken together, these reports indeed present substantial suggestive evidence of possible

functionality of microRNAs encapsulated within EVs. However, one common short-coming of almost all of these studies is most of these studies have been correlative in nature and direct evidence of microRNA mediated functionality through EVs is still lacking. While the abundance and transfer of microRNAs in EVs was demonstrated in these studies, downregulation of target messenger RNAs were demonstrated by treatment of target cells with isolated EVs. While this approach certainly suggests the functional role of microRNAs through EVs, it leaves a possibility that other factors present in the EVs, esp. proteins, may also play a role in the reported target downregulation or observed phenotypic response. Also, pre-treatment of EVs with RNAse was not performed in majority of these studies, leaving a possibility that the observed functionality occurred through micro-RNAs not encapsulated within EVs.

Indeed, recent studies have suggested that microRNA forms only a small component of EV RNA cargo and majority of the secreted microRNAs circulate membrane free and bound to ribo-nucleoproteins like Ago2 [292-294] and lipoprotein particles such as high density lipoprotein (HDL) [295]. Arroyo et.al [292] and Turkinovich et.al [294] reported nearly 90-95% of secreted microRNAs detected in cell-free blood plasma and nearly 99% of the secreted RNAs in cell culture medium is membrane free, protease sensitive and associated with Ago-2 ribo-nucleoprotein particles. Thus, these contradictory reports have further confounded the question of functionality of EV encapsulated RNA.

1.13 Rationale of the study

Investigations on EVs in various laboratories have used different methods of EV isolation, without proper benchmarking with established methods. Lack of standardized isolation methods may have led to these contradictory reports on EV RNA repertoire and has further

complicated the interpretation of functional studies of EV RNA. Moreover, cataloguing of the RNA repertoire of EVs using high throughput and relatively unbiased techniques like RNA-Seq has been limited; and few studies have explored the true diversity of the various classes of annotated RNA transcripts encapsulated within EVs in depth. Identification of transcripts specifically enriched within EVs, fragmentation patterns of EV RNA, cell type specificity and dynamicity of EV RNA cargo has also remained relatively unexplored.

Despite the vast spectrum of biological roles mediated by EVs in diverse physiological systems and pathological conditions, investigations on the involvement of RNA in EV mediated intercellular communication in the past have been relatively few and often lacked crucial controls. Moreover, almost all of these functional studies of EV RNA have been primarily limited to messenger RNA and micro-RNA component of EVs, which has left the biological role of other reportedly abundant and enriched classes of RNA molecules in EVs unexplored.

The objective of this study is to establish if EV mediated transfer of functional RNA molecules represents a novel mode of intercellular communication, with particular focus on the functionality of other classes of non-coding transcripts enriched in EVs. To that end, we first developed and validated a novel and efficient approach of isolation of EVs and bench-marked with existing methods of EV isolation. Armed with this approach, we performed a comprehensive characterization of RNA repertoire of EVs from nine different cell types of diverse developmental origins. Finally, we report a novel function of one of the most abundant non-coding RNA components in EVs and its possible involvement in EV mediated intercellular communication.

Chapter 2

Novel and efficient strategy for isolation of EVs.

Sudipto K. Chakrabortty[#], Ashwin Prakash[#], Alexandra Scavelli, Stephen Hearn and Thomas R. Gingeras

Authors contributes equally to this work.

2.1 Synopsis:

The strategies for isolation of EVs commonly used today vary greatly in their purity and efficiency; with each method having their unique advantages and disadvantages. In this chapter, we report a novel and efficient 'hybrid' strategy for isolation of EVs and systemically validate our EV preparations with multiple orthogonal techniques. Multi-parametric comparative analysis with existing methods of EV isolation indicated that our hybrid approach obtained higher yield of EVs and EV RNA in a reproducible and scalable manner, making it the method of choice for downstream investigations on EVs and EV RNA.

2.2. Introduction

Release of extracellular vesicles by cells apparently represents a universal feature of all mammalian and non-mammalian cells investigated, including bacteria and parasites [43]. EVs are detected in abundance in cell culture medium and various body fluids and carry a plethora of proteins, lipid and RNA molecules, known to be involved in diverse functional roles in cells [21, 22, 43]. While exchange of biomolecules through EVs represents a medium of communication between cells, the exact function of only a small subset of the molecules (especially RNA molecules) within EVs are well understood today. Moreover, in the recent years, detection of specific RNA and protein molecules in EVs derived from body fluids has emerged as a novel, minimally invasive way of identifying diagnostic and prognostic biomarkers of various pathological conditions, including cancer [13, 87]. Crucial to the success of such investigations, is the development of a reliable, efficient and consistent method of purification of EVs.

In the recent years, emerging technologies have resulted in the development of various novel and innovative methods of isolation of EVs. These include microfluidics based isolation [296], acoustics isolation [297], chromatography column based purification [298], magnetic beads [299], etc. While the traditional ultracentrifugation based approach of isolation of EVs is still regarded as the "gold standard" method of isolation [300, 301], precipitation based approaches using commercially available polymer based reagents such as Exoquick (System Biosciences) and Total exosome isolation reagent (Life Tech)[302]; ultrafiltration [303-306] and immuno-affinity capture based approaches [12, 32, 307] represents other popular approaches for purification of EVs .

Comparative analysis of these methods based on multiple parameters such as yield, efficiency and morphology of EVs and consistency in detection of EV cargo has reported unique advantages and limitations of each method [32, 301, 304, 308-313]. While the initial differential centrifugation steps in the ultracentrifugation based procedure ensure the depletion of majority of other contaminating particles present in the medium or body fluid, ultracentrifugation remains a laborious, time-consuming approach requiring expensive equipment that may not be affordable to many labs. The reproducibility and yields produced by the ultracentrifugation method are also extremely sensitive to parameters such as g force, rotor type, angle of rotor sedimentation, radius of centrifugal force, solution viscosity and vesicle density [301]. Moreover, the efficiency of EV isolation using ultracentrifugation is regarded to be relatively low [32, 301, 314-317] and importantly, the effect of high gravitational force on the integrity and morphology of EVs and its cargo is not well understood [301]. Alternatively, precipitation based purification is generally considered to be a 'gentle' approach of purification, but pure precipitation based approach are prohibitively expensive, especially when working with large quantities of conditioned medium required for RNA-Seq libraries and highly likely to isolate non vesicular contaminants such as lipoproteins [301, 311]. While sequential centrifugal ultrafiltration is fast, affordable and relatively simple approach, this method often runs the risk of loss of vesicles due to clogging or membrane fouling [301, 311].

The limitations of these individual approaches has led us to develop a novel 'hybrid' approach which combines the unique advantages of each of these individual methods into one unifying hybrid approach. The first three low speed differential centrifugation steps of ultracentrifugation method deplete larger vesicular and non-vesicular contaminants, which can be performed relatively quickly without an expensive ultracentrifuge. Ultrafiltration with

100kDa nominal molecular weight limit (NMWL) membrane reduces large volumes of media to only a few ml of EV enriched residue, which makes liquid handling quick and easy. Most importantly, this step allows quick and affordable downstream use of Exoquick based “gentle” precipitation of EVs from large volumes of media otherwise not possible. Thus, by combining low-speed differential centrifugation steps of ultracentrifugation with 100kDa membrane centrifugal ultrafiltration and followed by Exoquick based precipitation of EVs, we report a novel hybrid approach of EV isolation which is easy, highly efficient, consistent and scalable. We further present a comparative study of our approach with conventional ultracentrifugation, precipitation and ultrafiltration based approaches based on multiple parameters, including yield and size distribution of isolated EVs and EV RNA, scalability as well as reproducibility in detection of RNA to demonstrate the superiority of our hybrid approach.

2.3. Materials & Methods

Cell culture and isolation of EVs

K562 cells were grown in complete RPMI1640 medium up to 70% confluence. Cell culture medium is then replaced with serum deprived conditioned medium and further cultured for another 24 hrs. Approximately 4+E7 K562 cells were grown per replicate. EVs were isolated in replicates by four different methods, namely Ultracentrifugation, ultrafiltration, Precipitation using Exoquick-TC and Hybrid method (Fig 2.1).

Ultracentrifugation

Ultracentrifugation based isolation of EVs was performed as described in Thery et.al [300]. Briefly, 200 ml of conditioned medium was centrifuged at 300g for10 minutes to discard the cell pellet. The supernatant was centrifuged at 2000g for10minutes and the pellet comprising of cell debris was discarded. The supernatant was centrifuged again at 10000g for 30minutes and the pellet was discarded. The supernatant was ultra-centrifuged at 110, 000g for 70 minutes using Sorvall SW-28 rotor. The supernatant was discarded and the pellet composed of EVs and protein complexes were suspended in phosphate buffer saline (PBS). The EVs was centrifuged again at 110,000g for 70 minutes. The supernatant was discarded again and the pellet was suspended in 500 microliter PBS.

Precipitation

EVs isolation was performed by Exoquick-TC from 50ml of conditioned medium (1+E7 source cells approx.) due to prohibitive expense of the precipitation reagent Exoquick-TC (System Biosciences). Briefly, conditioned medium was centrifuged at 300g for 10 minutes. The

cell pellet was discarded and the supernatant was centrifuged at 2000g for10 minutes. The pellet, comprising of cell debris and apoptotic bodies was discarded. 10ml of Exoquick-TC was added to the 50ml supernatant (1:5 ratio) and incubated for 12 hours at 4 degrees. Next day, the conditioned media-Exoquick-TC mixture was centrifuged at 1500g for 30 minutes. The supernatant was discarded and the pellet was centrifuged again at 1500g for 5 minutes. The left over supernatant was discarded and the pellet was suspended in 500microliter PBS. Yield of EVs and EV RNA from 200ml conditioned medium using precipitation was extrapolated by multiplying the yield by a factor of 4.

Ultrafiltration

200ml of conditioned medium was centrifuged at 300g and 2000g to discard the cells and cell debris pellet respectively. Larger contaminants were first depleted from the supernatant by ultrafiltration using 0.45 micron filter (Sterivex, Millipore). The filtrate was then further filtered using Centricon Plus-70 100 kDa filters (10nm pore size approx.). The isolated EVs in the residue were collected and the filtrate was discarded. The volume of the collected EVs was brought to 500 microliters with PBS.

Hybrid

200ml of conditioned medium was centrifuged at 300g for 10 minutes. The cell pellet was discarded and the supernatant was centrifuged at 2000g for 10 minutes. The pellet, comprising of cell debris was discarded and the supernatant was centrifuged at 10000g for 30 minutes. The pellet was discarded and the supernatant was filtered with Centricon Plus-70 100kDa (10nm pore size approx.) centrifugal filters at 3500g for 15 minutes. The residue,

enriched in EVs was collected while the filtrate was discarded. The volume of the filtration residue was made to 500 microliters using PBS.

Nanoparticle Tracking Analysis (NTA)

Nanoparticle tracking analysis was performed on the purified EV samples using NanoSight LM10. The samples were run at 25 degrees using PBS as a diluent.

Transmission electron microscopy (TEM)

Aliquots of EVs suspensions were dispensed on Parafilm on a petri dish and Butvar coated EM grids were adsorbed on them for 5 minutes at room temperature and then kept on ice. The grids were transferred to drops of distilled water thrice for 30 seconds each to wash off excessive salts. The grids were then transferred to a drop of 1% uranyl acetate in 1% methyl cellulose for 30 seconds followed by another transfer to a second drop for 5 minutes. The grids were air dried and excess stain was blotted off. Imaging was performed using Hitachi H7000 electron microscope at 75kV.

Immuno-electron microscopy

Immuno-gold labeling for the CD9 EV surface protein was performed by re-suspending EVs in primary mouse antibody to human CD9 (Abcam) diluted in PBS for 30 minutes at room temperature. The antibody labeled vesicles were pelleted by centrifugation, re-suspended in a 1:10 solution of 5nm colloidal gold conjugated to rabbit anti-mouse IgM secondary antibody (Aurion, Electron Microscopy Sciences) for 30 minutes. The gold labeled vesicles were then adsorbed to Butvar-coated grids for 5 minutes and then rinsed through 3 drops of PBS to remove

unbound gold particles. Negative staining of the gold labeled vesicles was completed as described above

Isolation of RNA

Purified EVs, re-suspended in PBS, were treated with 15microliters of RNase cocktail (Ambion) at 37 degrees Celsius for 30 minutes to degrade any free RNA molecules that's not enclosed within EVs. The RNases were immediately inactivated with the lysis /binding buffer of Mirvana miRNA isolation kit (Ambion) and immediately proceeded to total RNA isolation using manufacturer's protocol and ethanol precipitated with 2.5 volumes of 100% ethanol and 1/10th volume 3M sodium acetate. The precipitated RNA was DNase treated with Turbo-DNase (Ambion) and ethanol precipitated. The re-suspended RNA was finally quantified using Agilent Bio-analyzer RNA pico-chip.

Small RNA-Sequencing

Small RNA libraries were constructed using Illumina TruSeq Small RNA Sequencing kit. The purified RNA samples were first treated with Tobacco acid pyro phosphatase (TAP) for 1 hour at 37deg to convert 5' (prime) capped and triphosphate RNA molecules into monophosphate and make then amenable to adapter ligation. The RNA was subsequently extracted using phenol-chloroform and precipitated with 2.5 volume 100% ethanol and 1/10th volume sodium acetate. The precipitated RNA sample was then used for adapter ligation, reverse transcription and PCR amplification according to Truseq protocol. While ultracentrifugation, hybrid and filtration libraries were amplified for 15 PCR cycles, libraries from precipitation method were amplified for 30 PCR cycles due to its extremely low starting input of RNA. The amplified cDNA was run on a 2% agarose gel and region pertaining to 20-200bp of RNA (145 -

350bp cDNA on gel) were cut out of the gel. The cDNA was then extracted using Qiagen gel extraction kit according to manufacturer's protocol, ethanol precipitated and quantified using Bioanalyzer HS-DNA chip. Finally, replicates of libraries were multiplexed and run on Illumina HiSeq 2000 or MiSeq.

Bioinformatics analysis

All data from RNA sequencing experiments in the study were mapped to Human Genome version 19 (hg19, GRCh37) obtained from the UCSC genome browser website (http://hgdownload.cse.ucsc.edu/downloads.html). RNAseq reads were aligned using the STAR v1.9 [318] software, and up to 5 mismatches per alignment were allowed. Only alignments for reads mapping to 10 or fewer loci were reported. Annotations were not utilized for mapping the data. The obtained BAM files were further processed using HTSeq [319] software in order to appropriate the number of reads originating from each annotated region of the genome, utilizing annotations obtained from Gencode v19 [320] of the human genome, using the "Union mode" option of the software for all libraries, tRNA annotations were obtained from tRNAscan database [321]. Reads per million (rpm) values for each gene were obtained by dividing the number of reads uniquely mapping within the limits of a gene annotation, by the total number of uniquely mapping reads in the library and multiplying by a million. These rpm values were used to establish correlation between biological replicates of RNA-Seq libraries from each isolation method (Table 2.2). Mean of rpm values of both replicates from each method were calculated first to estimate the correlation of RNA-Seq libraries across the four EV isolation methods (Table 2.3).

2.4. Results

2.4.1. Comparison by yield and size distribution of EVs:

The yield of purified EVs achieved is an important parameter to assess the isolation methods. Nanoparticle tracking analysis allowed us to quantify and compare the number of EVs isolated by each isolation method. While our hybrid method yielded 1.06E+11 and 7.59E+10 EVs, in contrast, conventional ultracentrifugation method isolated 7.27E+09 and 6E+09 EVs. Replicates of ultrafiltration yielded 1.31E+11 and 1.26E+11 EVs respectively and precipitation method yielded 5.10E+09 and 3.68E+09 EVs (extrapolated from 50 ml medium actually used). Thus, although the yield of EVs by our hybrid method was slightly lower than ultrafiltration method, the yield from hybrid method was higher than the traditional "gold standard" ultracentrifugation and filtration methods by at least an order of magnitude (Figure 2.2A).

NTA analysis also allowed us to compare the size distribution of the isolated EVs. The hybrid method isolated vesicles of remarkably similar size distribution when compared with other methods. The mean diameter of EVs isolated in replicates by hybrid method was 185 and 195nm, with standard deviation of 89 and 109nm respectively, while ultrafiltration method isolated EVs of mean 173 and 177nm with standard deviation 80 and 71nm respectively. Similarly, while precipitation method isolated EVs of mean diameter 173 and 188 nm with standard deviation 84 and 93nm respectively, the ultracentrifugation method isolated EVs of mean diameter 183 and173 nm with standard deviation 84 and 81nm respectively (Figure 2.2B). Thus, the size distribution profile of EVs isolated by the hybrid method are remarkably consistent with all other methods.

Transmission electron microscopy on EVs isolated by hybrid method revealed membrane vesicles of characteristic cup shaped morphology (Figure 2.3A). Detection of the protein CD9 on the surface of EVs by immune-electron microscopy further validated our purification of EVs by hybrid method (Figure 2.3B).

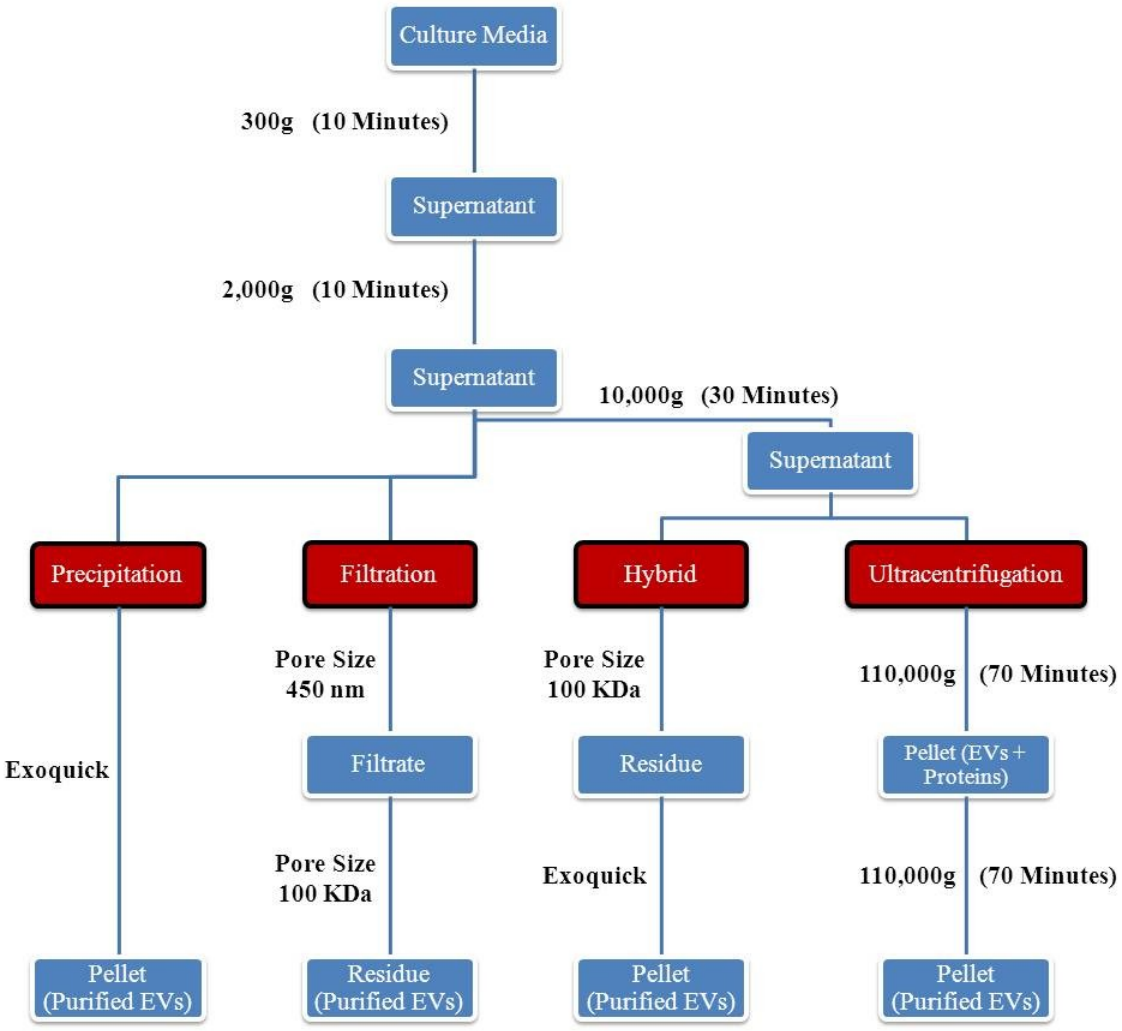

Figure 2.1: Methods of EV isolation. A schematic representation of the four methods of isolation of EVs used in this study, namely Ultracentrifugation, Filtration, Precipitation, and the novel Hybrid method**.**

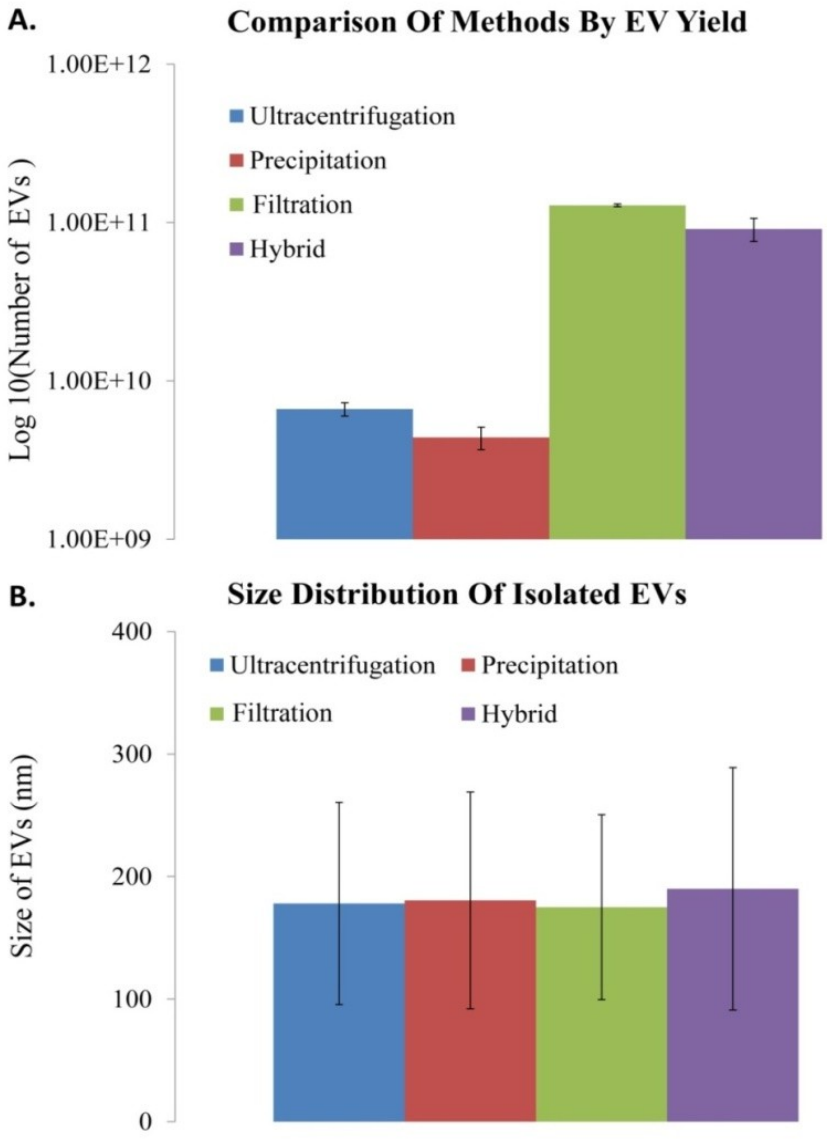

Figure 2.2: Comparison of EV isolation methods by yield and size distribution of isolated EVs. (A) The yield of EVs isolated by Ultracentrifugation, Precipitation, Filtration, and Hybrid method. Quantification of the yield of EVs was performed by Nanoparticle Tracking analysis (NTA). Mean of duplicates are presented. Y-axis represents the total number of isolated EVs in Log10 scale. **(B)** Size distribution of EVs. EVs were isolated in duplicates by Ultracentrifugation, Filtration, Precipitation, and Hybrid method and analyzed by NTA. Each bar represents the mean hydrodynamic diameter of EVs and the error bars represent mean standard deviation as reported by NTA. Y-axis represents size of EVs in Nanometers (nm).

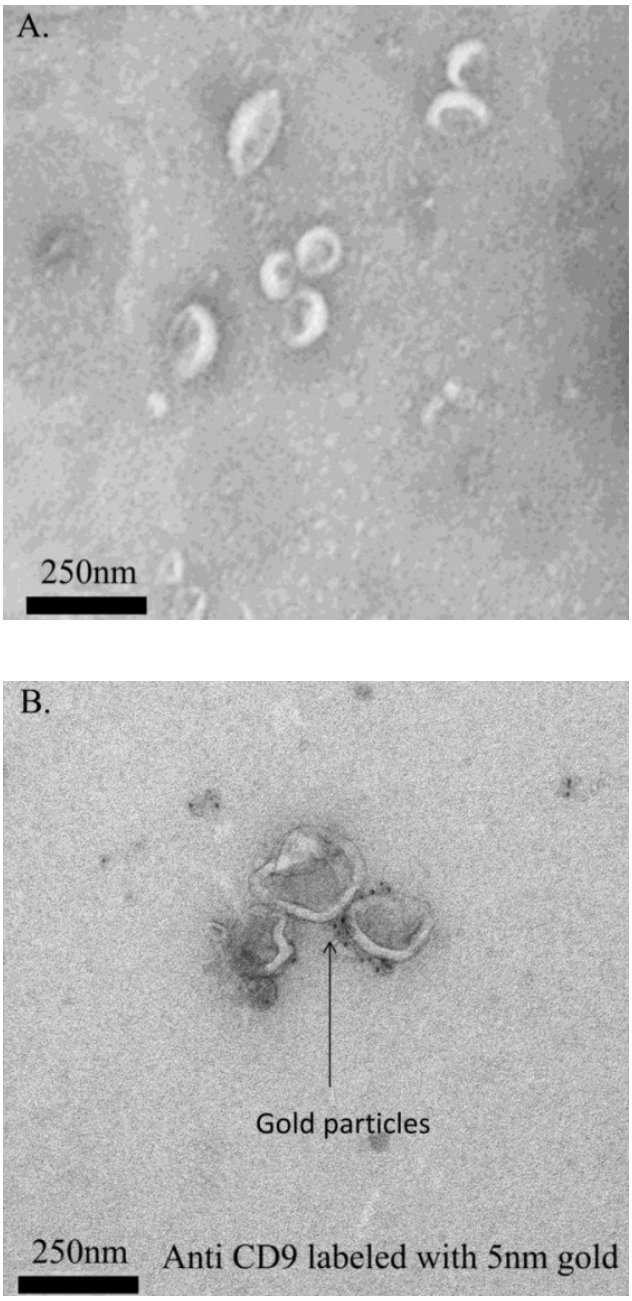

Figure 2.3: Validation of EV isolation from Hybrid method by Electron Microscopy. **(A)** Transmission electron microscopy image of K562 EVs after negative staining shows classic cup-shaped vesicles that are on average smaller than 200nm. **(B)** Immuno-electron microscopy image of purified EVs labeled with Anti-CD9 (mouse mAb) and detected by Goat anti-mouse IgG secondary conjugated with 5nm gold. Dark spots on the image are the electron dense gold particles conjugated to IgG secondary antibody. Scale bar represents 250nm.

2.4.2. Comparison by yield and size distribution of EV RNA

Next, we investigated the quantity and size distribution of the RNA molecules enclosed in EVs. Bioanalyzer profile showed each of the method isolated EVs consisting of mostly small RNA of size less than 200 nucleotides. The amount of long RNA (>200) present in EVs was found to be very low, although a slight bump around 18S and 28S ribosomal RNA region was observed. Thus, the RNA size distribution profile obtained by the hybrid method was found to be remarkably consistent and displayed huge overlap with the RNA size distribution obtained with established methods (Figure 2.4B).

Interestingly, the yield of RNA isolated by the four methods varied greatly as well as within the replicates of each method. Replicates of the Hybrid method isolated 356 and 292ng of RNA. In contrast, replicates of Ultracentrifugation method yielded 114ng and 38.8ng of RNA. Precipitation method would have yielded 48.8 and 22 ng of RNA (extrapolated from 12.2 and 5.5ng of RNA yield from 50ml conditioned medium). Surprisingly, RNA yield from ultrafiltration showed inconsistency among replicates. While, replicate1 of ultrafiltration method yielded 354ng of RNA, 2nd replicate yielded just 77.8ng of RNA. Thus, the highest and most consistent yield of RNA from EVs was achieved by the hybrid method which strongly underscores the ability of hybrid method to purify structurally intact EVs resulting in minimal RNA loss (Figure 2.4A). Further assessment of the scalability of the hybrid method was performed by isolating EVs from replicates of 25ml, 50ml and 100ml of conditioned medium. Linearity of the EV RNA yield from these different volumes of medium attested the down-scalability of hybrid approach (Figure 2.5).

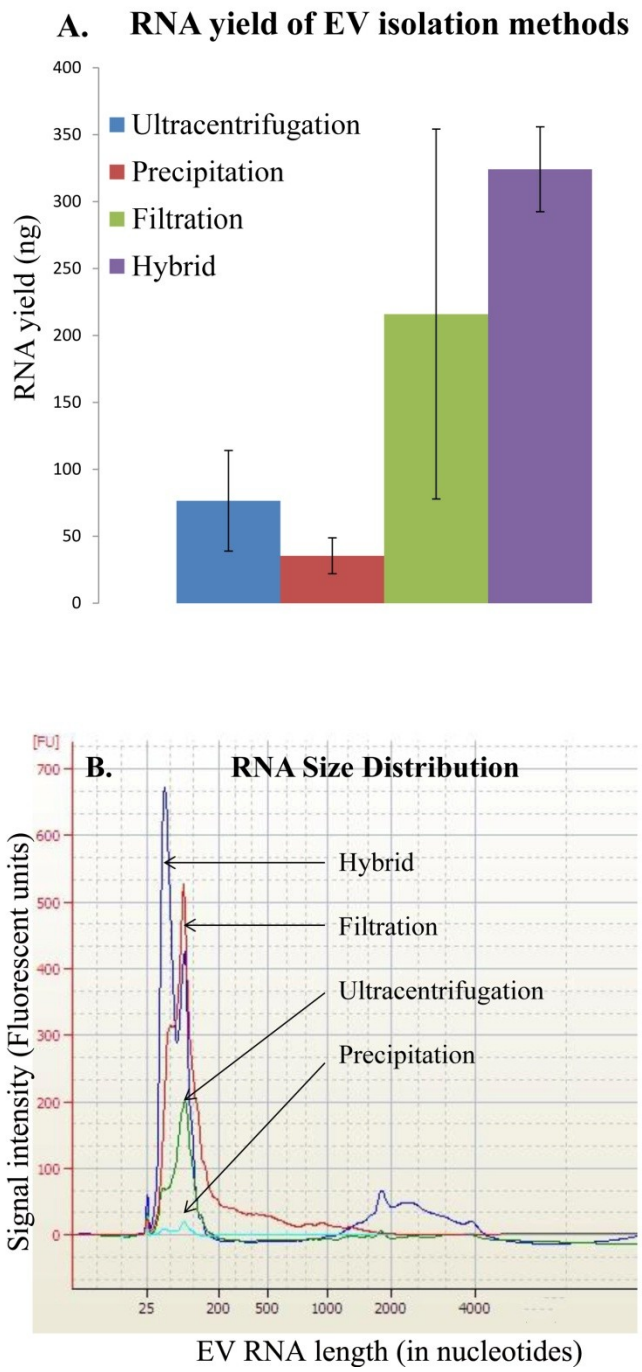

Figure 2.4: Comparison of EV isolation methods by RNA yield and RNA size distribution: (A) Yield of RNA obtained from EVs isolated by Ultracentrifugation, Precipitation, Filtration, and Hybrid method. Quantification of RNA yield was performed by Bioanalyzer (Pico-chip). Each bar represents mean of duplicates of RNA yield from the four isolation methods and the error bar represents variation from mean. Y-axis represents yield of RNA in nanograms (ng). **(B)** Size distribution of RNA isolated from EVs by Ultracentrifugation, Precipitation, Filtration, and Hybrid method. Analysis was performed on Bioanalyzer Pico-chip. X-axis represents the nucleotide length of isolated EV RNA and Y axis represents Bioanalyzer signal intensity.

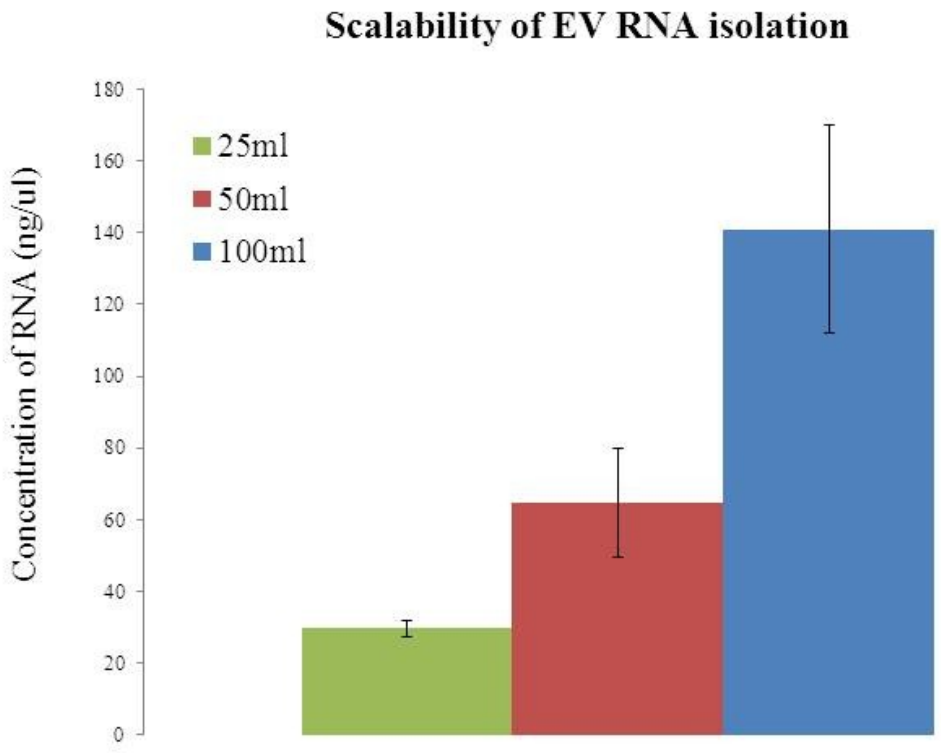

Figure 2.5: Scalability of EV isolation by hybrid approach. EVs were isolated by the hybrid method from 25, 50, and 100ml of K562 cells conditioned medium in duplicates followed by RNA isolation. Quantification of the RNA yield was performed by Nanodrop, which revealed linear increase in the yield of EV RNA with increase in the starting volume of conditioned medium. Each bar represents mean of duplicates and error bar represent variation from the mean yield. Y-axis represents the concentration of RNA in Nanograms / milliliter (Ng/ml).

2.4.3. Comparison by RNA-Seq

While Bio-analyzer analysis allowed us to compare the yield and size distribution of the RNA molecules enclosed in EVs, RNAseq analysis allowed us to assess the degree of reproducibility in detection achieved by each of the isolation methods as well as the consistency of detection among the four methods. Illumina TruSeq small RNA-Sequencing was performed on the EV RNA isolated by the four methods (in duplicates) as described in the methods. Each library was sequenced to a depth of 22.25 million reads approx. and mapped using STAR [318]. The proportion of reads mapping to the genome was approximately 61% and was highly consistent among the libraries. About 41 % reads mapped uniquely to the genome and approximately 21% of reads mapped to multiple locations in the genome. The read length distribution of the libraries was extremely similar to each other with average read length around 44bp (Table 2.1).

To investigate the inherent consistency of detection of EV RNA obtained by each method, we utilized the Pearson's correlation coefficient between the replicates of each method. While each method demonstrated strong correlation between its replicates, the highest correlation was observed in Precipitation (r^2 =0.91) method. Ultracentrifugation and hybrid method came a close second and third, with correlation coefficient of 0.89 and 0.87 respectively. Replicates of ultrafiltration had a relatively weak correlation with coefficient (R^2) around 0.8 (Table 2.2, Figure 2.6).

Since ultracentrifugation has traditionally been recognized as the "gold standard" method for isolation of EVs, we decided to compare the expression levels of RNA detected by the rest of the methods with ultracentrifugation. We computed the Pearson's coefficient of correlation of EV RNA expression detected between the four isolation methods. The hybrid method

demonstrated the strongest correlation with ultracentrifugation (correlation coefficient 0.92), followed by precipitation and ultrafiltration with 0.88 and 0.87, respectively. The hybrid method was also highly correlated with precipitation and filtration, with correlation of 0.87 and 0.84 respectively. The correlation between precipitation and filtration was 0.84 (Table 2.3.).

Sequencing statistics	Hybrid	Filtration	Ultracentrifugation	Precipitation	Mean
Library Size (No. of reads)	26710609	28525331	17335359	16433015	22251079
Percentage Unique Mappers	37.63	46.08	34.16	45.8	40.9175
Percentage Multi-Mappers	23.27	16.13	15.3	28.95	20.9125
Average mapped read length	43.58	35.76	49.12	45.68	43.535

Table 2.1 Sequencing statistics: Mapping statistics of RNA-Seq libraries from EVs isolated by Ultracentrifugation, Filtration, Precipitation and Hybrid methods. Mean of the library size, percent of uniquely and multiply mapped reads and mapped read length from the replicates of RNASeq libraries from each isolation method are presented. The mean column represents the mean across the four isolation methods.

EV Isolation Method	Correlation
Filtration	0.8
Hybrid	0.87
Precipitation	0.91
Ultracentrifugation	0.89

Table 2.2 Correlation between RNASeq replicates of EV isolation methods: Pearson correlation coefficient of gene expression between replicates of RNASeq libraries from Ultracentrifugation, Precipitation, Filtration and Hybrid method.

Methods	Hybrid	Precipitation	Ultracentrifugation
Filtration	0.84	0.849	0.879
Hybrid		0.878	0.927
Precipitation			0.88

Table 2.3 RNASeq correlations between EV isolation methods: Pearson **c**orrelation coefficient of gene expression in RNASeq libraries from EVs isolated from Ultracentrifugation, Precipitation, Filtration and Hybrid methods.

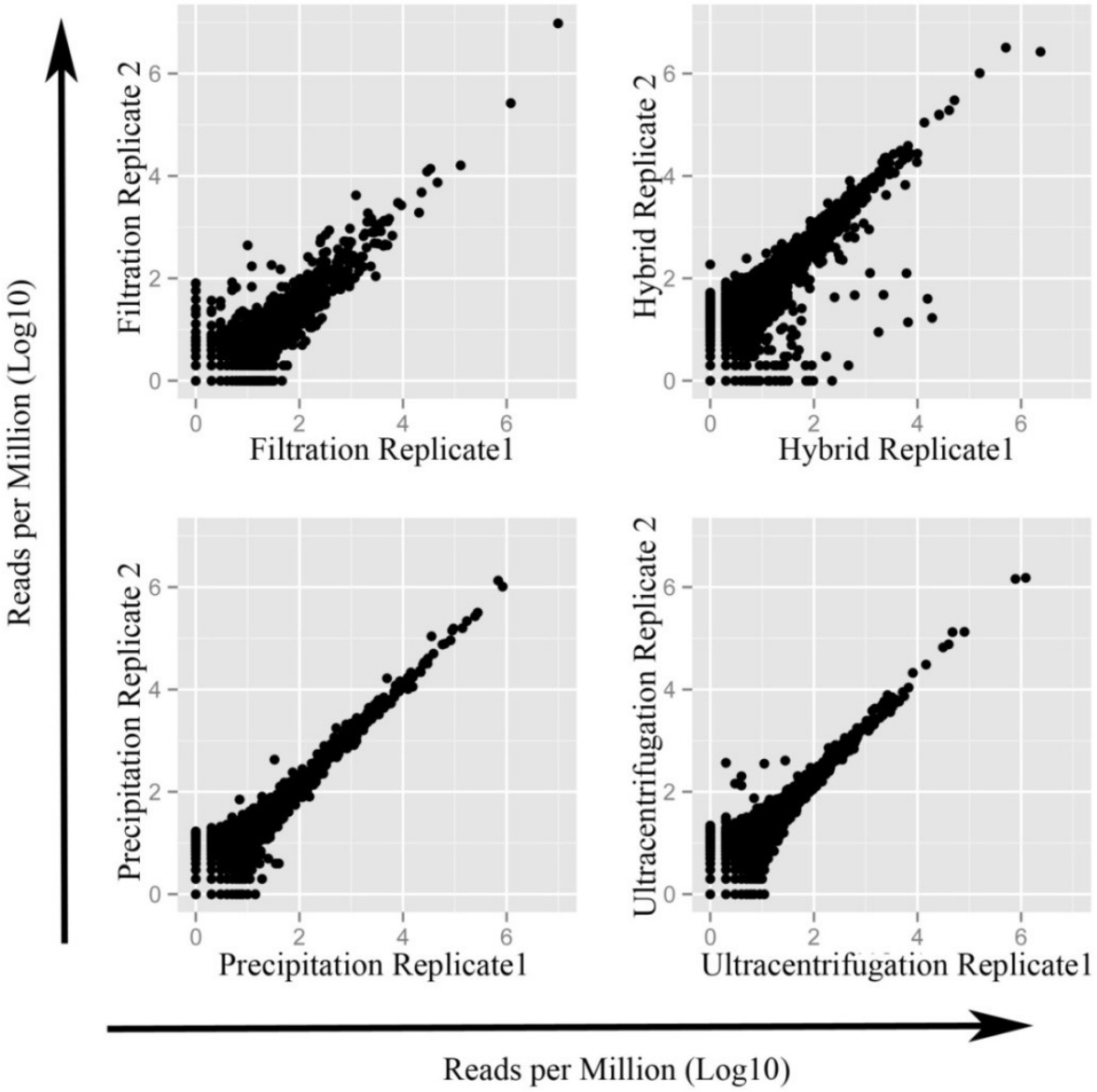

Figure 2.6: Correlation between RNASeq replicates of EV isolation methods. Scatter plots representing correlation in gene expression levels, between replicates of EV small RNA libraries isolated by Filtration, Precipitation, Ultracentrifugation, and Hybrid method.

2.5. Discussion

In this study, we report a novel approach of isolation of EVs from cell culture medium and systematically compare it with current methods of isolation of EVs. We show that yield and size distribution of EVs isolated by hybrid method are remarkably consistent with currently existing methods. Bioanalyzer profiles further indicated the consistency in RNA size distribution with existing methods. While other methods result in comparatively lower and inconsistent yield of EV RNA, our hybrid method consistently yields highest quantity of RNA from EVs. While we demonstrated the scalability of our hybrid approach down to 25ml volume of conditioned media, this method could be easily scaled down to even lower volumes of media or body fluid. RNA-Seq analysis further confirmed the hybrid method's ability to consistently and reproducibly isolate RNA transcripts from EVs. Moreover, strong correlation of gene expression observed between hybrid method and each of the existing methods, including the gold standard ultracentrifugation method underscored the reliability of its performance. Taken together, these results coupled with highest and consistent yield of RNA, argue in favor of hybrid method as the method of choice for isolation of EVs for downstream EV RNA oriented studies.

Chapter 3

Comprehensive characterization of the RNA contents of extracellular vesicles.

Sudipto K. Chakrabortty[#], Ashwin Prakash[#], Alexandra Scavelli, Jorg Drenkow, Stephen Hearn and Thomas R. Gingeras

# Authors contributed equally to this work

3.1 Synopsis:

Characterization of the RNA cargo of EVs has been performed in a limited fashion as yet. Armed with the efficient 'hybrid' approach of EV preparations, we perform a comprehensive characterization of RNA repertoire of EVs from 9 different cell types of diverse developmental origins by RNA-Seq, which revealed the diversity and cell type specificity of EV RNA, non-random sorting of RNA in EVs, gene family specific fragmentation patterns and dynamic nature of EV RNA with changing physiological conditions of the source cell. We then explored the temporal dynamics, spatial localization and integrity of EV RNA upon transfer into another cell. Finally, we investigate the ability of EV and EV RNA to induce a cell type specific and context dependent molecular response upon uptake in recipient cells.

3.1. Introduction

The complex landscape of transcription in multi-cellular organisms is modulated by multi-layered processes that are endogenous as well as exogenous to cells. Endogenous factors include transcription factors, three-dimensional DNA/genome organization [322-325], chromatin modifications [326, 327], DNA methylation [328-330], as well as post-transcriptional molecular processes such as alternative splicing [331], microRNA mediated regulation [332, 333] and RNA degradation [334, 335]. Exogenous factors traditionally refer to extra-cellular conditions (temperature, pH, oxygen, etc.) and secreted factors (proteins, hormones, metabolites, etc.) which stimulate various signaling pathways in the cell. Recently, extracellular vesicles have garnered substantial appreciation as a key component of the extracellular milieu. While several studies have implicated EVs in various physiological roles, majority of these studies failed to attribute the observed effects to responsible biomolecules encapsulated in them.

Recent studies on EVs have shown the presence of both small and long RNA molecules encapsulated within EVs [76, 82, 84, 90]. However, majority of these studies have limited their attention on two categories of RNA, namely micro-RNA and messenger RNA. Moreover, recent studies have contradicted the earlier observation on the presence of intact messenger RNA [86] and has questioned the presence of substantial amounts of microRNA within EVs as well [292, 294]. Furthermore, limited studies on EV RNA cargo using next generation sequencing has reported the enrichment of other classes of non-coding RNAs within EVs, not microRNA or messenger RNA [94, 95, 98, 99]. These contradictory reports on EV RNA contents have further convoluted the picture of the true nature and extent of EV RNA repertoire released by cells, and emphasizes the need for a comprehensive characterization of the RNA contents encapsulated within EVs.

Nevertheless, EV mediated transfer of RNA between cells has been suggested to represent a novel mode of communication between cells. Indeed, the ability of RNA to compactly store and transmit information, to produce base pair specific interaction and to act as molecular adaptors for incoming signals (e.g. ribo-switches) makes it an ideal molecule of information transfer [336]. Such exchange of genetic information may confer specific advantages to the recipient cell. Uptake of mRNA and its subsequent translation can complement a cell's own protein repertoire by augmenting its endogenous protein level or by providing it with a completely new protein molecule that may not be produced by that cell, thereby priming the cell for a new function or state. Micro-RNA or other regulatory RNA, upon uptake, may act on its endogenous targets and modulate their expression level, thereby adding a new layer of regulation of gene expression in-trans [336]. Unlike other single molecular signaling mechanisms, EVs possess the unique ability to accommodate several RNA and protein molecules within them which can potentially act *en masse* on the recipient cells to elicit a far more complex response.

However, mere transfer of genetic information between cells may not be sufficient to be termed as a mode of communication, as it must satisfy basic properties that any form of communication must possess. Firstly, the message must be meaningful and non-random. This not only requires an understanding of the exact nature and diversity of the messages being exchanged, but more importantly, a specific sorting and packaging of certain messages over others for delivery must be established. Secondly, the message must be dynamic, as a monotonous transfer of a static signal cannot be termed as meaningful communication and it must reflect in some sense the changes in physiological state of the source cell. Thirdly, the message must be delivered safely to the recipient in a manner such that the message remains

available to the recipient's signal interpretation machinery. Finally, the message must be functional and interpretable, capable of eliciting a meaningful response in the recipient.

In this study, we perform a comprehensive characterization of the distribution, enrichment and cell type specificity of annotated RNA cargo within EVs derived from 9 different human cell types by RNA sequencing. While previous studies have reported the presence of a few RNA fragments derived from longer annotated genes, we demonstrate an enrichment of family specific RNA fragmentation patterns across cell types, suggesting a conserved processing and sorting machinery of EV RNA. Next, we explore the dynamic nature of the EV RNA cargo, with changing physiological conditions of the source cell. Although others have demonstrated the transfer of EVs between cells, we demonstrate the inter-cellular delivery and subsequent sub-cellular localization of EV RNA. We further characterize the cell type specific and temporal dynamics of the molecular response elicited by EV RNA in multiple cell types.

3.3. Results

3.3.1 Validation and quantification of EVs

The presence of various species of RNA was first demonstrated in extracellular vesicles (EV) in an attempt to define a potential mechanism by which EVs may mediate intercellular transfer of genetic material [82, 101]. In this study, isolation of EVs derived from 9 different cell lines was performed using a method adapted from the original ultracentrifugation method described by [300]. Empirical validation of the purification was performed using Transmission electron microscopy (Figure 3.1A) which confirmed the presence of vesicles of size < 200nm and cup-shaped morphology typically described in literature. Immuno-electron microscopy with 5nm gold conjugated antibodies demonstrated the presence of EV surface markers such as CD81 on purified EVs (Figure 3.1B). Western blot analysis further confirmed the enrichment of EV markers and depletion of other sub-cellular organelle markers [data not shown]. Nanoparticle Tracking Analysis (NTA) further quantified the enrichment of vesicles <200nm (Figure 3.1C). Consistent with previous studies, Bioanalyzer analysis showed an overwhelming majority of the EV RNA are small RNA with size distribution between 20-200 nucleotides (Figure 3.1D). Intra-vesicular origin of the EV RNA was confirmed by RNase treatment prior to RNA isolation and small RNA sequencing.

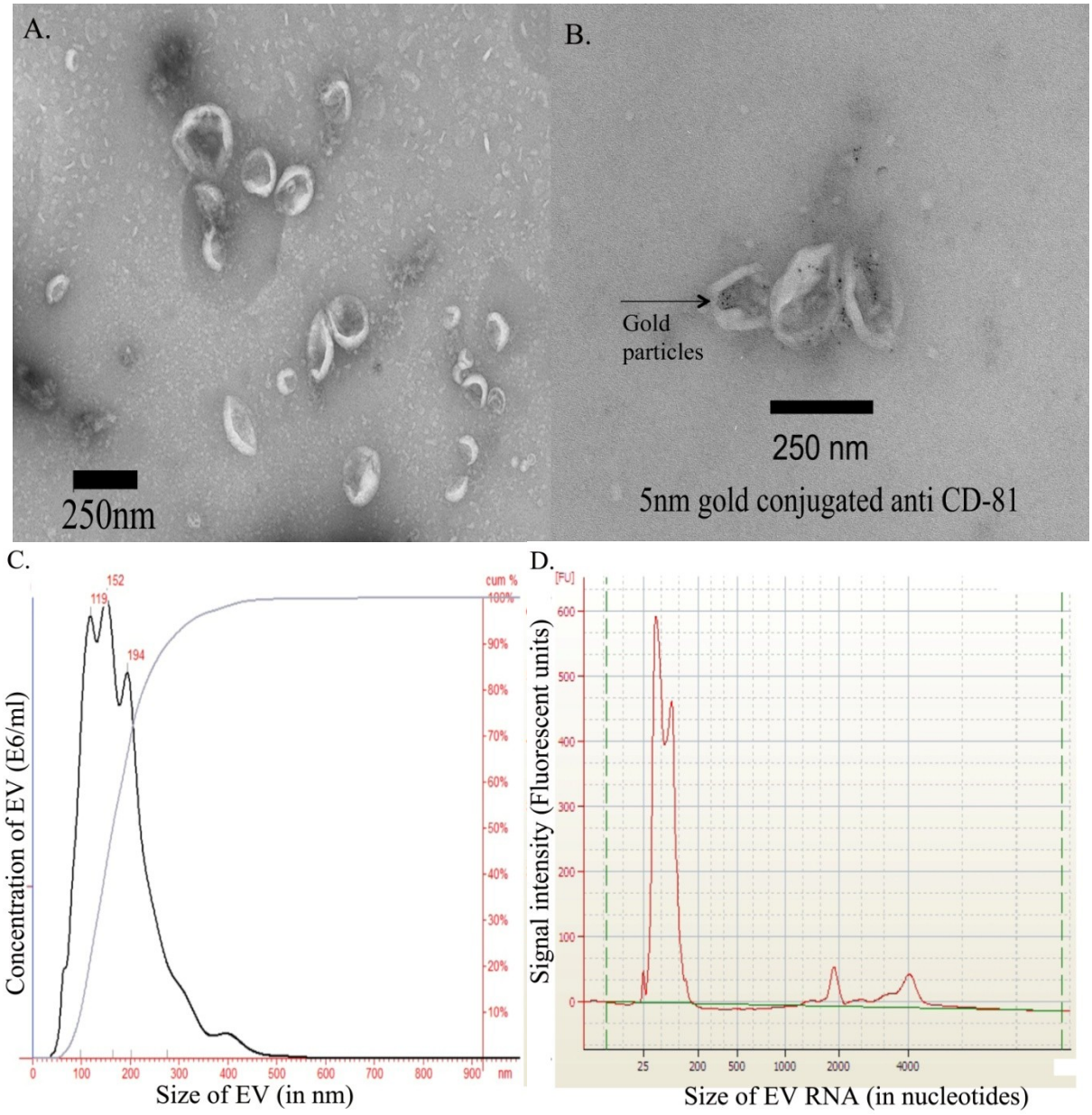

Figure 3.1: Validation of purification of extracellular vesicles (EVs). (A) Transmission electron microscopy image of K562 EVs after negative staining shows classic cup-shaped vesicles smaller that are on average smaller than 200nm. **(B)** Immuno-electron microscopy image of purified EVs labeled with Anti-CD81 (mouse mAb) and detected by Goat anti-mouse IgG secondary conjugated with 5nm gold. **(C)** Size distribution of K562 EVs by NTA. **(D)** Bioanalyzer RNA profile (RNA Pico-chip) of K562 EVs. X-axis is nucleotides length and Y-axis is Fluorescent Units.

3.3.2. Diversity of EV RNA

Deeply sequenced RNA (RNA-Seq) data from EVs derived from a diverse group of cell types (five cancer cell lines, including K562 (chronic myelogenous leukemia), HeLa (cervical adenocarcinoma), MCF7 (breast adenocarcinoma), A549 (lung carcinoma) and U2-Os (Osteosarcoma) and four primary cell types, including BJ (skin fibroblast), HUVEC (human umbilical vein endothelial cells), HFFF (human fetal foreskin fibroblasts) and IMR90 (lung fibroblasts), allowed us to perform comprehensive bio-informatics analyses of global EV RNA diversity both specific to and common between cell types. An essential qualification for EV RNA to be considered as a viable medium of cell-cell communication is to demonstrate reproducibility under similar growth conditions, a lack thereof being indicative of an inability to disseminate meaningful information. Hence we administer the Pearson's correlation coefficient here to test reproducibility. A very strong correlation was observed between whole cell small RNA replicates, suggesting that the population of cells were in similar transcriptional states when EVs were isolated from them (Figure 3.2A). The EV RNA profiles derived from them were also very well correlated, suggesting the presence of a relatively consistent RNA appropriation process (Figure 3.2B, Table 3.1). This raises the question whether the relatively correlated distribution of EV RNA, is but a reflection of their expression profile within their source cells. However, consistent with previous studies [84, 101], we observed a very poor correlation between EVs and their source cells, suggesting only a subset of cellular RNA are being exported into EVs (Figure 3.2C).

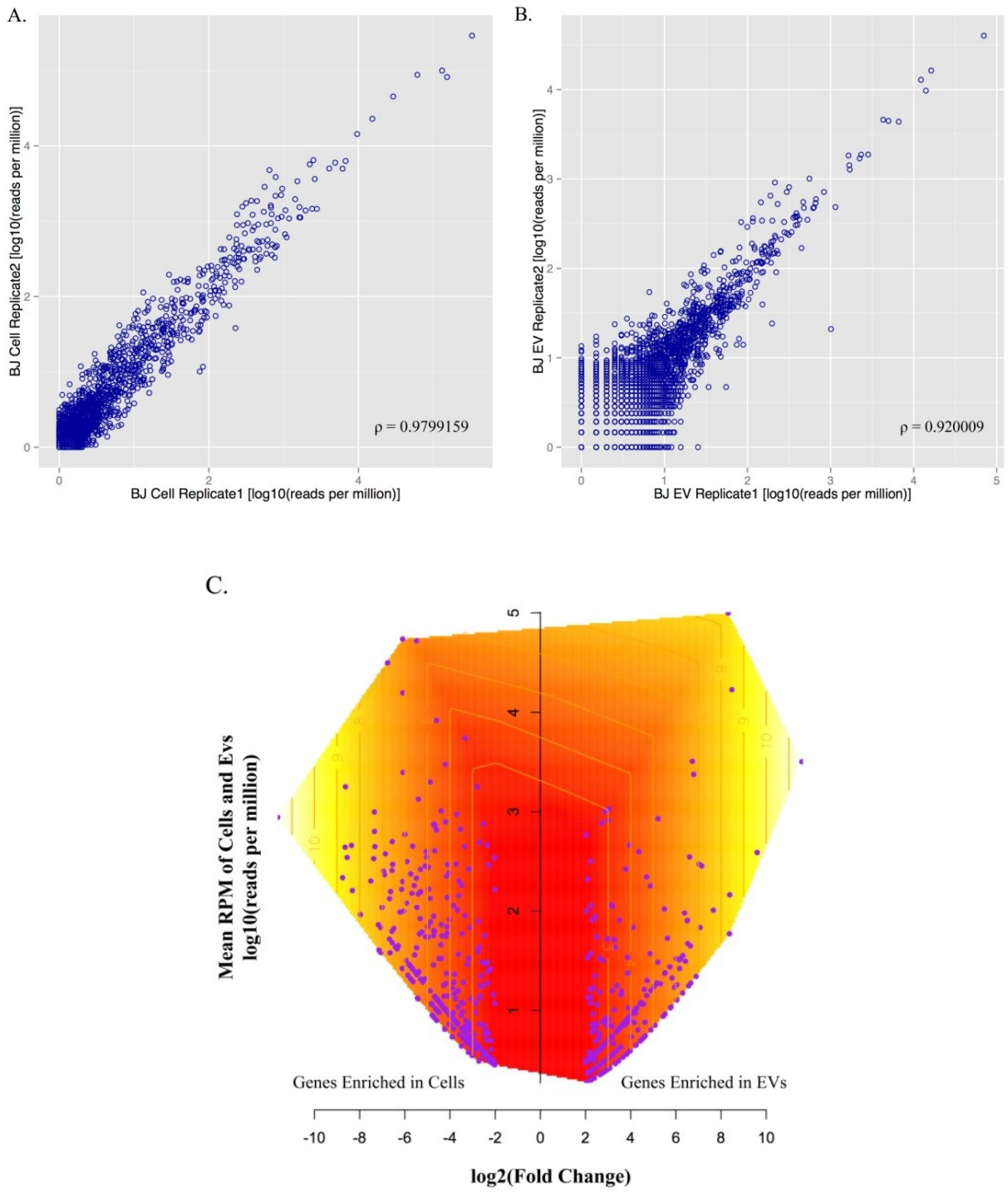

Figure 3.2: Correlation between EV and cellular RNA by RNASeq. Scatter plots representing correlation in gene expression levels between replicates of **(A)** BJ EVs and **(B)** cellular small RNA. **(C)** Volcano plot representing poor correlation in gene expression between BJ EVs and Whole cell. Each purple dot represents an annotated gene. X-axis represents fold change in expression levels between BJ EV and whole cell (log2 scale) and Y-axis represents mean levels of expression of each gene in BJ EVs and Whole cell (reads per million in log10 scale). Genes with fold change less than 2 (on log2 scale) between EVs and cell are not represented.

Short RNA Sequencing	
EV Correlation	
Cell Type	Correlation
A549	0.9797434
BJ	0.920009
HELA	0.889628
HMEC	0.9584124
HUVEC	0.9736823
IMR90	0.9918295
K562	0.9843029
MCF7	0.9473313
U2-Os	0.8670823

Table3.1 Pearson correlation coefficient between replicates of small RNA-Seq libraries from EVs derived from nine different cell types.

A detailed characterization of EV RNA from all the 9 cells types revealed that EVs are overwhelmingly populated by families of small RNA (sRNA) such as miRNA, miscellaneous RNA, tRNA, rRNA, snRNA and snoRNA. tRNA transcripts are the most diverse of all the sRNA families ranging from 202 to 346 transcripts depending on the source cell. These are followed by miscRNA (167-328 transcripts), rRNA (153-301 transcripts), snoRNA (103-188 transcripts), snRNA (38-118 transcripts) etc. In addition to these small RNA families EVs also contain fragments of longer annotated RNA families such as protein coding genes (1476 to 8775 transcripts), pseudogenes (44-751 transcripts) and long non-coding RNA (64-301 transcripts).

The relative abundance of sRNA families within EVs is demonstrated by their share of reads within the RNAseq library (Figure 3.3). Though the specific proportions of EV RNA families detected in EVs varies widely from cell to cell, we observe that miscRNA are the most abundant family across cell types with an average share of 33% of the reads, followed by rRNA

with a median of 30% of the reads, tRNA with 11 %, miRNA with 11% of the reads, and fragments of protein coding transcripts with 7%. This is however in contrast to the distribution of small RNA families seen in the whole cells, where rRNA forms the largest family with 26% followed by snoRNA with 22%, miRNA with 12% and snRNA 10%. MiscRNA (0.37 %) and tRNA (cell mean 1.74%) which are extremely abundant within EVs are significantly depleted in the cells. On the other hand, the GENCODE annotation family "Processed transcript", described as non-ORF containing RNA, and thus encompassing several possible biotypes, are significantly enriched in the cells (26%) and very rare within EVs (0.6 %). This hints at a strong likelihood of concerted sorting mechanisms responsible for the enrichment of certain EV RNA families relative to others, in a manner independent of their intracellular abundance.

Despite the diversity of sRNA families within EVs, expression level of genes within each family indicates a more homogenous picture (Figure 3.3). The top five most expressed genes within the miscRNA and rRNA families account on average for 98% of the reads originating from genes within these families. On the other hand, miRNA and tRNA families are more heterogeneous in comparison, where the top five genes accounted for only 68% and 72% of the reads originating from these respective families. Further examination revealed that some of these genes in miscRNA (RNY5, RNY1 and RN7SL2) and rRNA (RNA5-8SP6, RNA5-8SP2 and RNA5-8SP4) contributed to over 60% of the total reads in EVs in most cell types.

Since the overwhelming majority of sRNA genes (99%) within EVs have expression levels less than 100 reads per million (rpm), we define genes with expression levels above this threshold to be abundant. Interestingly, we find that there are only 9 genes that are abundantly detected across our cell types, of which two are rRNA (RNA5-8SP2 and RNA5-8SP6), two miscRNA (RNY5 and RPPH1) and five tRNA (tRNA23550, tRNA23569, tRNA23643,

tRNA23827 and tRNA7867). 23 abundant genes were common across all the primary cells, while 15 genes were common to all the cancer cell lines (Figure 3.4 A, B).

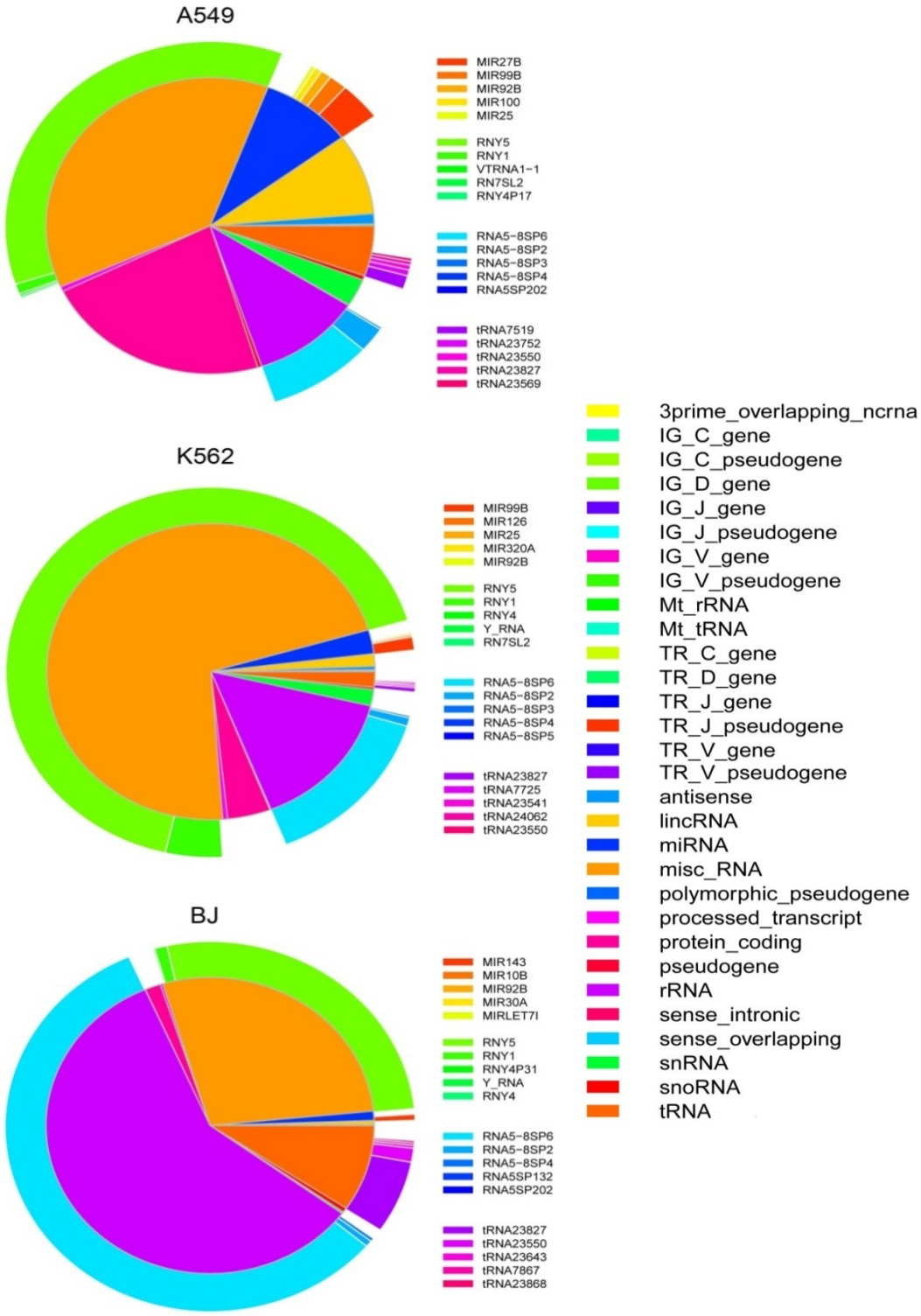

Figure 3.3 (A): Relative abundance of gene families in EVs. Pie-charts representing the distribution of various Gencode annotated gene families in EVs derived from A549, K562 and BJ cells. The inner pie-chart represents the relative abundance of gene families within EVs (by percent of reads mapped to each gene family). The outer pie-chart represents the relative abundance of the top five annotated transcripts within the respective gene families that are abundant in EVs.

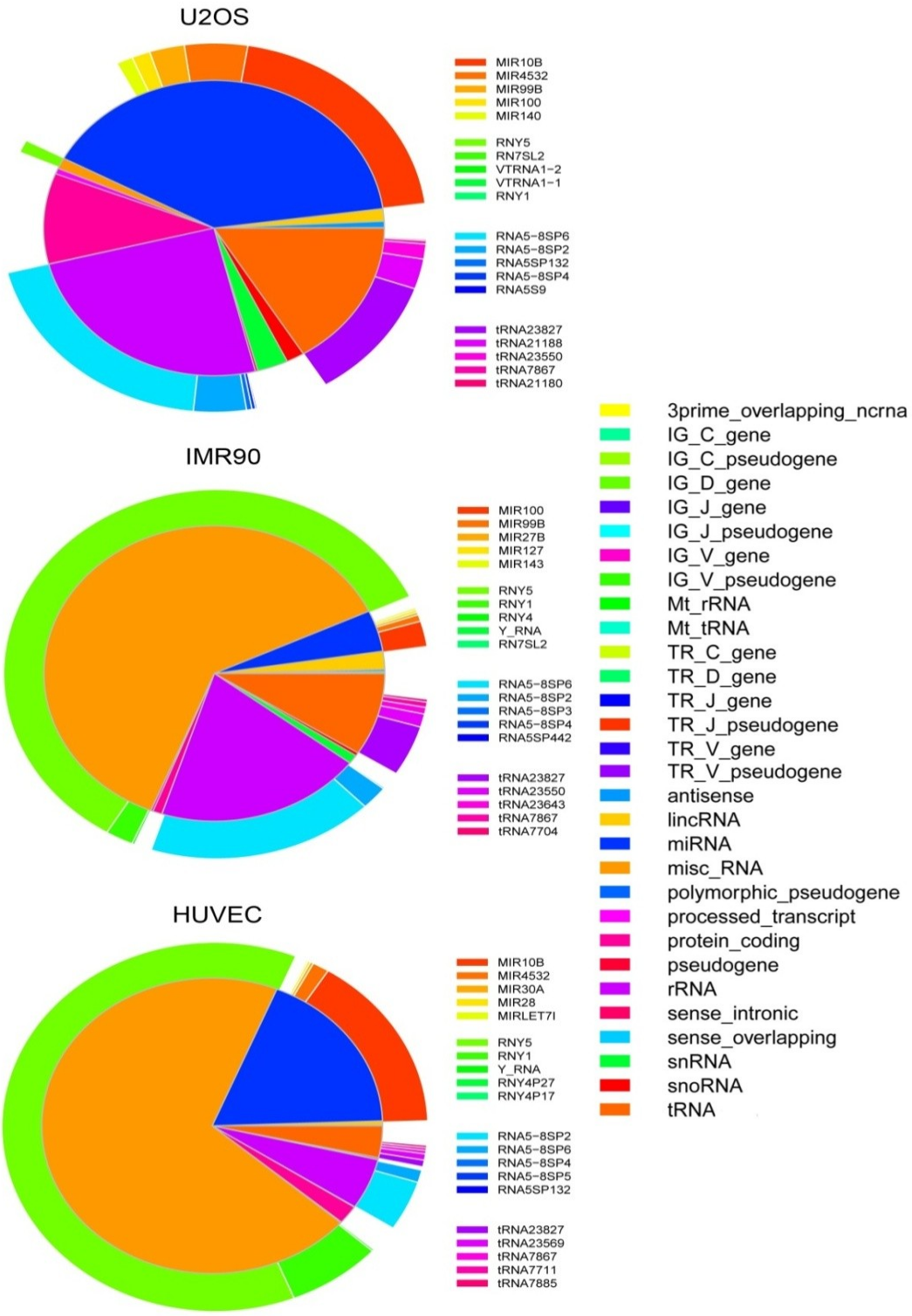

Figure 3.3 (B): Relative abundance of gene families in EVs. Pie-charts representing the distribution of various Gencode annotated gene families in EVs derived from U2-Os, IMR90 and HUVEC cells. The inner pie-chart represents the relative abundance of gene families within EVs (by percent of reads mapped to each gene family) and the outer pie-chart represents the relative abundance of the top five annotated transcripts within the respective gene families that are abundant in EVs.

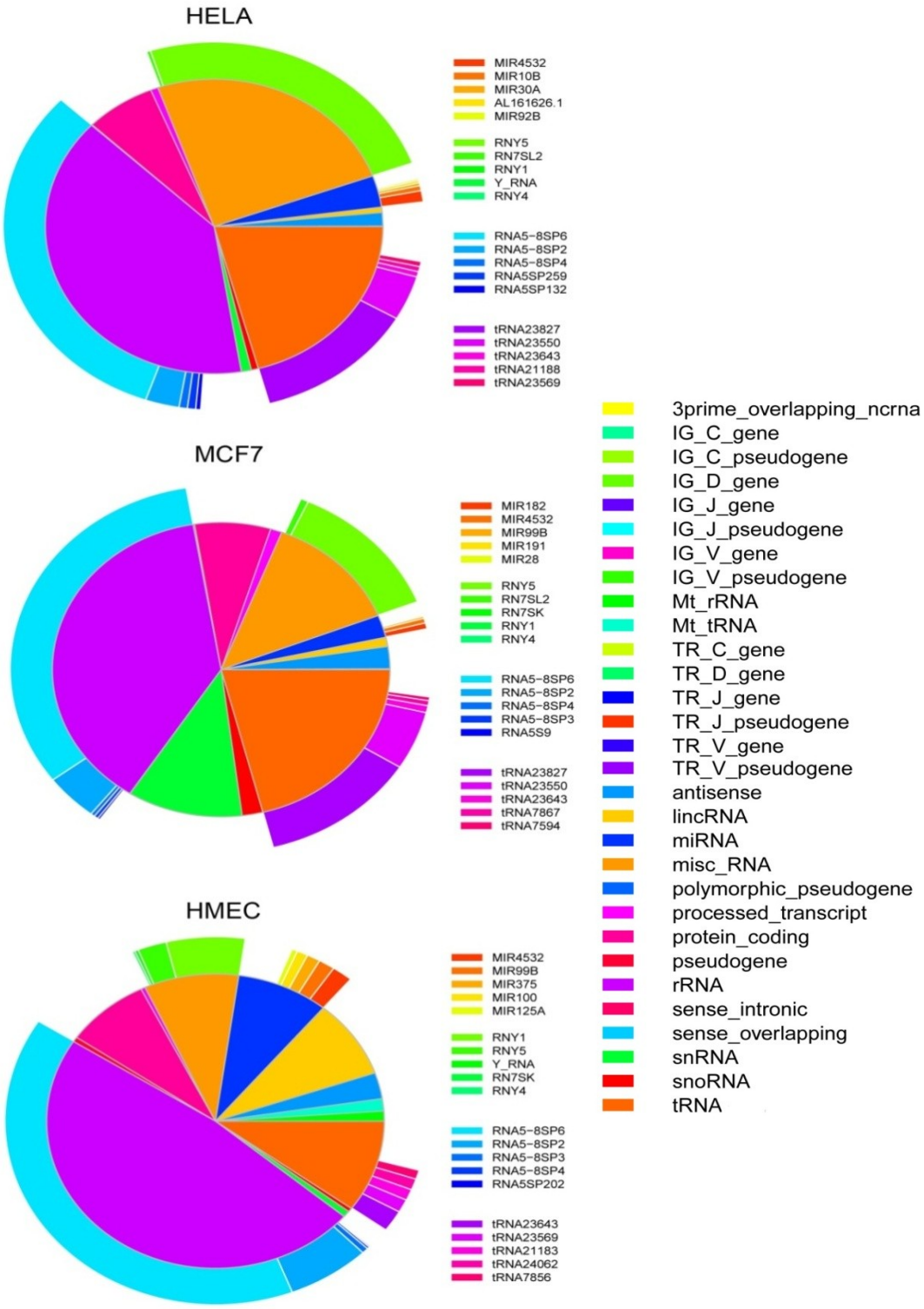

Figure 3.3 (C): Relative abundance of gene families in EVs. Pie-charts representing the distribution of various Gencode annotated gene families detected within EVs derived from HeLa, MCF7 and HeLa cells. The inner pie-chart represents the relative abundance of gene families within EVs (by percent of reads mapped to each gene family). The outer pie-chart represents the relative abundance of the top five annotated transcripts within the respective gene families that are abundant in EVs.

3.3.3. Cell type Specificity of EV RNA

Next, we determined whether the transcriptome landscape within EVs of different cell types are stochastic or are truly cell type specific. A global representation of all RNA across EVs of our nine cell types in a Heatmap with unsupervised hierarchical clustering using Euclidian distance, revealed a cell type specific RNA signature for each cell (Figure 3.4C). After adjusting for differences in library sizes using size factor estimations using the DESeq [337], we administer the negative binomial test by grouping EV RNA libraries of one cell type as a group and all the other cell types as another, and in turn obtained genes which are enriched in one cell type as compared to all the others in our study. Once we obtained the list of genes which are specifically enriched in each cell type, we obtained p-values to test significance using a one-sample t-test. The analysis showed that A549 has the largest number of genes which are uniquely enriched over 4 fold–1082 genes (p-value<0.0003315796), K562–938 genes (p-value<0.03462435), HUVEC–358 genes (p-value<0.02523887), U2OS–295 genes (p-value<0.00564851), HMEC–275 genes (p-values<0.02635909), MCF7–103 genes (p-value<0.02247853) and HELA–83 genes (p-value<0.02370253). In BJ we found 14 genes (p-value<0.03699261) which are more than 6 fold enriched compared to all the other cell lines. With IMR90, even though we found over 116 genes enriched over 4 fold, none of them were statistically significant (p-value<0.0785996), but there are 613 genes (p-value<0.001907386) which are over 4 fold enriched in all other cells but IMR90. Furthermore, this cell type specificity was not limited to low abundance transcripts, but many of the cell type specific transcripts were found to be extremely abundant (greater than 100 rpm). Among the cancer cell lines, U2-Os had 48 cell type specific genes, A549 had 41 genes, K562 26 genes, while MCF7 and HELA had 3 genes each (Figure 3.4A). HUVEC had 34 genes, HMEC 31 genes, IMR90 20

genes and BJ had 11 genes that are specifically enriched within EVs from each primary cell type in this study (Figure 3.4B).

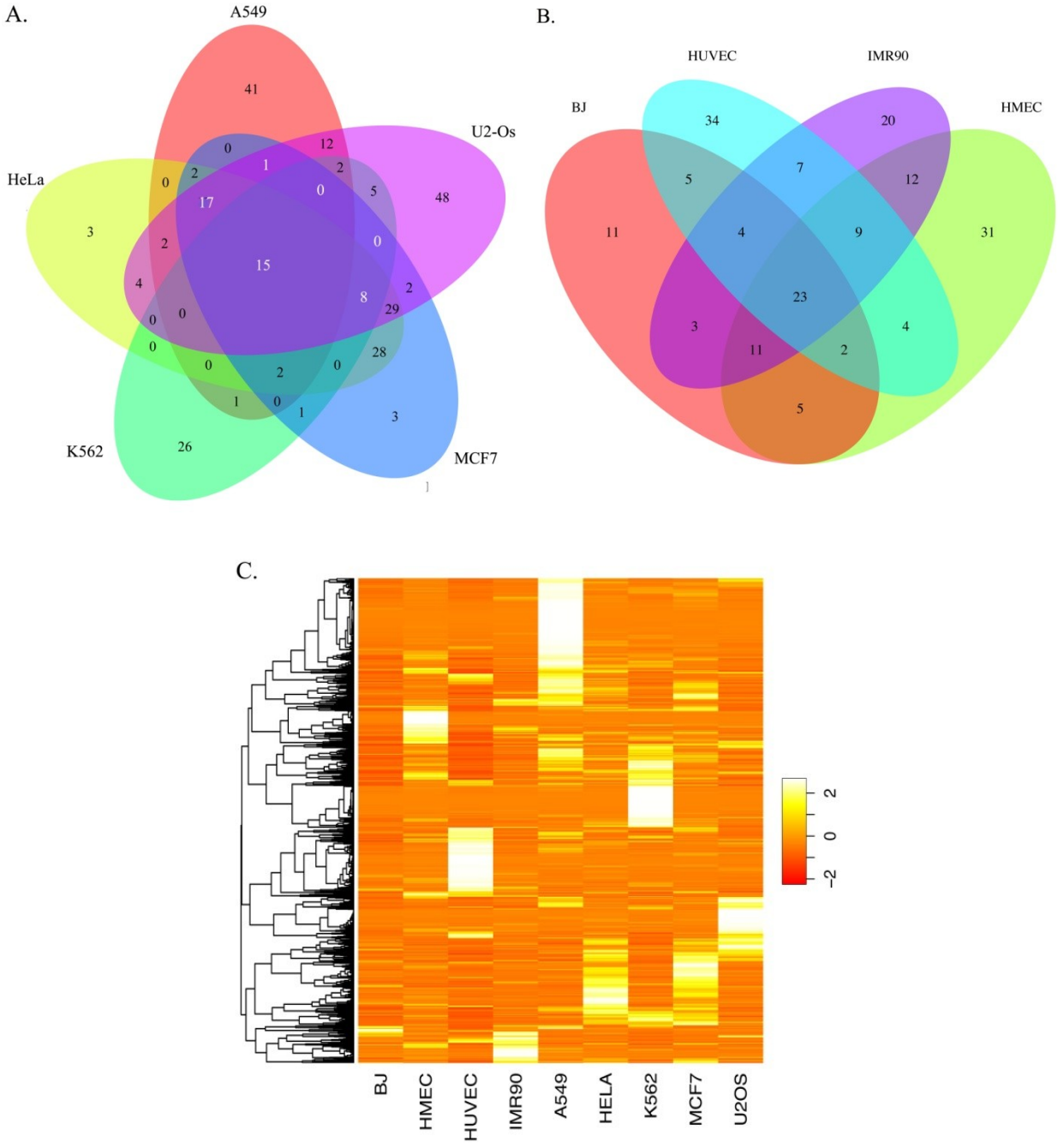

Figure 3.4: Cell type specificity of EV RNA cargo. **(A, B)** Venn diagrams representing the cell type specificity of abundant RNA transcripts (expression levels greater than 100 reads per million) in EVs derived from **(A)** 5 different cancer cell lines and **(B)** four different primary cell types. **(C)** Heatmap representation of cell type specificity of EV RNA cargo derived from nine different cell types.

3.3.4. Enrichment of specific small RNA fragments within EVs

The average fragment length observed in the EV RNA sequencing libraries from all the 9 cell types is 31.67 nucleotides, corroborating other observations that EV RNA are mainly populated by shorter RNA fragments of annotated genes [86, 94-96, 338, 339]. As there has been some speculation whether EV RNA are comprised of random fragments or functional parts of their parent RNA molecules, we examined which portions of the RNA from these genes populate EVs. Analysis of the read length distributions by gene families, suggests that fragmentation patterns is non- random and gene family specific (Figure 3.5). Over half of the reads mapping to miRNA genes are about 22 nucleotides long, both in EVs as well as in cells. Reads mapping to tRNA genes within EVs tend to be larger than miRNA reads, with about half of them being about 35 nucleotides long. In contrast, tRNA read distribution in cells tend to be considerably different, with a sizable proportion of them around ~75 nucleotides) which is not observed in EVs. Similarly a large population of rRNA (40%) are over 101 nucleotides long in cells, while in EVs reads are considerably shorter, with the majority of reads (>90%) being less than 30 nucleotides long. Reads mapping to snRNA also tend to be shorter in EVs than in cells, with about 80% of snRNA reads being less than 60 nucleotides long in EVs, while over 80% are over 100 nucleotides long in cells. However, comparable proportion of reads mapping to snoRNA in both EVs (30%) and cells (35%) tend to be over 70 nucleotides in length. EVs also contain reads that map to protein coding genes, but almost all these reads are short fragments (<30 nucleotides) of larger mRNA. These findings suggest the enrichment within EVs of RNA fragments that have a family specific length distribution.

Previous study by Chen et.al has suggested that miRNA within EVs are longer pre-miRNA [85], which could be processed in the recipient cell after transfer from the source cell,

while other studies have suggested that there might be mature miRNA within EVs [87, 88, 99]. To obtain a global perspective across all precursor miRNA genes, we analyzed reads mapping to these genes, whose lengths were normalized to 100 nucleotides. Reads mapping to 10% upstream and downstream of the gene were also included in the analysis. The probability of finding a read spanning each normalized position within a gene was used to derive the probability density across all genes within the family. This analysis on miRNA demonstrates that though there is a significant enrichment of 3' mature miRNA reads in EVs, this does not seem to be different from the distribution in source cells (Figure 3.6A). However there is a significantly lower probability of 5' mature miRNA reads in BJ EVs. Additionally, in over 97% of the cases, miRNA 22-mers detected in EVs came from the same side as found to be predominant in their source cell, further diminishing the possibility that miRNA within EVs are other than the cellular mature miRNA.

A similar fragmentation analyses on tRNA gene family within EVs provides a significantly different fragmentation profile compared to cells. Given the difference in read length distribution between tRNA reads from EVs and cells, a look at the probability density distributions in cells and EVs makes it apparent that while cells tend to have greater proportions of full length tRNAs, EVs are enriched in only 3' tRNA halves. Interestingly there is also a significant paucity of reads upstream and downstream of mature tRNA genes in EVs (previously described as tRF-5 and tRF-1 series [340]), suggesting prior processing of tRNA before sorting into EVs (Figure 3.6B).

Reads mapping to snoRNA transcripts in BJ whole cell were primarily full length reads. While majority of snoRNA transcripts within EVs are full length, a small subset of reads map to fragments of snoRNA which are almost never observed in the cells. However, a gradual 5'-

3’drop in the proportion of the reads mapping to snoRNA were observed in EVs, suggesting at least some of the snoRNA reads detected in EVs are snoRNA degradation (Figure 3.6C).

EVs are also significantly enriched with fragments of snRNA, most of which start at the 5’ end of the genes but vary in length considerably (from halves to full length transcripts), while reads mapping to snRNA in cells are overwhelmingly full length (Figure 3.6D). In contrast to the small-RNA families, fragments from protein coding genes in EV as well as in whole cell does not demonstrate enrichment of any specific gene fragment, which suggests that reads detected in EVs from protein coding genes are randomly derived fragments of protein coding transcripts (Figure 3.6E).

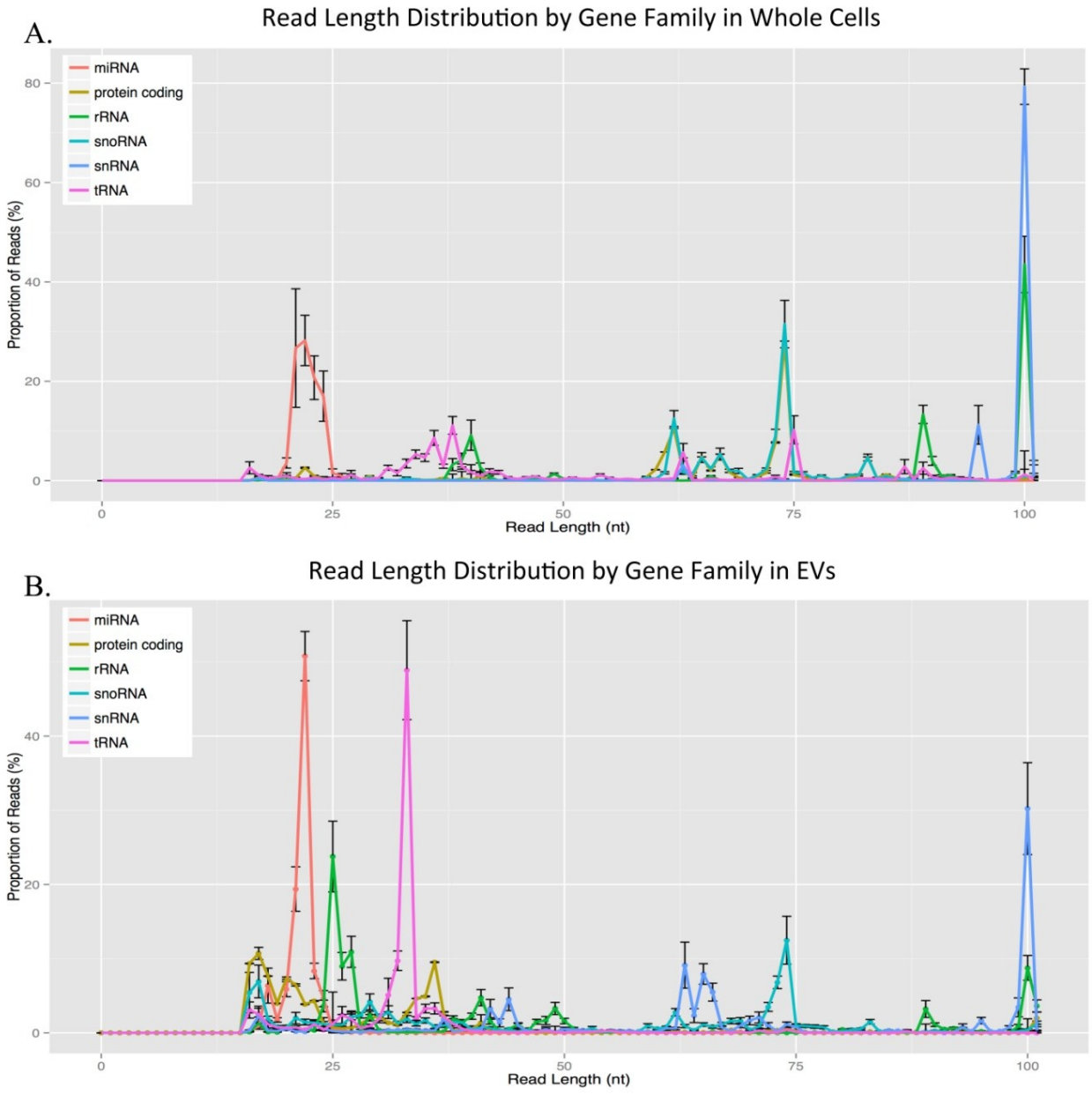

Figure 3.5: Read length distribution by gene family in BJ EVs and whole cell. Read length distribution by annotated gene families in **(A)** BJ whole cells and **(B)** BJ EV small RNA-Seq libraries. X-axis represents the nucleotide length of reads. Y-axis represents the proportion of all reads mapped to each gene family of a given nucleotide length.

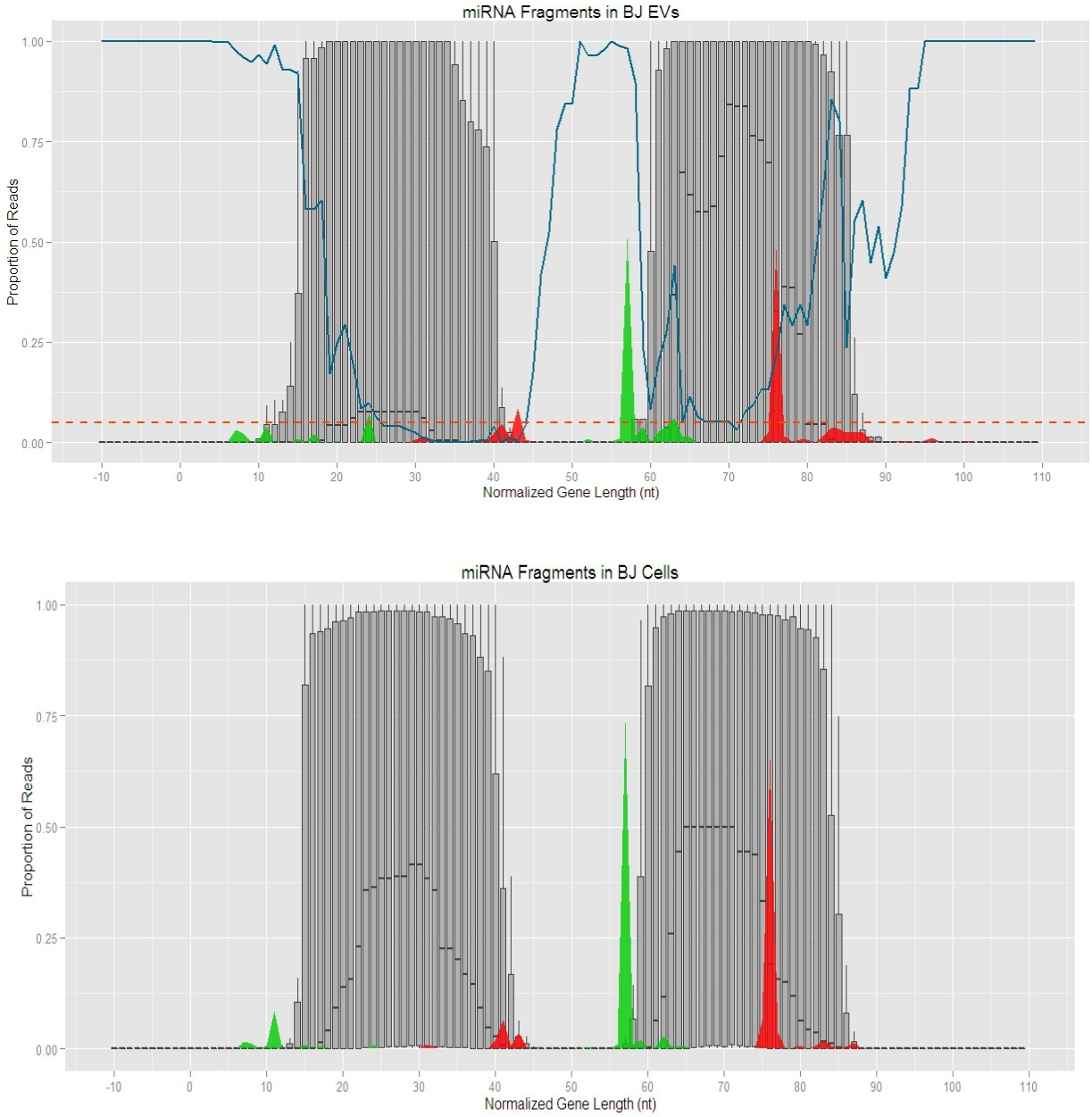

Figure 3.6(A): Gene family specific fragmentation patterns in BJ EV and cellular RNA. Box plot representation and comparison of gene family specifc RNA fragmentation patterns in EV and whole cell. Since different genes families vary in their size, all gene lengths were normalized to 100 nucleotides. Read mapping to 10% of the normalized gene length upstream or downstream of the gene are included in the analysis.Green and red peaks represent the start and stop position of all reads mapping to specific gene family respectively. The blue line represents p-value significance of difference in fragmentation patterns of RNA between EV and Whole cell at each normalized position across the gene length. The red dotted line represents the level of significance (p value<0.01). X-axis represents normalized gene length (in nucleotides). Y-axis reprsents the probability of reads at each normalized position across the gene length. **(A)** Micro-RNA fragmentation patterns in BJ EVand whole cell. MicroRNA reads map to mature microRNA region within the microRNA precuror gene in both EVs and whole cell. Probability of reads mapping to the 3' mature side of microRNA precursor are higher in EV compared to the 5' side while probability of reads mapping to either side of the mature micro-RNA are similar in whole cell.

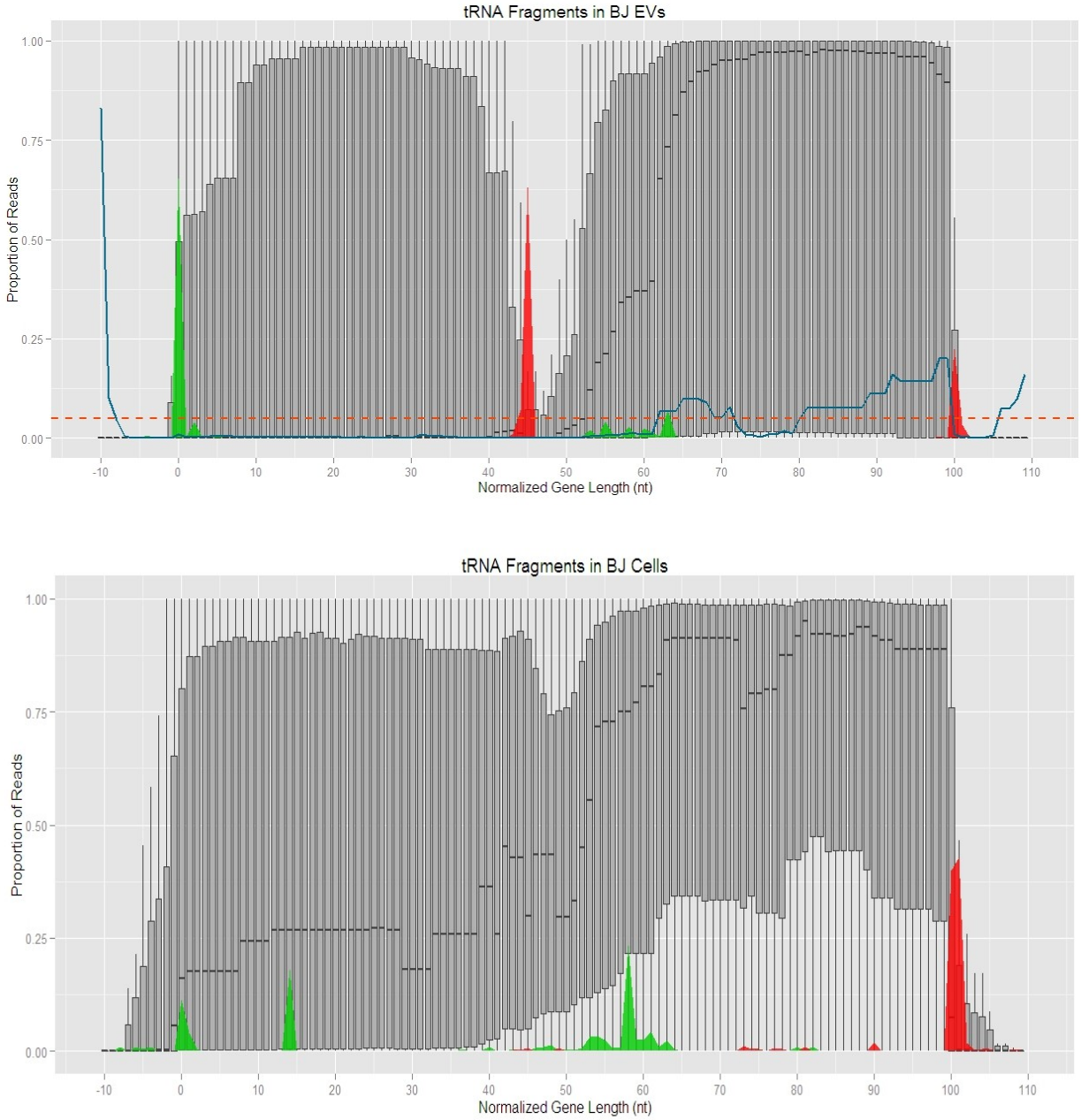

Figure 3.6 (B): tRNA fragmentation patterns in BJ EV and whole cell. Read mapping to 10% of the normalized gene length upstream or downstream of the gene are included in the analysis. Green and red peaks represent the start and stop position of all reads mapping to specific gene family respectively. The blue line represents p-value significance of difference in fragmentation patterns of RNA between EV and Whole cell at each normalized position across the gene length. The red dotted line represents the level of significance (p value<0.01). X-axis represents normalized gene length (in nucleotides). Y-axis reprsents the probability of reads at each normalized position across the gene length. In whole cell, reads mapping to tRNAs are a mixture of longer full length tRNAs and 3' tRNA halves. On the other hand, EVs are enriched with reads mapping to 3' halves of the tRNA genes. Reads mapping to the 5' half of few tRNA genes can also be detected in EV. Full length tRNA reads are depleted from EV.

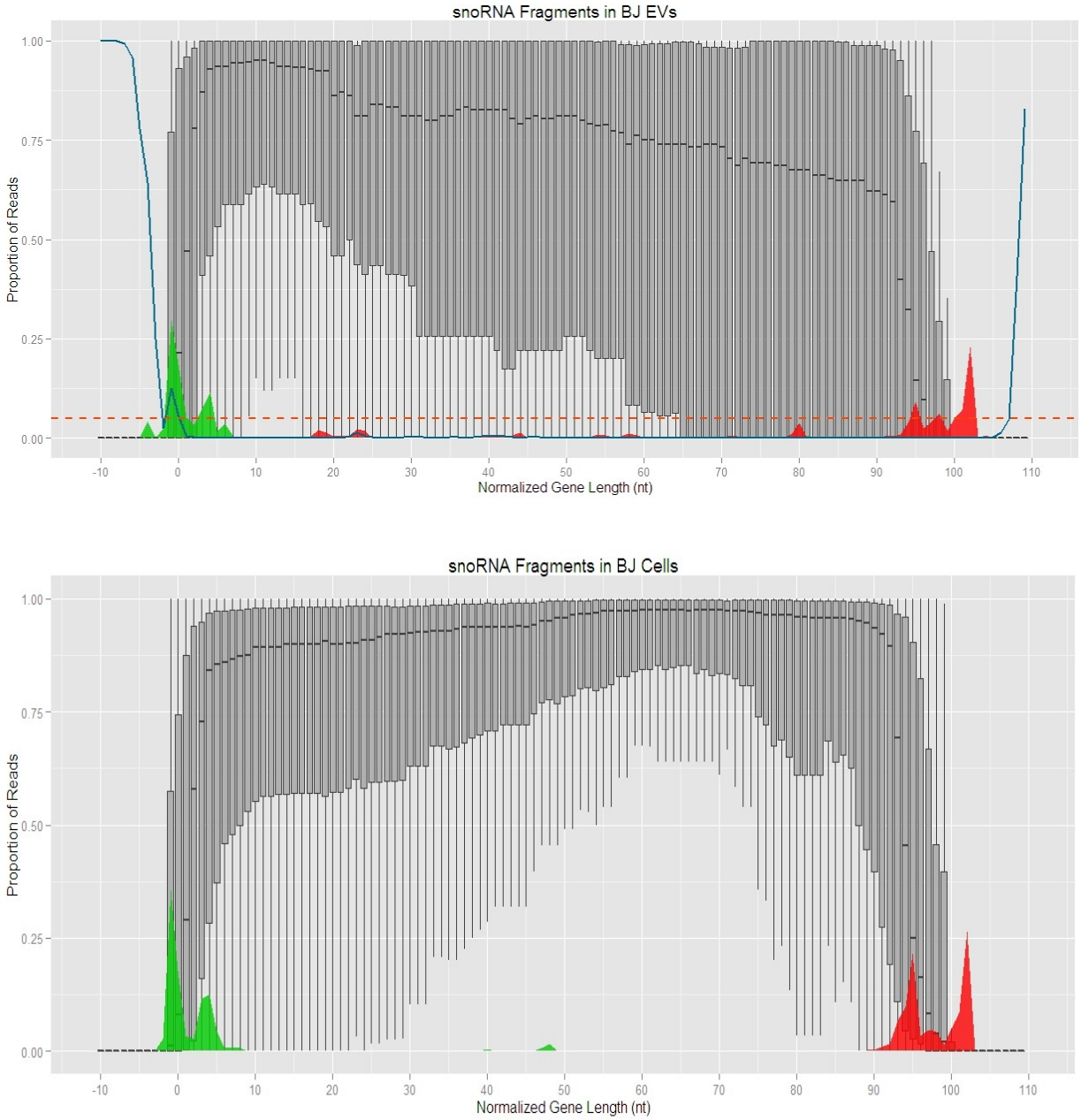

Figure 3.6 (C): snoRNA fragmentation patterns in BJ EVand whole cell. Read mapping to 10% of the normalized gene length upstream or downstream of the gene are also included in the analysis. X-axis represents normalized gene length (in nucleotides). Y-axis reprsents the probability of reads at each normalized position across the gene length. Green and red peaks represent the start and stop position of all reads mapping to specific gene family respectively. The blue line represents p-value significance of difference in fragmentation patterns of RNA between EV and Whole cell at each normalized position across the gene length. The red dotted line represents the level of significance (p value<0.01). snoRNA reads in the cell are almost always full length. Both fragmented and full length reads mapping to snoRNAs are detected in EVs, with a gradual 5' to 3' drop in proportion of mapped reads .

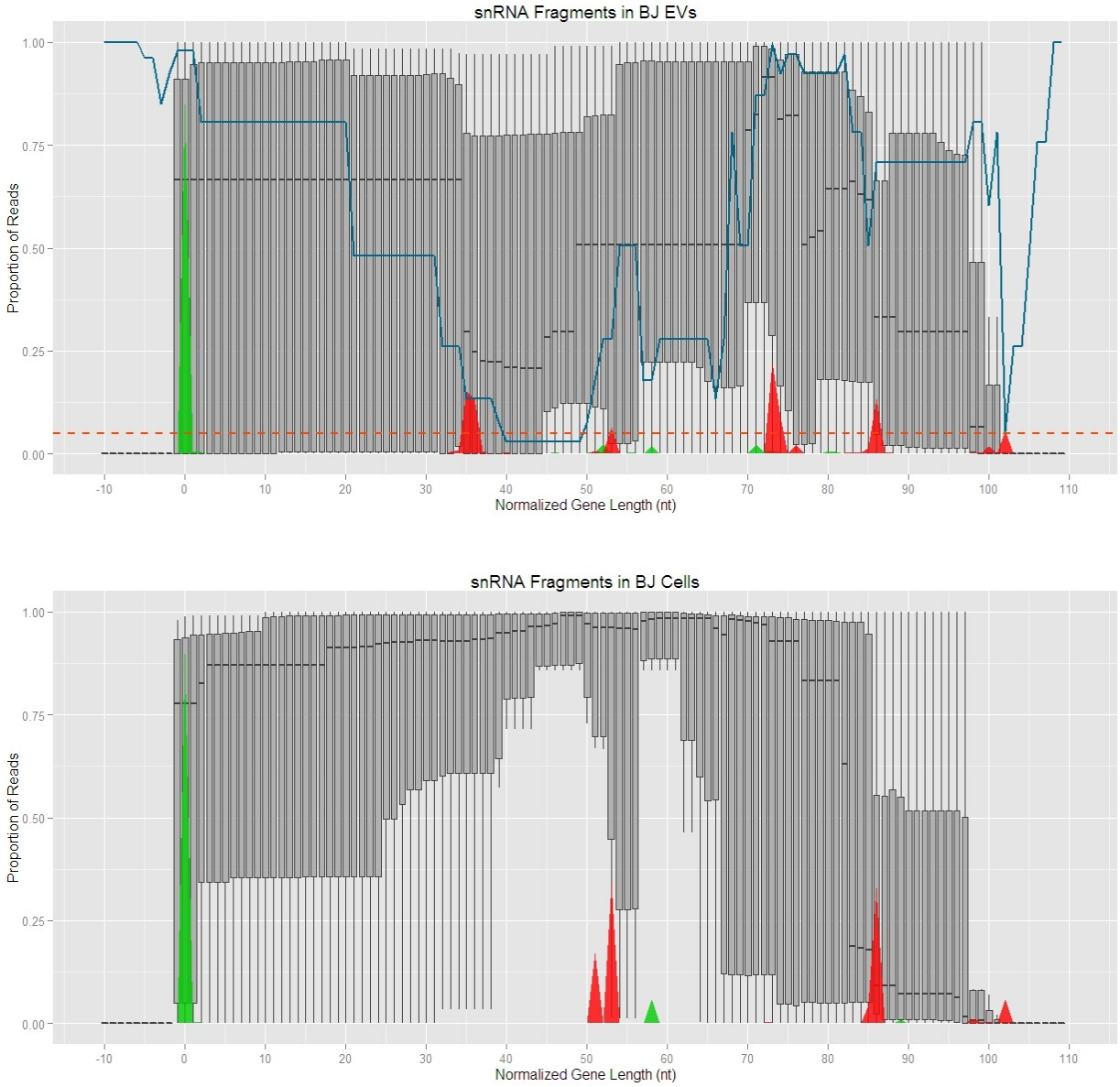

Figure 3.6 (D): snRNA fragmentation patterns in BJ EV and whole cell. Read mapping to 10% of the normalized gene length upstream or downstream of the gene are also included in the analysis. X-axis represents normalized gene length (in nucleotides). Y-axis reprsents the probability of reads at each normalized position across the gene length. Green and red peaks represent the start and stop position of all reads mapping to specific gene family respectively. The blue line represents p-value significance of difference in fragmentation patterns of RNA between EV and Whole cell at each normalized position across the gene length. The red dotted line represents the level of significance (p value<0.01).Reads mapping to snRNAs in whole cell map to either full length molecule or to the 5' half of the molecule. Although reads mapping to snRNAs start at the annotated 5' start position of the gene, most of these reads in EVs map to fragments of snRNA of varying lengths, and only a small subset of reads mapping to full length snRNA molecules.

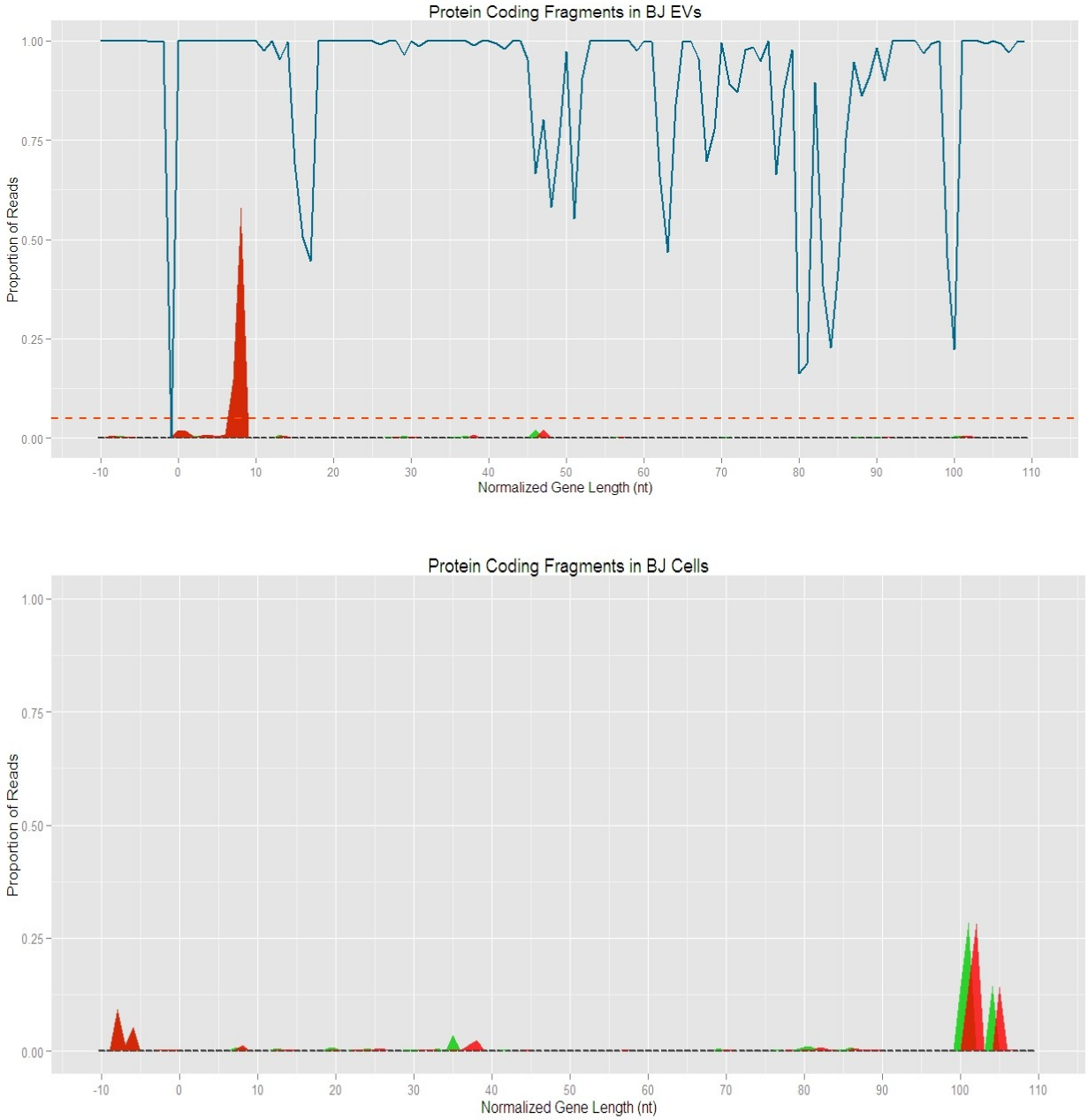

Figure 3.6 (E): Protein coding RNA fragmentation patterns in BJ EV and whole cell. Read mapping to 10% of the normalized gene length upstream or downstream of the gene are also included in the analysis. X-axis represents normalized gene length (in nucleotides). Y-axis reprsents the probability of reads at each normalized position across the gene length. Green and red peaks represent the start and stop position of all reads mapping to specific gene family respectively. The blue line represents p-value significance of difference in fragmentation patterns of RNA between EV and Whole cell at each normalized position across the gene length. The red dotted line represents the level of significance (p value<0.01).Reads mapping to protein coding genes does not show any family specific fragmentation patterns, both in EV and whole cell, suggesting that reads mapping to protein coding genes are randomly derived fragments from their parental transcripts.

3.3.5. Variability of EV RNA content

Armed with evidence of cell type specificity of EV RNA, we investigated variability of the EV RNA landscape with change in environmental conditions of source cells. Total EV RNA was sequenced from EVs of K562 cells grown under three different conditions – in presence of EV depleted fetal bovine serum, nutritionally constrained media by serum deprivation and chemotherapeutic treatment with DNA cross-linker MitomycinC (Figure 3.7A, B and C). While 76 highly abundant genes (expression levels greater than 100 rpm) were common between EVs from all three conditions, considerable numbers of genes are uniquely abundant in EVs from each of these conditions (Figure 3.7F). For example, while 102 genes were abundantly and uniquely detected in K562 EVs derived from cells cultured with EV-depleted serum, 12 genes were unique and abundant in K562 EVs derived from K562 cells cultured in serum deprived conditioned medium. 18 genes were uniquely and abundantly detected in EVs derived from MitomycinC treated K562 cells. EV RNA derived from cells grown in EV depleted serum contained 571 genes enriched (over 4 fold, p-values<1.260859e-100) and 51 genes down-regulated (over 4 fold, p-value<3.274755e-11) compared to cells from serum deprived condition (Figure 3.7D). Treatment with MitomycinC resulted in enrichment of 135 genes (p-value < 6.368023e-16) and depletion of 108 genes (p-value<2.162584e-21) in comparison to serum deprived state (Figure 3.7E). These results suggest that the EV RNA cargo is not static but continuously varies with changing environmental conditions.

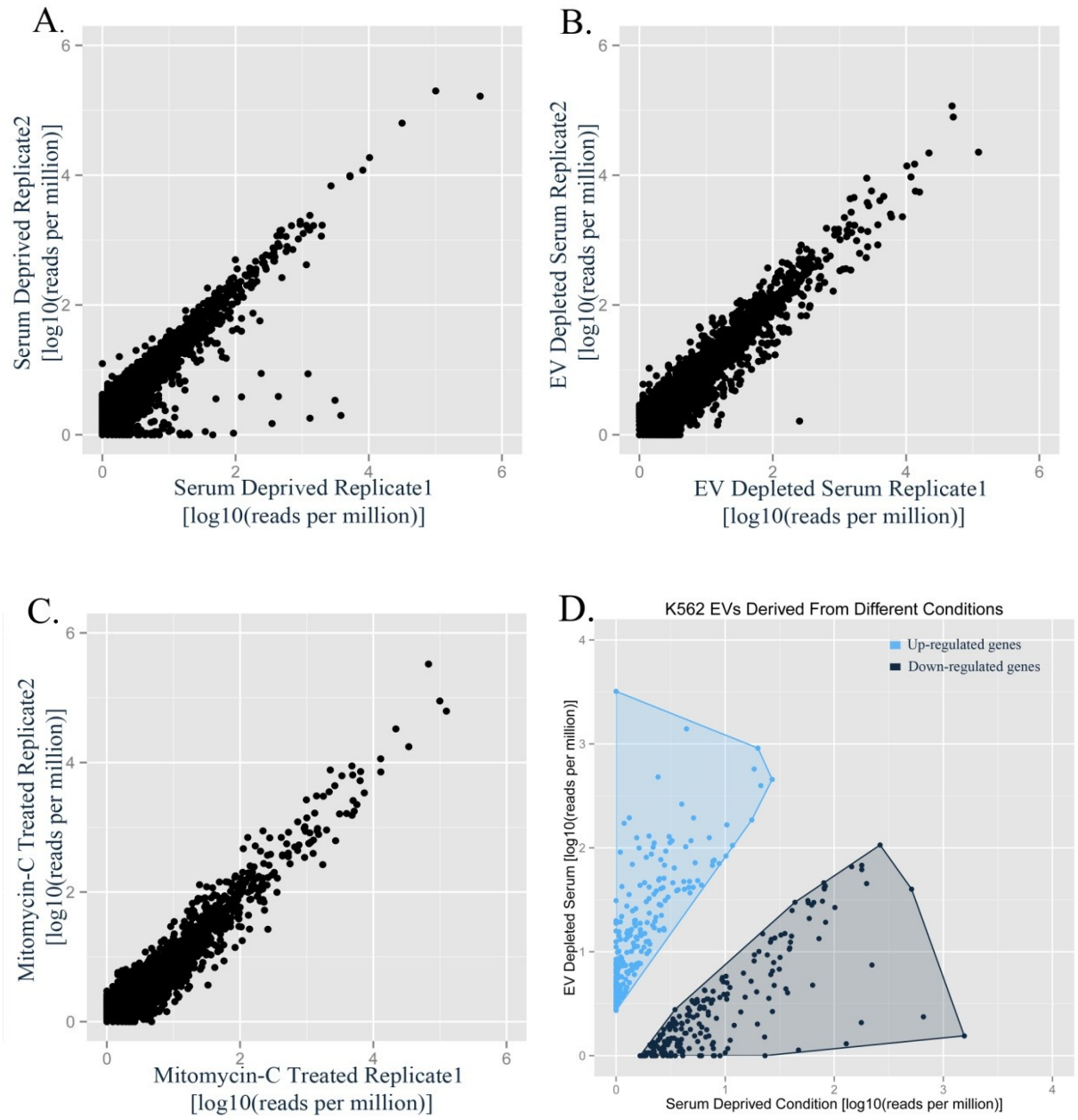

Figure 3.7: Dynamicity of EV RNA cargo. (A, B and C) Scatter plot representation of correlation of small RNA gene expression between replicates of K562 EVs isolated from different culture conditions. X and Y axis represents levels of gene expression in reads per million (log10 scale). **(A)** Correlation between replicates of K562 EV isolated from serum deprived conditioned medium, **(B)**. Correlation between replicates of EV derived from K562 cells cultured in EV-deleted serum containing medium. **(C)** Correlation between replicates of EV derived from K562 cells treated with MitomycinC in serum deprived conditioned medium. **(D)** Differential expression analysis between K562 EV derived from serum deprived conditioned medium and EV derived from K562 cells cultured in EV-deleted serum containing medium. X axis represents levels of gene expression in K562 EV from serum deprived conditioned medium (reads per million in log10 scale), while Y axis represents gene expression levels of EVs derived from K562 cells cultured in EV-deleted serum containing medium (reads per million in log10 scale). Only genes that are differentially expressed over four fold are shown in the figure.

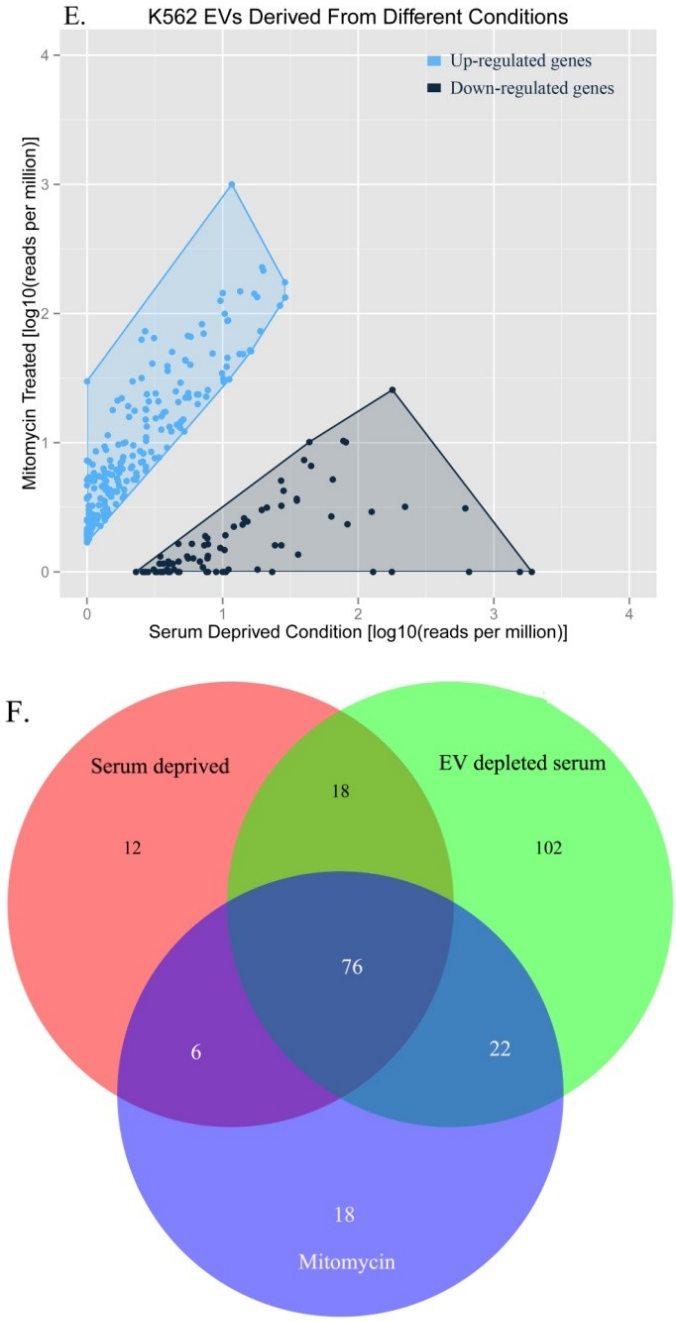

Figure 3.7: Dynamicity of EV RNA cargo. (E) Differential expression analysis between K562 EV derived from serum deprived conditioned medium and EVs derived from K562 cells treated with MitoMycinC in serum deprived medium. X axis represents levels of gene expression in K562 EV from serum deprived conditioned medium (reads per million in log10 scale), while Y axis represents gene expression levels of EV derived from K562 cells treated with MitomycinC in serum deprived medium (reads per million in log10 scale). Only genes that are differentially expressed over four fold are shown in the figure. **(F)** Venn diagram representing number of unique and shared abundant genes (genes with expression level greater than 100 rpm) detected in K562 EVs from different culture conditions.

3.3.6 Intercellular transfer of EV RNA

The functionality of the diverse repertoire of RNA packaged in EVs relies on its ability to transfer them from one cell to another in the extracellular milieu. Previous studies have demonstrated transfer of EVs from one cell type to another, primarily through labeling lipid and protein components of EVs [ref], Here we extend these studies by demonstrating intra and inter-species transfer of EVs and EV RNA cargo, as well as report its subsequent subcellular localization in the recipient cell. To begin with, K562 EVs, labeled with lipid dye PKH67 were added to K562, HeLa and BJ cells which confirmed transfer of EVs in each of the three cells (Figure 3.8A). Transfer of K562 EVs, with its RNA cargo labeled with Sytoselect RNA green dye to HeLa cells confirmed the actual transfer of the RNA cargo within the vesicles to another cell (Figure 3.8B). The subcellular localization of EVs and EV RNA were found to be exclusively cytoplasmic (Figure 3.8B). Co-labeling of subcellular organelles such as mitochondria, lysosomes and endoplasmic reticulum did not point to any preferential co-localization with any of the labelled structures (Figure 3.8C, D and E). The integrity of the transferred RNA and dynamics of EV RNA transfer was studied by tracking the level of human specific transcript RNY5 by RNAseq in mouse HB4 cells, both by direct incubation of GM12878 EVs with HB4 cells and transwell co-culture of GM12878 and HB4 cells, for 24 hours and 48 hours (Figure 3.8F). These results underscore the lack of selectivity displayed by cells in transfer and uptake of EVs *in-vitro*.

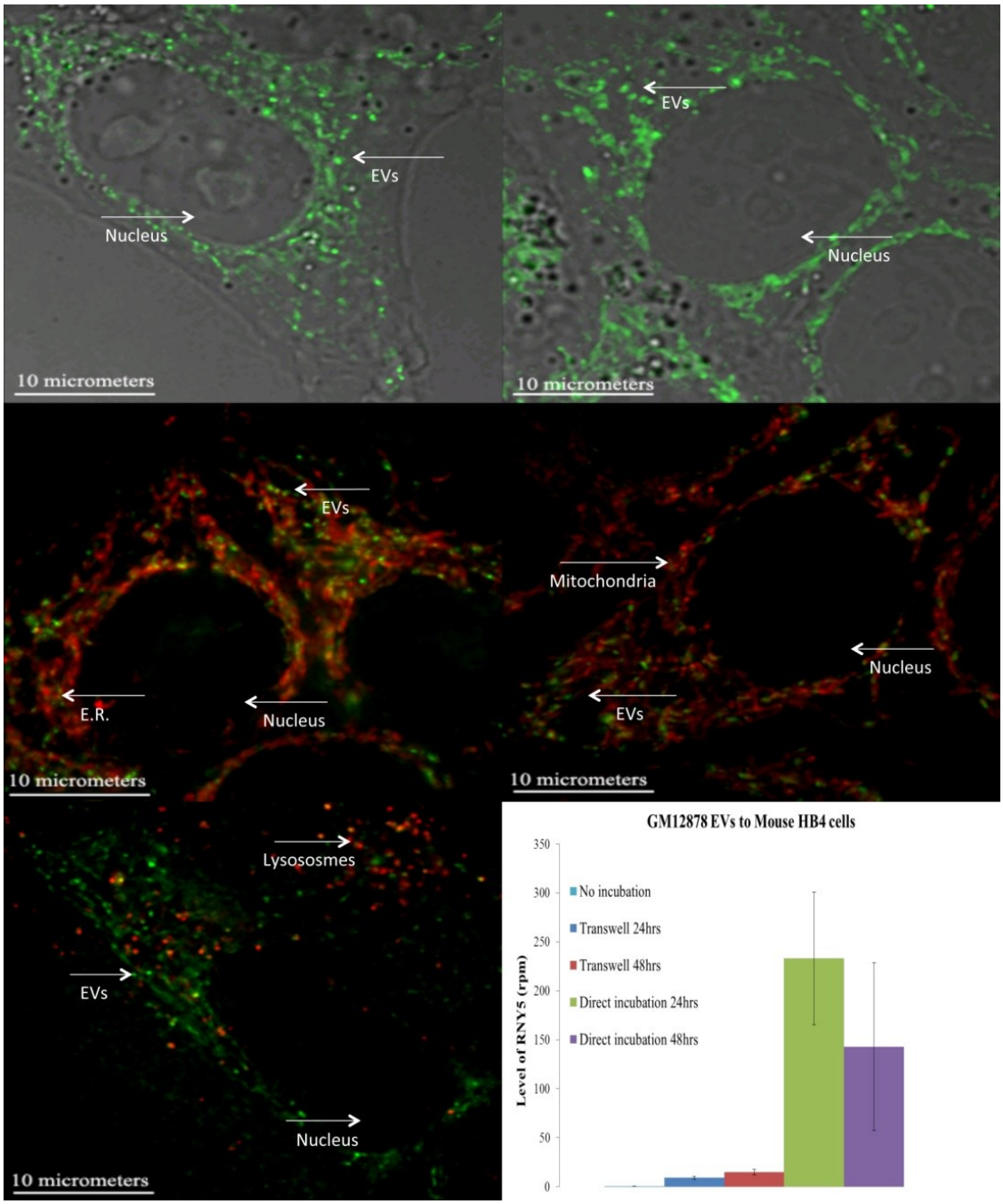

Figure 3.8: Intercellular transfer and subcellular localization of EV and EV RNA. (A) Transfer and subcellular localization of K562 EVs labeled with lipid dye PKH67 (green) in HeLa cells. **(B)** Transfer and subcellular localization of Syto RNAselect Green labeled K562 EV RNA in HeLa cells. **(C)** Subcellular localization of Syto RNAselect Green labeled K562 EV (Green) in recipient HeLa cells with its Endoplasmic reticulum (Red) co-labeled with ER-Tracker Red. **(D)** Subcellular localization of Syto RNAselect Green labeled K562 EVs (Green) in recipient HeLa cells with its Mitochondria (Red) co-labeled with Mito-Tracker Red. **(E)** Subcellular localization of Syto RNAselect Green labeled K562 EV (Green) in recipient HeLa cells with its Lysosomes (Red) co-labeled with Lyso-Tracker Red. **(F)** Inter-species transfer of EV RNA by RNASeq. Time course analysis of the level of human specific *RNY5* 31-mer RNA in mouse HB4 cells when mouse HB4 cells are incubated with human GM12878 EVs or co-cultured across Transwell membrane with GM12878 cells for 24 and 48hrs. Y-axis indicates the level of RNY5 (in reads per million) in mouse HB4 cells.

3.3.7 EV mediated transcriptional response in recipient cells

Correlated response between EVs and EV RNA treatment

EVs derived from K562 cells grown in serum deprived state were added to BJ cells and, their long RNA sequenced 2 and 24 hours post-treatment to capture both acute and delayed variations in the RNA landscape of these cells (Figure 3.9A, B). A look at the differentially expressed protein coding genes when compared to untreated controls at 2 hours after treatment, demonstrated 205 genes upregulated and 438 genes down-regulated (over four fold), while 24 hours after treatment, 47 genes were upregulated over 4 fold and 60 genes were down-regulated. This result suggests a relatively acute onset of transcriptional changes in the recipient cells after treatment with EVs, and the persistence of significant altered transcriptional state changes even 24 hours post treatment.

In order to demonstrate that at least some of the transcriptional response by BJ cells after EV treatment is attributable to the EV RNA cargo, the above experiment was replicated with EV RNA isolated from K562 EVs and transfected onto BJ cells. Long RNA sequenced 24 hours post treatment, revealed a very good correlation (Pearson's correlation coefficient = 0.934) between the transcriptional landscape of BJ cells treated with both EVs and EV RNA (Figure 3.9C). However, despite these seemingly similar responses to both EVs and EV RNA, we also observed that of the 237 protein coding genes that were differentially expressed after EVs treatment, as many as 213 protein coding genes behave differently between the two treatments, underscoring that the response induced by the EVs are not just a result of EV RNA but rather a complex synergistic effect induced by the RNA and protein cargo together within EVs.

Cell type specific response to EVs

Given the lack of specificity with which EVs from one cell are transferred to other cells *in-vitro*, we studied the transcriptional changes after EVs treatment in two different cell types to investigate if a similar response occurred irrespective of recipient cell type. BJ and HUVEC cells were treated with K562 EVs for 24 hours, and long RNA from each cell and their untreated controls were sequenced in replicates (Figure 3.9D). In BJ cells 47 protein coding genes were upregulated and 60 genes were down-regulated (four fold threshold), while in HUVEC cells 25 genes were upregulated and no genes were significantly down-regulated (Figure 3.9F). Interestingly, no overlap was detected among differentially expressed genes in the two cell types at this time point. This suggests a differential molecular response by BJ and HUVEC cells even though they were treated by EVs from the same source cells.

Differential response with variability of EVs

Owing to the dynamicity in the EV RNA cargo, we investigated if this changed cargo is capable of inducing a differential response. Upon treatment of BJ cells with EVs derived from MitomycinC treated K562 cells, long RNA was sequenced at 24 hours post treatment. It was observed that over 254 protein coding genes behaved differently when compared to treatment with EVs derived from serum deprived K562 cells, of which 149 genes were upregulated and 105 genes were down-regulated over 4 fold (Figure 3.9E).

Long RNA Sequencing	
Replicates Correlation	
Cell Type	Correlation
BJ cells Untreated	0.9730287
BJ cells treated with K562 EV 2hrs	0.9975198
BJ cells treated with K562 EV for 24hrs	0.9975976
BJ cells treated with K562 EV RNA	0.9984934
BJ cells treated with K562 EVs (MitomycinC treated) 24hrs	0.9992484
HUVEC cells Untreated	0.9350982
HUVEC cells treated with K562 EV 24hrs	0.8989747

Table3.2 Pearson correlation coefficient between replicates of long RNASeq libraries of BJ and HUVEC cells with various treatments.

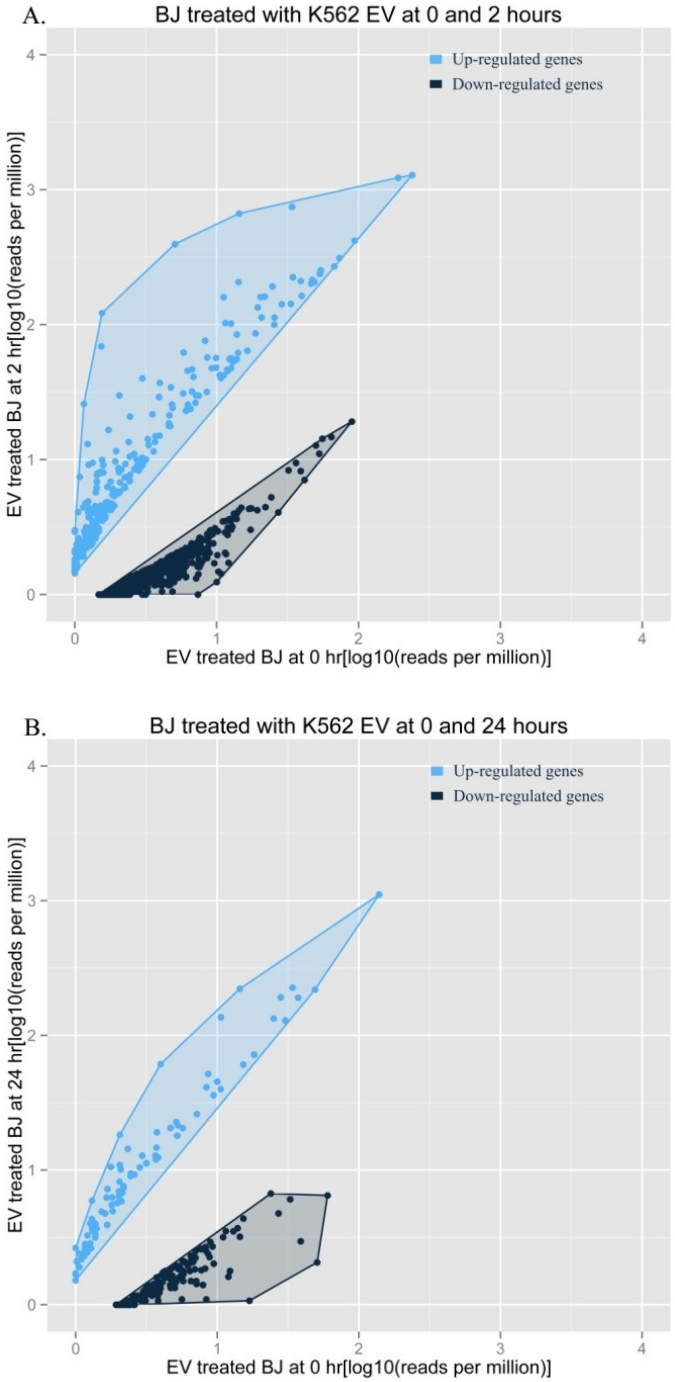

Figure 3.9: Differential and cell type specific molecular response in recipient cells by K562 EV and EV RNA. (A, B) Differential molecular response by BJ cells when treated with K562 EV for **(A)** 2hrs and **(B)** 24hrs compared with 0 hours control. Only genes that are over four fold differentially expressed are shown in the figure. The axis represents gene expression levels of BJ cells with different treatments (reads per milion in log10 scale).

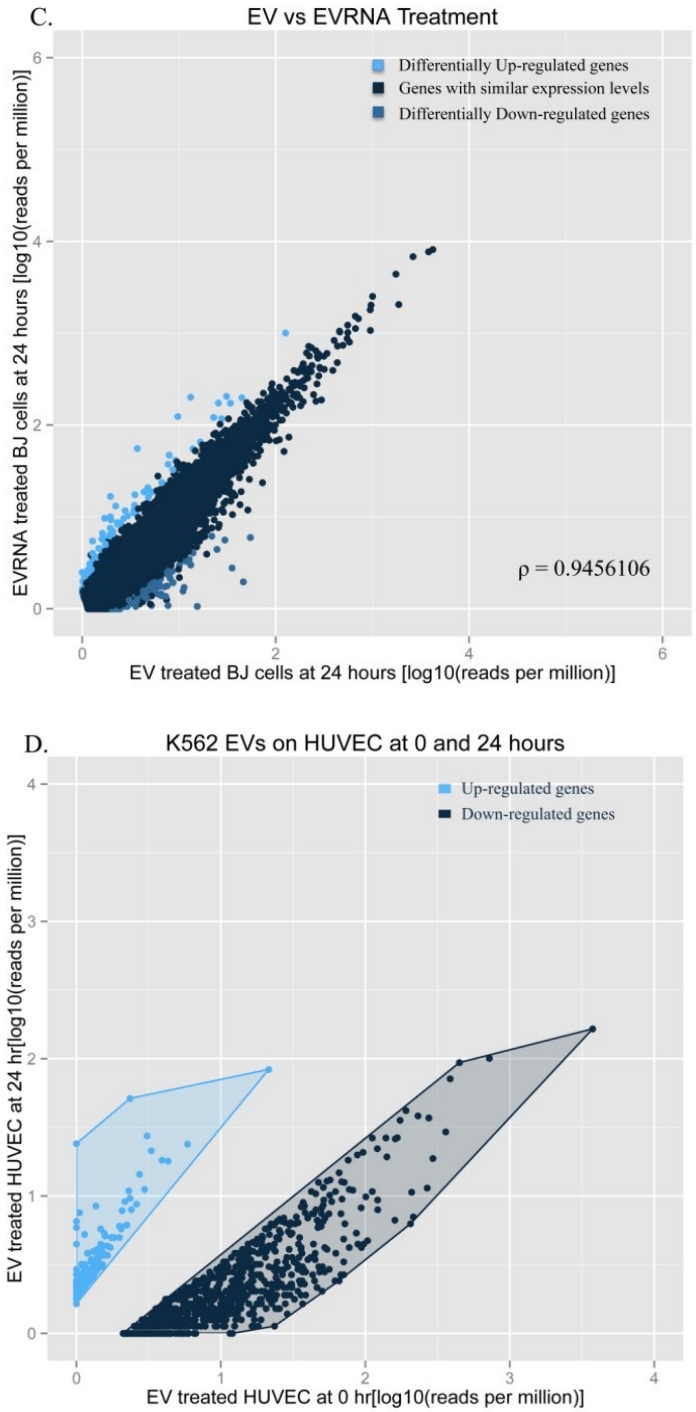

Figure 3.9: Dynamic and cell type specific molecular response in recipient cells by K562 EV and EV RNA. (C) Correlation in molecular response by BJ cells when treated with K562 EVs and K562 EV total RNA for 24hrs. Pearson correlation coefficient between EV and EV RNA treatments was estimated as 0.94. X and Y axis represents gene expression levels in BJ cells with 24hr K562 EV and K562 EV RNA treatment (rpm in log10 scale), respectively. **(D)** Differential molecular response by HUVEC cells when treated with K562 EVs for 24hrs compared with 0 hours control. X and Y axis represents gene expression levels in HUVEC cells with 0hr K562 EV treatment and 24hrs K562 EV treatment (rpm in log10 scale), respectively.

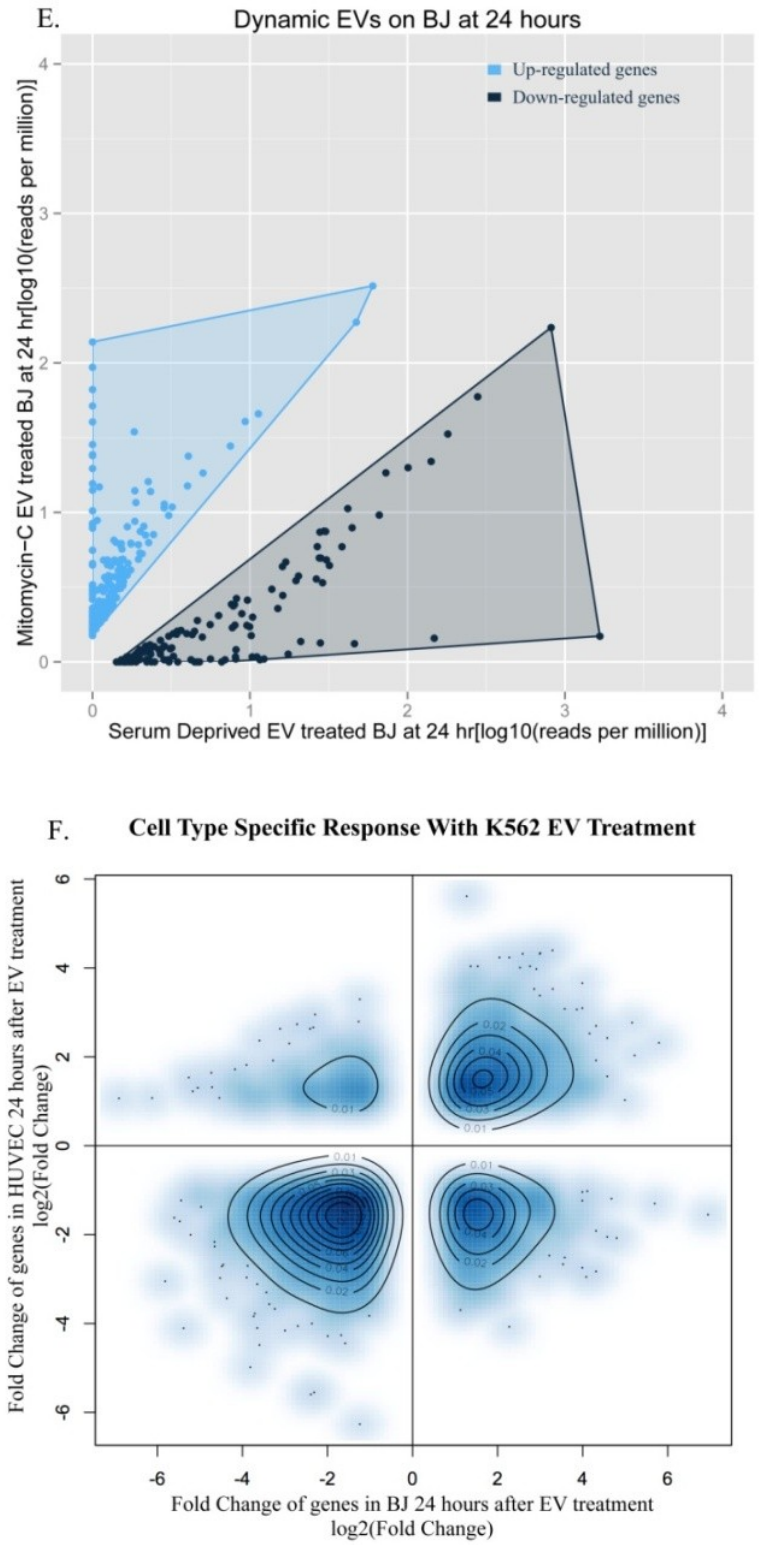

Figure 3.9: Dynamic and cell type specific molecular response in recipient cells by K562 EV and EV RNA. (E) Dynamic molecular response in BJ cells when treated with K562 EVs from serum deprived conditioned medium and K562 EVs derived from MitomycinC treated K562 cells for 24hrs. X-axis

represents gene expression levels in BJ cells when treated with serum deprived K562 EVs (rpm in log10 scale) while Y-axis represents gene expression levels in BJ cells when treated with MitomycinC treated K562 EVs (rpm in log10 scale). Black dots represents genes downregulated by more than four fold while blue dots represents genes upregulated by more than four fold. Genes that are not differentially expressed by four fold are not shown. **(F)** Cell type specific molecular response by K562 EVs in BJ and HUVEC cells. Contour plot representation of the density of genes that are differentially expressed (more than two fold) in BJ and HUVEC cells when treated with K562 EVs for 24hrs. X-axis represents fold change of genes in BJ cells with 24hrs K562 EV treatment (log2 scale) and Y-axis represents fold change of genes in HUVEC cells with 24hrs K562 EV treatment. 1st and 3rd quadrant represents genes which are similarly differentially expressed between the two cell types, while 2nd and 4th quadrant represents genes that differentially expressed in a cell type specific manner by the same K562 EV treatment.

3.4 Discussion

In this study, we present evidence which support EV mediated transfer of RNA between cells indeed represents a novel mode of intercellular communication. A comprehensive characterization of the nature and diversity of RNA messages packaged in EVs by at least 9 different cell types revealed a non-random and specific sorting of the messages into EVs by cells. Moreover, the message sorted into EVs was found to be highly cell type specific. We further establish that the sorting of RNA messages into EVs is a dynamic process which broadly reflects the physiological state of the cell. While others have demonstrated the transfer of EVs between cells, we demonstrate the transfer of the RNA molecules by EVs as well as their subcellular localization in the recipient cells. Most importantly, we establish that the transferred RNA molecules are intact, functional and able to elicit a system-wide transcriptional response in recipient cells. We further establish the molecular response by recipient cells to the incoming message is dynamic and varies with change in the composition of EVs. Finally, we reveal the complexity of such a mode of communication by demonstrating that the same EV RNA message may elicit distinct molecular response in different recipient cells, depending on the signal interpretation machinery enabled by the transcriptional and translational landscape of that cell. Thus, our study demonstrates the involvement of the total EV RNA cargo in EV functionality and forces us to investigate further the potential involvement of the individual members of the RNA cargo of EVs in inducing a response. Taken together, these results highlight a novel and underappreciated mode of gene regulation in multicellular organisms.

The unique fragmentation patterns of each class of small non-coding transcripts and their enrichment in EVs, points towards specific processing and sorting mechanisms in the cell that are not well understood. Interestingly, tRNA fragments have been previously observed in body

fluids [96, 339] as well and have been implicated in translation repression and regulation of cell death [341-343]. This raises an interesting possibility that these processed fragments from non-coding RNAs may represent a novel class of short RNAs with as-yet-undiscovered functions. The enrichment of such transcripts makes EV a valuable source to explore their potential functional role in intercellular communication.

The beauty of EV lies in their ability to enclose multiple RNA messages within one packet and deliver them to recipient cells. It is tempting to speculate that during the course of evolution, increased complexity of living organisms necessitated the need to transmit multiple messages (such as replicative, transcriptional or translational status, nutritional or other environmental stress signals, etc.) at the same time to neighboring cells. Instead of evolving distinct regulatory mechanisms for each and every signaling molecule, life may have evolved a common medium/platform of communication in the form of lipid vesicles, which could provide exceptional stability and protection from harsh extracellular environment and robustly and faithfully enclose and deliver multiple messages to intended recipients. Interestingly, the most abundant class of transcripts detected in EVs is Y-RNAs, a class of short non-coding transcripts that has been implicated in DNA replication and has been termed as “replication licensing factors” [344-347]. It is tempting to speculate that Y RNAs in EVs may play the role of a quorum sensing molecule (similar to bacterial quorum sensing systems) and regulate DNA replication in neighboring cells in mammalian systems.

3.5. Material and Methods

Cell culture and isolation of EV

Cells were grown in their respective complete medium until they reached 70-80% confluence when the medium was replaced with serum-free conditioned medium and incubated for another 24 hours. The Conditioned medium was centrifuged at 300g for 10 minutes and the cell pellet was discarded and the supernatant was further centrifuged at 2000g for 10 minutes. The Pellet, comprising of mostly cell debris was discarded and the supernatant was again centrifuged at 10000g for 30 minutes. The pellet was discarded and the supernatant was filtered at 3500g for 15 minutes using Centricon Plus70 100KDa NMWL membrane (Millipore). The filtrate was discarded and the residue, enriched with EVs and other proteins was collected. The collected residues were precipitated overnight using ExoQuick-TC (System Biosciences) and the EVs were recovered next day by low speed centrifugation and suspended in 500microliter PBS.

Electron microscopy of EV

Aliquots of EVs suspensions were dispensed on parafilm on a petri dish and Butvar coated EM grids were adsorbed on them for 5 minutes at room temperature and kept on ice. The grids were transferred to drops of distilled water thrice for 30 seconds each to wash off excessive salts. The grids were then transferred to a drop of 1% uranyl acetate in 1% methyl cellulose for 30 seconds followed by another transfer to a second drop for 5 minutes. The grids were air dried and excess stain was blotted off. Imaging was performed using Hitachi H7000 electron microscope at 75kV.

Nanoparticle Tracking Analysis of EVs

Quantification of the extracellular vesicles was performed by Nanoparticle Tracking Analysis (NTA) using NanoSight LM10 at 25 degrees Celsius. PBS was used as a diluent.

RNA isolation and small RNA sequencing

EVs were treated with Ambion RNase cocktail at 37 degrees Celsius for 15 minutes. RNA isolation was performed immediately using Ambion's Mirvana miRNA Isolation kit using manufacturer's protocol. The purified RNA samples were first treated with Tobacco acid pyro phosphatase (TAP) for 1 hour at 37deg and DNase treated with Ambion Turbo-DNase (Life Tech). Ribosomal RNA depletion was performed on Whole cell RNA using Eukaryote Ribominus kit (Life Tech) using manufacturer's protocol. Libraries were constructed using Illumina TruSeq small RNA kit according to manufacturer's protocol, except reverse transcription was performed using Superscript III. Amplified libraries were run on 2% agarose gel and 20-200nts region was cut and gel-purified with Qiagen gel extraction kit. Libraries were quantified on Agilent Bio-analyzer HS-DNA chip and sequenced on Illumina HiSeq2000.

Long RNA Sequencing

Long RNA was isolated with Mirvana miRNA isolation kit and DNase treated with Ambion Turbo-DNase using manufacturer's protocol. Construction of complementary-DNA libraries was performed using Illumina TruSeq stranded total RNA kit (cat. no.RS-122-2201). Libraries were quantified using Agilent Bioanalyzer HS-DNA chip and run on Illumina Hi-Seq 2000 or NextSeq 500 platform.

Mapping & analysis

All data from RNA sequencing experiments in the study were mapped to Human Genome version 19 (hg19, GRCh37) obtained from the UCSC genome browser website (http://hgdownload.cse.ucsc.edu/downloads.html). RNAseq reads were aligned using the STAR v1.9 [318] software, and up to 5 mismatches per alignment were allowed. Only alignments for reads mapping to 10 or fewer loci were reported. Annotations were not utilized for mapping the data. The obtained BAM files were further processed using HTSeq software [319] in order to appropriate the number of reads originating from each annotated regions of the genome, utilizing annotations obtained from Gencode v19 [320] of the human genome, using the "Union mode" option of the software for all libraries, tRNA annotations were obtained from tRNAscan database [321]. Reads per million (rpm) values for each gene was obtained by dividing the number of reads uniquely mapping within the limits of a gene annotation, by the total number of uniquely mapping reads in the library and multiplying by a million. These rpm values were used between replicates to establish correlation between biological replicates of RNA-Seq libraries (Table 3.2, Table 3.3). Relative abundance of RNA families in Figure 3.3 was calculated using the cumulative rpm values of all genes within the Gencode defined RNA families such as miRNA, snoRNA, miscellaneous RNA (miscRNA), protein coding etc. Differential expression analysis of RNAseq libraries was performed using DESeq [348] and plots for data visualization were made using R statistical package.

Dynamicity of EV RNA

K562 cells were grown to 70% confluence in complete medium following which cells were transferred to conditioned medium. Replicates of 1+E8 cells were cultured in serum deprived conditioned medium, conditioned medium supplemented with EV depleted serum (10% final concentration) or in conditioned medium treated with MitomycinC (Sigma) at a final

concentration of 20ng/ml for 24 hours. Isolation of EVs, EV RNA and small RNAseq was performed as described above. Bioinformatics analysis of RNASeq libraries were performed using STAR mapping software and HTSeq as described above. Differential expression analysis was performed using DESeq [348] and plots for data visualization were made using R statistical package.

Microscopy

Transfer of EVs was demonstrated using lipid labeling of EVs. Briefly, 2 microliter of PKH67 (Sigma) was re-suspended in 500microliter diluent and added to purified K562 EVs for 4 minutes in dark and subsequently EVs were isolated using Exoquick-TC according to manufacturer's protocol. The labelled EV pellet was re-suspended in complete medium (DMEM +10% FBS+1% Penicillin-Streptomycin) and added to HeLa cells for overnight incubation. Imaging was done on Deltavision OMX microscope and image analysis was performed with Delta-vision SoftWorx software.

Transfer of EV RNA was demonstrated by labeling EV RNA with Syto RNAselect green dye (Life Tech). Briefly, K562 EVs were incubated with Sytoselct RNA green dye in dark and precipitated overnight using ExoQuick-TC. HeLa cells were then incubated overnight with RNA-labeled EVs and next day, imaging was performed using Deltavision OMX microscope and image analysis performed with Deltavision SoftWorx software.

Subcellular localization of EVs was studied by live imaging in HeLa cells by labeling mitochondria with MitoTracker Red (Life Tech), lysosomes with Lysotracker Red (Life Tech) and endoplasmic reticulum with ER-tracker Red (Life Tech) according to manufacturer's protocols and then incubating labeled HeLa cells with Syto RNAselect green labeled K562 EVs

(as described above) for 30 minutes. Imaging was performed on Deltavision OMX microscope and image analysis was performed using SoftWorx software.

Inter-species transfer of EV RNA

Interspecies transfer of EV RNA was determined by direct incubation with EVs as well as by transwell co-culture. In direct EV incubation, approx. 3+E5 mouse HB-4 cells were incubated with EVs isolated from human GM12878cells (1+E8 cells, in replicates) for 24 and 48 hours, while in transwell co-culture, mouse HB4 cells were co-cultured with human GM12878 cells (3+E5 cells each, at 1:1 ratio) across 1 micron transwell membrane for 24 and 48 hours. Mouse HB4 cells were then washed and pelleted with low speed centrifugation. RNA isolation was performed with Mirvana miRNA isolation kit as described above and small RNA sequencing was performed using an A-tailing approach as described in [349]. The data was mapped using STAR [318] against combined Human and Mouse genome and reads which mapped uniquely to humans only were considered for further analysis. *RNY5*, a human specific gene enriched in EVs was used to determine inter-species transfer of human GM12878 EV RNA to Mouse HB4 cells.

Correlated transcriptional response in cells with EV and EV RNA treatment `

Treatment of cells with EVs was performed by incubating 2+E5 BJ cells with EVs isolated from 1+E8 K562 EVs for 0, 2 and 24hrs. Alternatively, 2E5 BJ cells were transfected with K562 EV RNA (RNA isolated from EVs derived from 1+E8 K562 cells, in replicates) using Lipofectamine for 6 hours in Opti-MEM medium. Lipofectamine medium was replaced with fresh complete medium (DMEM+10% FBS +1% penicillin-Streptomycin) and incubated for another 24hrs. BJ cells were then washed and pelleted and long RNA isolation was performed

subsequently using Mirvana miRNA isolation kit. Long RNA libraries were prepared using Illumina total RNA stranded kit, using manufacturer's protocol and libraries were sequenced on Illumina HiSeq2000. Bioinformatics analysis of RNASeq libraries were performed using STAR mapping software and HTSeq as described above.

Dynamic response by EVs

Replicates of K562 cells were grown to 70% confluence and then transferred to serum free conditioned medium with and without MitomycinC (final concentration of 20ng/ml) for 24hrs. EVs were then isolated from both treated and untreated K562 cells. Replicates of 2+E5 BJ cells were incubated with K562 EVs (derived from cells with and without MitomycinC treatment) for 24 hrs. Subsequently, cells were pelleted and long RNA isolation was performed using Mirvana miRNA isolation kit. Long RNA libraries were constructed using Illumina Truseq total RNA stranded kit using manufacturer's protocol and sequenced on Illumina NextSeq. Bioinformatics analysis of RNASeq libraries were performed using STAR mapping software and HTSeq as described above. Differential expression analysis was performed using DESeq [348] and plots for data visualization were made using R statistical package.

Cell type specificity of EV response

Replicates of 2+E5 BJ and HUVEC cells were incubated with EVs (derived from 1+E8 K562 cells) for 0hr and 24hrs, following which cells were pelleted and long RNA isolation was performed using Mirvana miRNA isolation kit. Long RNA libraries were constructed using Truseq total RNA stranded kit using manufacturer's protocol and sequenced on Illumina NextSeq 500. Bioinformatics analysis of RNASeq libraries were performed using STAR mapping software and HTSeq as described above. Differential expression analysis was

performed using DESeq [348] and plots for data visualization were made using R statistical package.

Chapter 4

Extracellular vesicle mediated transfer of processed and functional RNY5 RNA

Sudipto K. Chakrabortty[#], Ashwin Prakash[#], Gal Nechooshtan, Stephen Hearn and Thomas R. Gingeras

# Authors contributed equally to this work

4.1 Synopsis:

Extracellular vesicles (EVs) have been proposed as means to communicate with and influence neighboring and distal cells. Analysis of the RNA content of K562 EVs identified a 5' 31 nucleotide processed fragment of human *RNY5* gene as one of the most abundant and specifically enriched transcripts in EVs. Full length RNY5 is processed into shorter fragments of distinct lengths, and factors responsible for this activity seem to be enriched within EVs. We demonstrate EV mediated transfer of RNA to other cells and study kinetics and subcellular localization of EV-RNA in recipient cells. As a specific example of EV RNA functionality, we show that ectopic expression of 31 nucleotide processed RNY5 transcripts using synthetic oligonucleotides induces cell death in primary cells of distinct developmental lineages in a dose dependent manner, while cancer cells do not display a similar response. Treatment of primary BJ cells with total RNA from K562 EVs as well as with K562 EVs recapitulated the response observed with synthetic oligonucleotide treatment, suggesting the possible involvement of the 5' 31nt *RNY5* fragment encapsulated within these EVs in mediating this response. Finally, we report an 8 nucleotide motif in the 5' *RNY5* fragments that is required for its functionality.

4.2. Introduction

Since the observation that various types of RNAs are part of the cargo of EVs [83, 350, 351], numerous efforts have been made to catalogue RNA cargos and determine if these RNAs are biologically functional [187, 352-354]. The question of the functionality of the RNA cargos have been made complicated by the observation that a large proportion of the detected RNA biotypes are represented by a mixture of full length and shorter fragments [97, 339, 355, 356]. With perhaps the exception of micro- (mi) RNA cargos, the issue of the functionality of RNAs released and carried by EVs remains largely unresolved. We describe a study of the human (h)Y RNA family that seeks to address this issue.

The *hY* RNA family consists of four genes (*RNY1, RNY3, RNY4, RNY5*) that are transcribed by RNA polymerase III, whose primary transcripts range in length from approximately 83- 112 nucleotides (nts) [357-359]. The evolutionary conservation of this gene family is underscored by the sequence similarity of these RNA genes seen in all vertebrates and more recently in invertebrates [360]. Additionally, the presence of 966 *hY* RNA pseudogenes, of which *hY5* has 8 in the human genome, also underscores their long evolutionary heritage [361, 362]. An understanding of the underlying biological roles of this class of RNAs developed slowly since their discovery in 1981 [357]. At the outset, the associations of the *hY* RNAs with both Ro60 and La proteins in ribonucleoprotein complexes found in normal and in systemic Lupus Erythematosus and Sjogren Syndrome samples [363] were the first indications of possible biological roles of these short (s)RNAs. Since these original observations, multiple other ribonucleoprotein complexes involving Y RNAs have been described, prompting the hypothesis that *Y*-RNAs may have multiple functions based on the protein-partners present in the complexes [364]. More recently, support for this hypothesis has been provided by reports that

cellular *Y*-RNAs have specific functional roles including forming part of the initiation of DNA replication complex [344, 345], the chaperoning of misfolded RNAs [345, 365] and assisting in the quality control of *5S* ribosomal RNAs [366]. Correlated with each of these functional roles has been the identification of a variety of distinct proteins associated with the *Y*-RNAs involved. Finally, *hY* RNAs are significantly up-regulated between 5-13-fold in human cancer tissues, compared to normal tissues [367]

In addition to the presence of the full length *hY* RNAs, fragments of each of the four *hY* RNAs have been found inside and outside of cells. Northern analyses of human Jurkat T-lymphocyte cell line induced into apoptosis showed rapid Ago 2 independent processing of the *hY* RNAs into fragments of multiple lengths [368]. Fragments of *hY* RNAs have also been detected outside of cells in healthy human serum and plasma isolates, using RNA sequencing (RNAseq) [97]. While the lengths of the processed RNAs observed outside of cells were seen to be similar to that observed within cells, approximately 95% of the sequences detected were mapped to *hY4* with only a minor fraction mapping to the other three *hY* RNAs. The detected fragments consisted of the 5' end sequences of each of the full-length *hY*RNA transcript but were determined not to be cargoes of EVs. It has been conjectured that they are part of circulating ribonucleoprotein complexes. Extracellular fragments of *hY* RNAs have also been found in EVs isolated from human semen [356] and mouse co-cultured dendritic-T cells [354]. A 30-33nt *RNY4* fragment and a 28nt fragment from unspecified mouse YRNA, both starting from the 5' end of the annotated genes have also been detected.

Although various members of the *hY* RNA families have been observed to be selectively enriched and made part of EV RNA cargo, a comprehensive study of the relationship of the full length primary transcript *hY* RNAs to processed forms and if any of these forms are biologically

active has yet to be carried out. Additionally, any differences in the processed vs. the primary transcripts for the *Y*-RNAs found in the EVs released by different types of normal and transformed cells has yet to be reported. This study explores the processing and transfer of specific RNY5 fragments within EVs derived from cancer cells and their cellular phenotype associated with induction of primary cell death.

4.3 Results

4.3.1 Isolation, quantification and characterization of EV RNA cargo of primary and cancer cell lines

Enriched preparations of EVs were carried out using the modified version of the protocol first described by Thery, et al [300] (Figure 4.1A). Verification of the isolation and enrichment of EVs compared to the cells of origin (K562 myelogenous leukemia and BJ primary fibroblast) was carried out using three methods: transmission electron (Figure 4.2A) and immuno-electron micrographic techniques (Figures 4.2B) and western blot analyses of the EV specific membrane proteins compared to several cellular protein markers (Figure 4.2C). The determination that the detected RNAs are cargos of the EVs rather than an artifact associated with EV purification was made by treatment of preparation of EVs prior to RNA isolation with RNase A and T1 and compared to RNA isolated from untreated EVs as well as EVs treated with detergent followed by RNase (Figure 4.2.D.). These results indicate the RNAs isolated from EVs were internalized within vesicles and thus protected from nuclease attack. Using a nanoparticle tracking technology (NanoSight Inc.) the number of EVs isolated from cultured 10^8 K562 and BJ cells was estimated to be approximately 1.1×10^{11} and 4.8×10^9, respectively (Figure 4.1B, Table 4.1).

To study the RNA content of isolated EVs, we carried out an RNAseq profile analysis on replicates of whole cells and EV cargoes derived from K562 (myelogenous leukemia) and BJ (foreskin fibroblast) cells. Profiles obtained from both cell lines and enriched EVs were highly reproducible (Figure 4.3). However, a low degree of correlation between RNA profiles in EVs and their source cells was readily evident. A detailed quantification of annotated sRNAs (reads

per million [rpm]) isolated from BJ and K562 whole cells (Figure 4.4. A, B) indicated a predominance of rRNA, snoRNA, and miRNAs. In contrast, the relative distribution of sRNAs in EVs from the same cells indicates almost a considerable enrichment of the miscellaneous RNA (miscRNA) group and predominance of rRNA and tRNA (Figure 4.4. C, D). A comparison of the relative abundance of sRNA families between source cells and their EVs specifically highlights the enrichment of genes within the miscRNA group, consisting of several families of sRNAs – *small Cajal body* (*sca*), *Y*-RNA and *vault* (*vt*) RNAs (Figure 4.5). *RNY5* was the most abundant miscRNA gene present in EVs, composing 35% of all sRNAs in BJ EVs and 48% in K562 EVs. In contrast, *RNY5* accounts for only 0.1% and 0.2% of all reads from sRNAs within BJ and K562 whole cells, respectively. In EVs from both BJ and K562, the *RNY5* gene contributes over 89% of the reads from miscRNA, whereas in whole cells it constitutes only 40% of miscRNA reads, emphasizing the particular enrichment of this gene within EVs Enrichment levels of *RNY5* in EVs compared to whole cell RNAs from BJ and K562 were 196 and 68 fold, respectively.

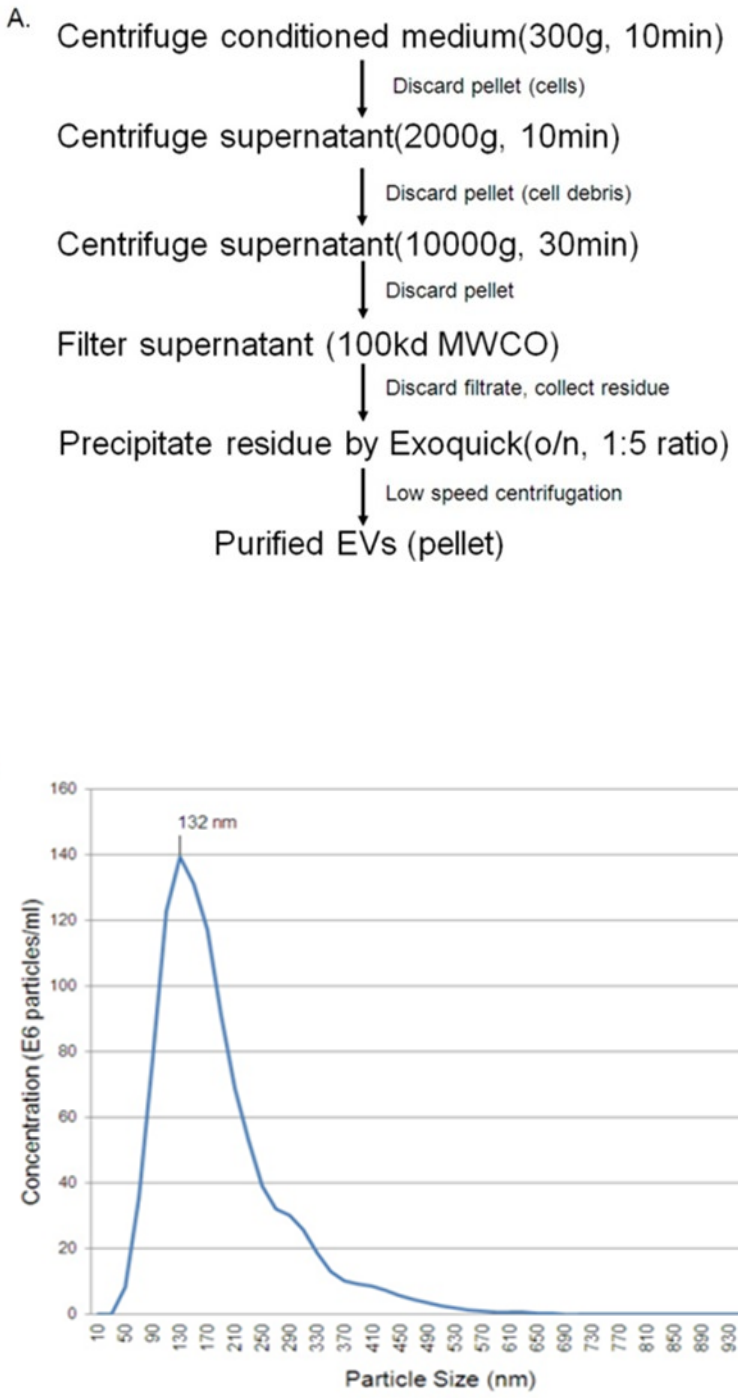

Figure 4.1: Isolation and quantification of EVs. (A) Protocol for isolation of EVs from conditioned cell culture medium. **(B).** Quantification and Size distribution of K562 EVs by Nanoparticle Tracking analysis (NTA). X-axis represents particles size (in nm) while Y-axis represents concentration of particles (E6)/ml.

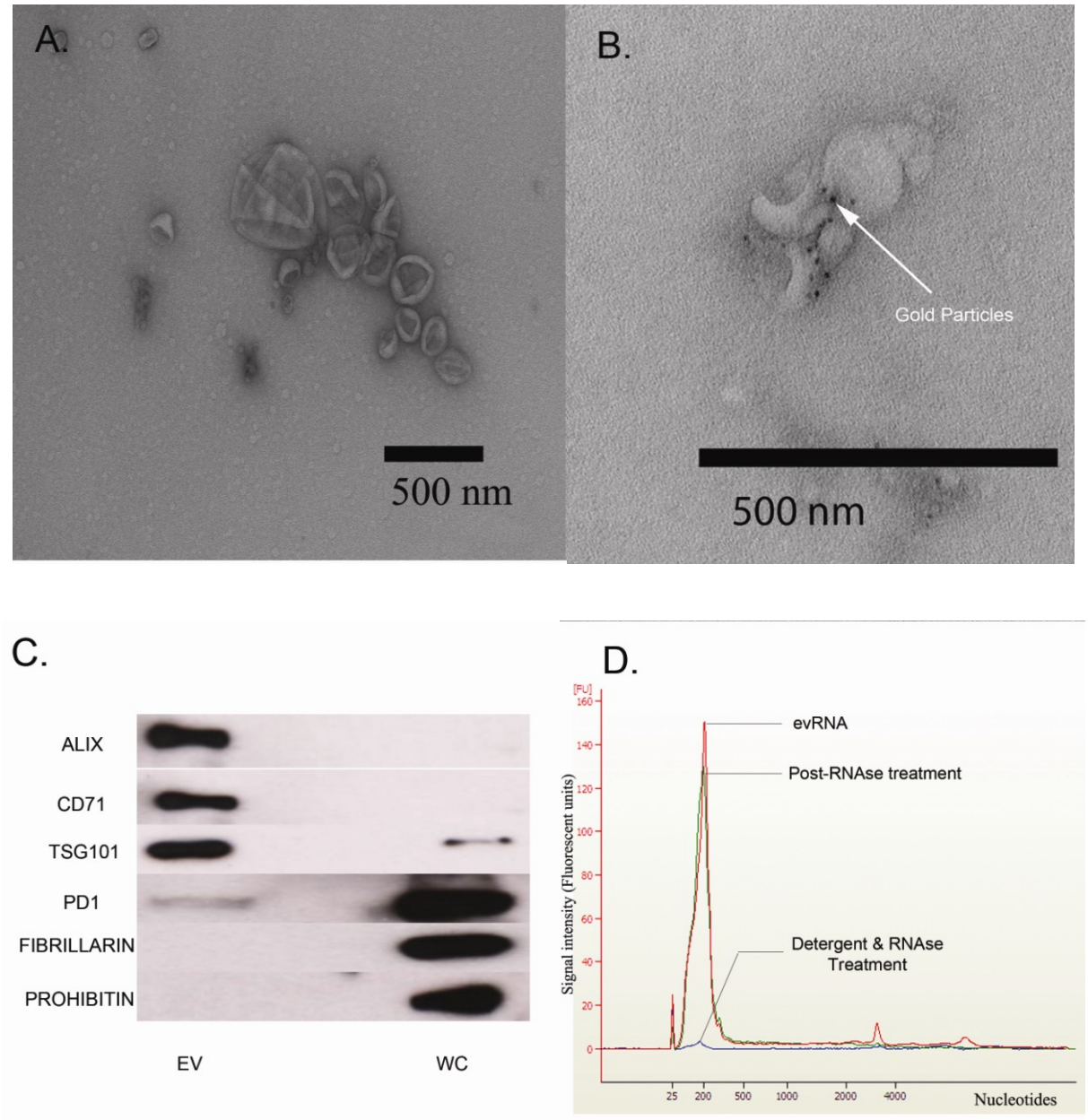

Figure 4.2: Validation of purification of extracellular vesicles (EVs). (A) Transmission electron microscopy image of K562 EVs after negative staining shows classic cup-shaped vesicles smaller that are on average smaller than 200nm. **(B)** Immuno-electron microscopy image of purified EVs labeled with Anti-CD81 (mouse mAb) and detected by Goat anti-mouse IgG secondary conjugated with 5nm gold. Dark spots on the image are the electron dense gold particles conjugated to IgG secondary antibody. **(C)** Bioanalyzer RNA profile (RNA Pico-chip) of untreated EVs(red), RNA profile of EVs treated with RNAse(green) and RNA profile of EVs treated with detergent and RNase(blue). X-axis is nucleotides length and Y-axis is Fluorescent Units. **(D)** Western Blot analysis of proteins from K562 EVs and whole cell. Proteins selected for detection were previously identified to be enriched in EV or whole cell. EV enriched: ALIX (Programmed cell death6 interacting protein), CD71 (Transferrin receptor) and TSG101 (tumor susceptibility 101 gene). Whole cell: PDI (Protein disulphide Isomerase), FIBRILLARIN *(FBL* gene), PROHIBITIN (*PHB* gene).

Cells	Number of EVs	Quantity of RNA
K562	1.135E+11	2-3ug
BJ	4.75E+09	800ng-1ug

Table4.1: Number of EVs (quantified by Nanoparticle Tracking analysis) and quantity of RNA (quantified by Nanodrop) isolated from 1+e8 K562 and BJ cells.

	K562 EV1	K562 EV2	K562 WC1	BJ EV1	BJ EV2	BJ WC1	BJ WC2
Number of input reads	15312204	38109015	37450624	12805596	13757050	13474063	18944518
Average input read length	28	38	60	30	43	62	55
UNIQUE READS:							
Uniquely mapped reads number	5021255	16183627	28362474	3821688	5881994	10658696	13182629
Uniquely mapped reads %	32.79	42.47	75.73	29.84	42.76	79.11	69.59
Average mapped length	38.12	49.03	63.5	33.06	56.73	63.26	57.73
MULTI-MAPPING READS:							
Number of reads mapped to multiple loci	3778069	11996007	5116446	6452579	5784261	1620129	3399157
% of reads mapped to multiple loci	24.67	31.48	13.66	50.39	42.05	12.02	17.94
UNMAPPED READS:							
% of reads unmapped	42.54	26.05	10.61	19.76	15.2	8.87	12.47

Table 4.2: Mapping statistics of the different RNASeq libraries from both K562 and BJ EVs and whole cells.

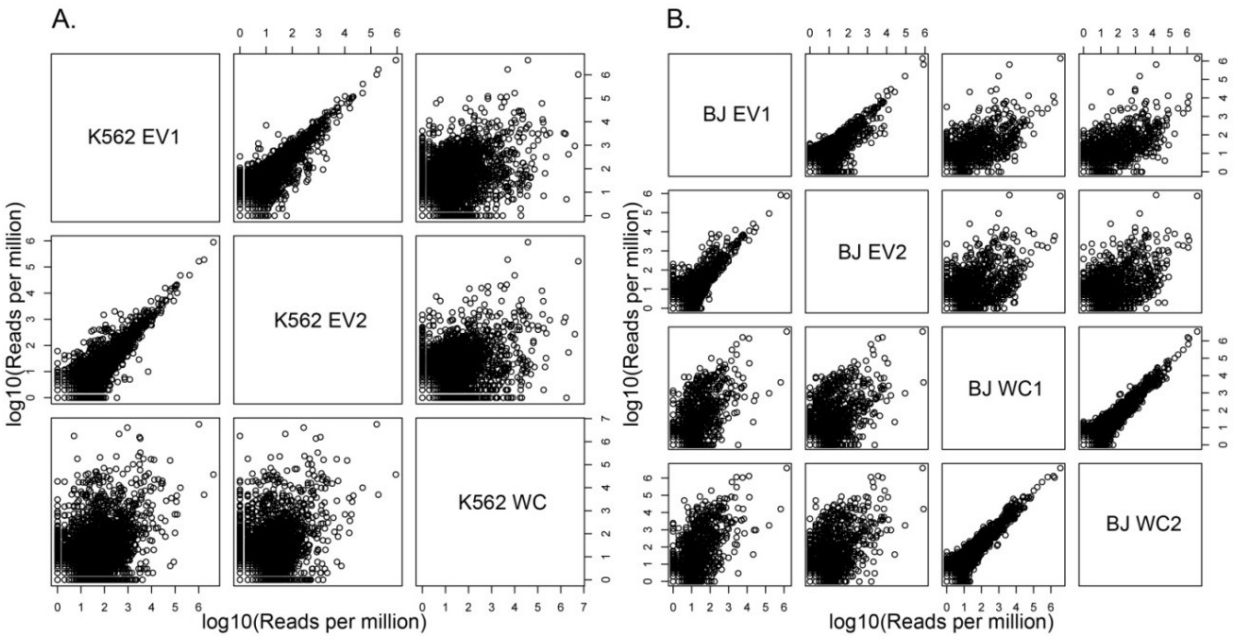

Figure 4.3: Correlation analysis of EV and whole cell. Scatter plots represent correlation in gene expression levels, between replicates of EVs and cellular small RNA in **(A)** K562 and **(B)** BJ.

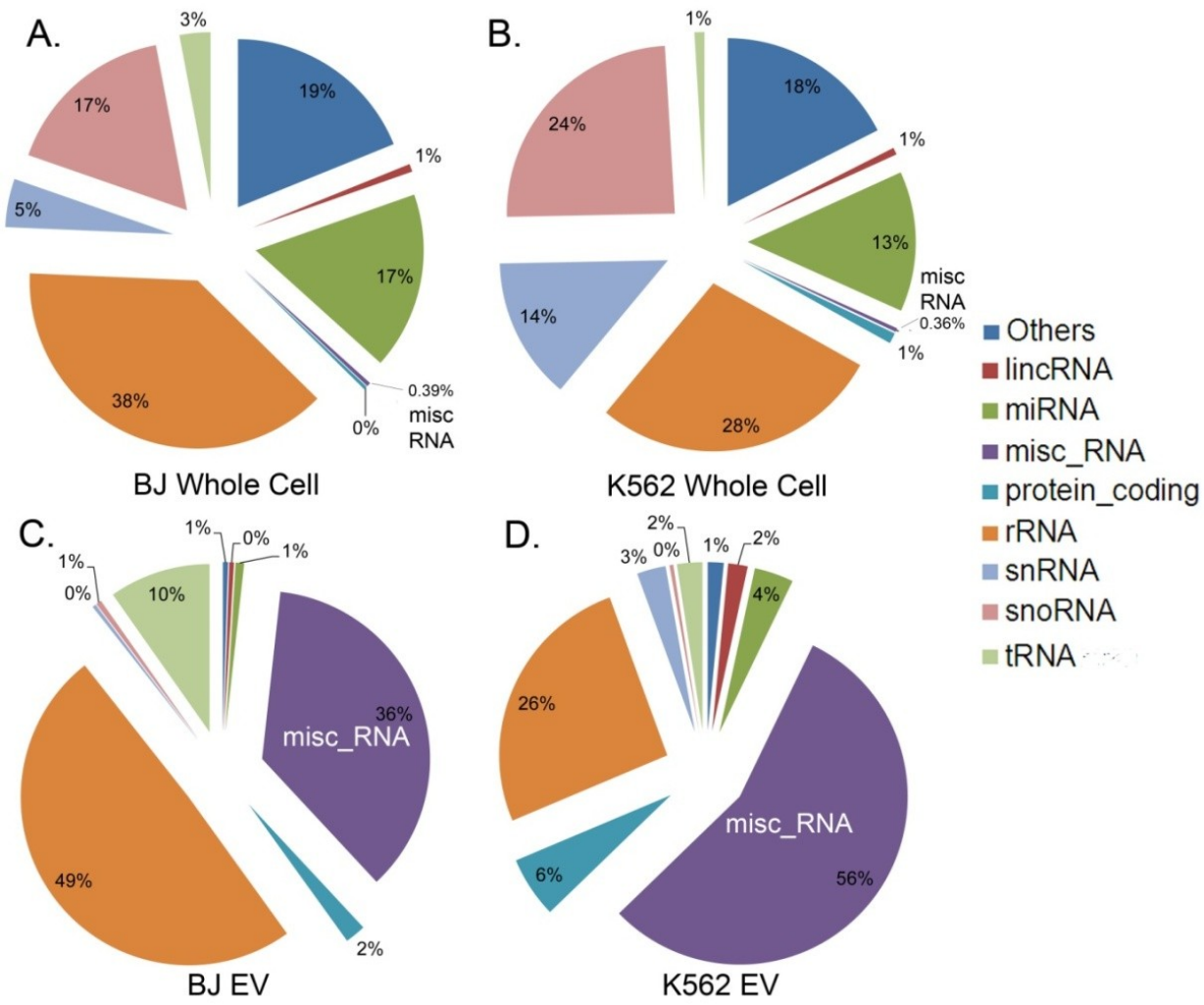

Figure 4.4: Relative abundance of annotated gene families in EVs and whole cell. Pie-charts representing the relative abundance of families of RNA within BJ whole cell **(A)**, K562 whole cell **(B)**, BJ EV **(C)**, and K562 EV **(D).** The group labeled as "Others" in the pie-charts are representative of reads derived from several Gencode annotation categories such as pseudogenes, antisense intronic, mitochondrial t-RNA, vault RNA, immunoglobulin genes etc.

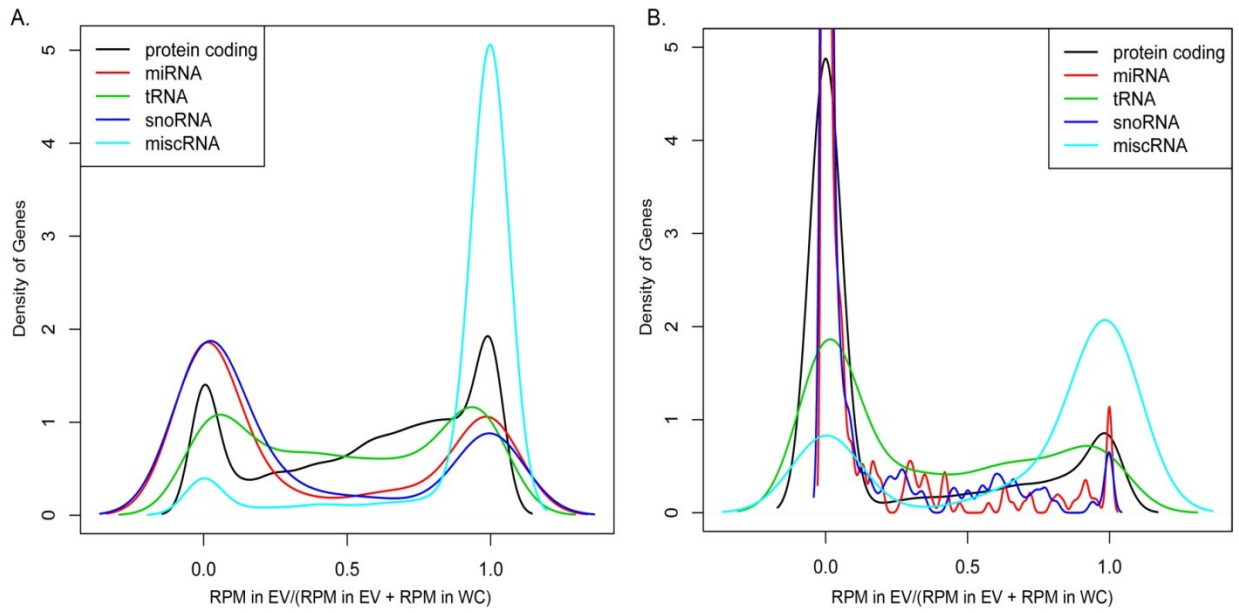

Figure 4.5: Enrichment analysis of genes in EVs. Graphs depicting kernel density plots of the ratio of rpm in EV and the sum of rpm in EV and corresponding whole cell in K562 **(A)** and BJ **(B).** Each line in the plots depicts the number of genes belonging to each RNA family, and genes which have a ratio of 0 represents genes that are more abundant in cells compared to EVs, which a ratio of 1 represents genes that are more abundant in EVs when compared to their source cells.

4.3.2. Processing of *RNY5* RNAs likely occurs within EVs.

In the EVs, using RNAseq data, the 83nt *RNY5* primary transcript (Figure 4.6A) was detected as well as shorter products of 23nt, 29nt and 31nt in length, with start and end positions for each of these forms located at the 5' end of the Gencode gene annotation (Figure 4.6B) . Additionally, a separate 31nt product mapping between nucleotide positions 51 to 83 (3'end of RNY5) of the primary transcript was observed, which is partially complementary to the 31 nucleotide 5' fragment (Figure 4.6B).

Northern hybridization analyses using a probe complementary to the first 31nts of the *RNY5* showed that the form of *RNY5* present in the whole cell was the full length 83nt transcript (Figure 4.6C). While the RNA extracted from EVs contained the 83nt transcript, it was highly enriched for the 29-31nt forms, as well as a modest amount of a 23nt product, which is in agreement with the RNAseq results observed for the EV RNAs (Figure 4.6B).

To further investigate the processing of *RNY5* seen in the EVs, we incubated a synthetic form of the 83nt *RNY5* transcript with K562 whole cell and EV protein extracts, followed with detection by northern analysis. We found that synthetic copies of the 83nt *RNY5* incubated with K562 whole cell extracts exhibit no detectable processing (Figure 4.6D), whereas incubation with K562 EV extracts leads to dose dependent formation of all processed forms (23, 29, 31nt) detected *in vivo* (Figure 4.6E). Additionally, a prominent *RNY5* processed species larger than 31nt is detected. The altered ratios of processed products and the appearance of a larger species *in-vitro* may well be caused by the different conditions in an *in-vitro* reaction (Figure 4.6E). Treatment of the synthetic version of the 31nt RNA with K562 EV extract produced the same 23nt product as seen using the 83nt substrate (Figure 4.6F) confirming that the 23nt product can

be produced from either an 83nt or 31nt substrate. However, when a shuffled version of the 31nt RNA was treated with EV extract, no 23nt product is observed, demonstrating the sequence specificity of the processing activity of the EV extract (Figure 4.6F).

Gardiner, et al [345] reported that a conserved double stranded sequence motif in the upper stem of all vertebrate *Y*-RNAs correlated with their participation in initiating DNA replication. Each of the products processed from the 5' side of *RNY*5 *in vivo* and *in-vitro* contains a single stranded version of this motif. The motif is 8 nucleotides long (5'GUUGUGGG 3') extending from nucleotides 14-21 of *RNY5* (Figure 4.6A). An alternate form of the 31nt substrate carrying a shuffled motif only exhibits residual processing into a 23nt product (Figure 4.6F), underscoring the importance of the motif for processing of *RNY5* transcripts into the smaller fragments.

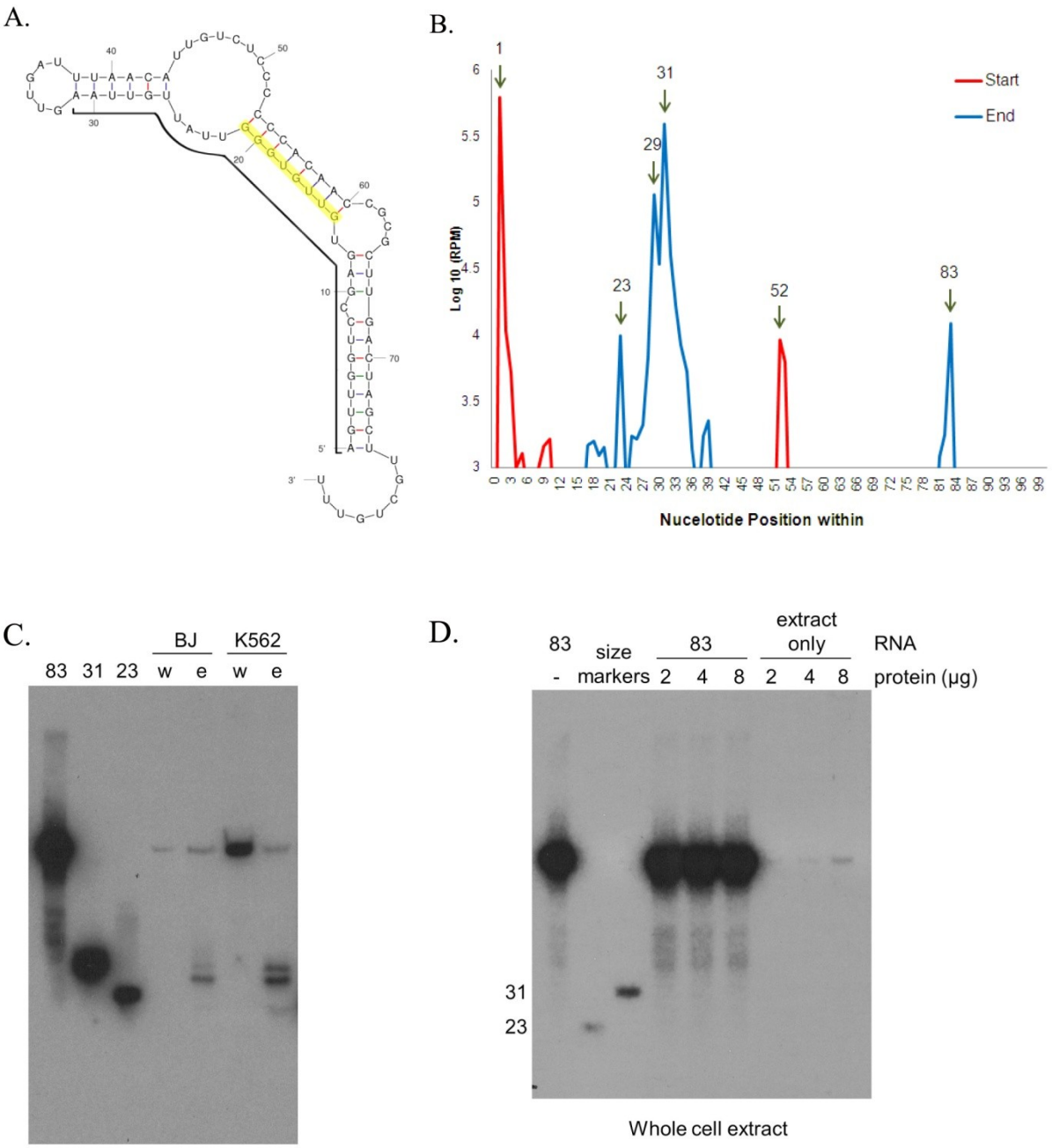

Fig 4.6: Fragmentation patterns of RNY5 (A) Full length *RNY5* structure**.** The structure was drawn using Mfold. Bold line indicates the 5' 31nt processed product and the 8nt motif is highlighted. **(B)** Graph depicting the most frequent (>1000 reads per million) start and stop positions of reads mapping to the human *RNY5* gene. The most frequent start positions marked as the 5' start position of the *RNY5* annotation, and position 52 of the annotation. And the most frequent stop positions being 23, 29, and 31 for the reads which start at the 5' end of the *RNY5* gene, and position 83 which has reads starting at 52 and also some reads that start at position 1. **(C)** Northern blot of RNY5 RNA purified from K562 and BJ cells and EVs. Synthetic versions of Y5 processing products were used as size markers. RNA was detected by a probe complementary to the 5' 31nt processed product. w- Whole cell RNA, e- EV RNA**. (D)** *In- vitro* processing of *RNY5* transcript. Synthetic full length RNY5 was incubated for 30 minutes at 37° with 0, 2, 4, or 8 µg of K562 whole cell.

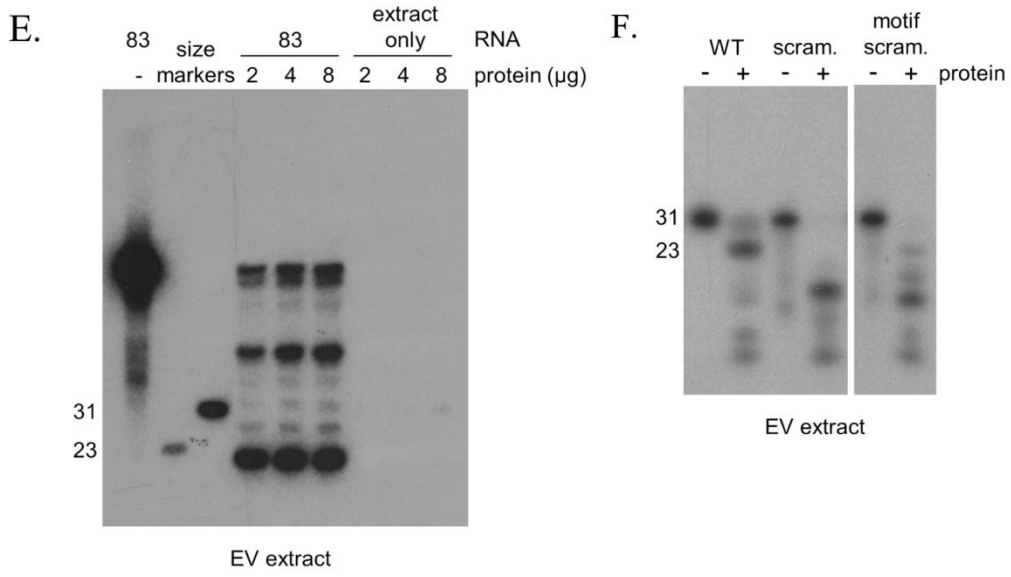

Fig 4.6: Fragmentation patterns of RNY5. (E) *In- vitro* processing of *RNY5* transcript. Synthetic full length RNY5 was incubated for 30 minutes at 37° with 0, 2, 4, or 8 µg of K562 EV protein extract. Samples containing only the extracts and treated identically were used to control for the existence of Y5 RNA in protein extracts. Detection was done as in C. 23nt and 31nt size markers are not equimolar. **(F)** *In vitro* processing of Y5 5' 31-mer variants. Wild type (WT), scrambled (scram.) and 8nt motif scrambled (motif scram.) versions of the *RNY5* 5' 31-mer were radioactively end-labeled and incubated with K562 EV protein extract for 2 hours at 37°C.

4.3.3. Intercellular transfer and subcellular localization of EVs and their RNA cargoes

The transfer of EVs and their molecular cargoes from one cell type to another has previously been documented by use of both microscopic and molecular methods [369]. We have extended these studies by monitoring the transfer of EVs between K562 and BJ cells and between K562 and two mouse cell lines (3T3 and HB4). The goals of these experiments were to confirm the transfer of RNA content of EVs from one cell type to another in a species independent manner and to identify the subcellular localization and kinetics of the transferred EVs and RNA contents.

K562 EVs were first labeled with the lipid dye PKH67 after isolation. Following exposure of human BJ cells to labeled EVs, the EVs were found to be localized almost exclusively in the cytosol (Figure 4.7A). To monitor the transfer of EV RNA, K562 cells were metabolically labeled with 5' ethynyl uridine, and EVs were isolated. Transfer of labeled RNA contained in EVs was monitored after entry into mouse 3T3 cells. The localization of the labeled RNAs was also found to be primarily cytoplasmic (Figure 4.7 B). The same cytosolic localization was observed when primary human fibroblasts (BJ cells) were transfected with synthetic 31nt oligonucleotides versions of *RNY5* via lipofection (Figure 4.7C). These data also point to a lack of cell-type and species specificity in the transfer of the EVs.

The kinetics of intercellular transfer of EV RNAs was studied by treating mouse HB4 cells with EVs from human K562 cells followed by RNAseq analysis. Mouse cells were chosen for this experiment as a recipient cell type because of the absence of the *RNY5* gene in the mouse genome, allowing for the unambiguous monitoring of human *RNY5* transcripts. A temporal

study lasting 24hrs revealed that maximum levels of *RNY5* were achieved by 12 hours post exposure followed by a progressive decrease in *RNY5* levels (Figure 4.7 D).

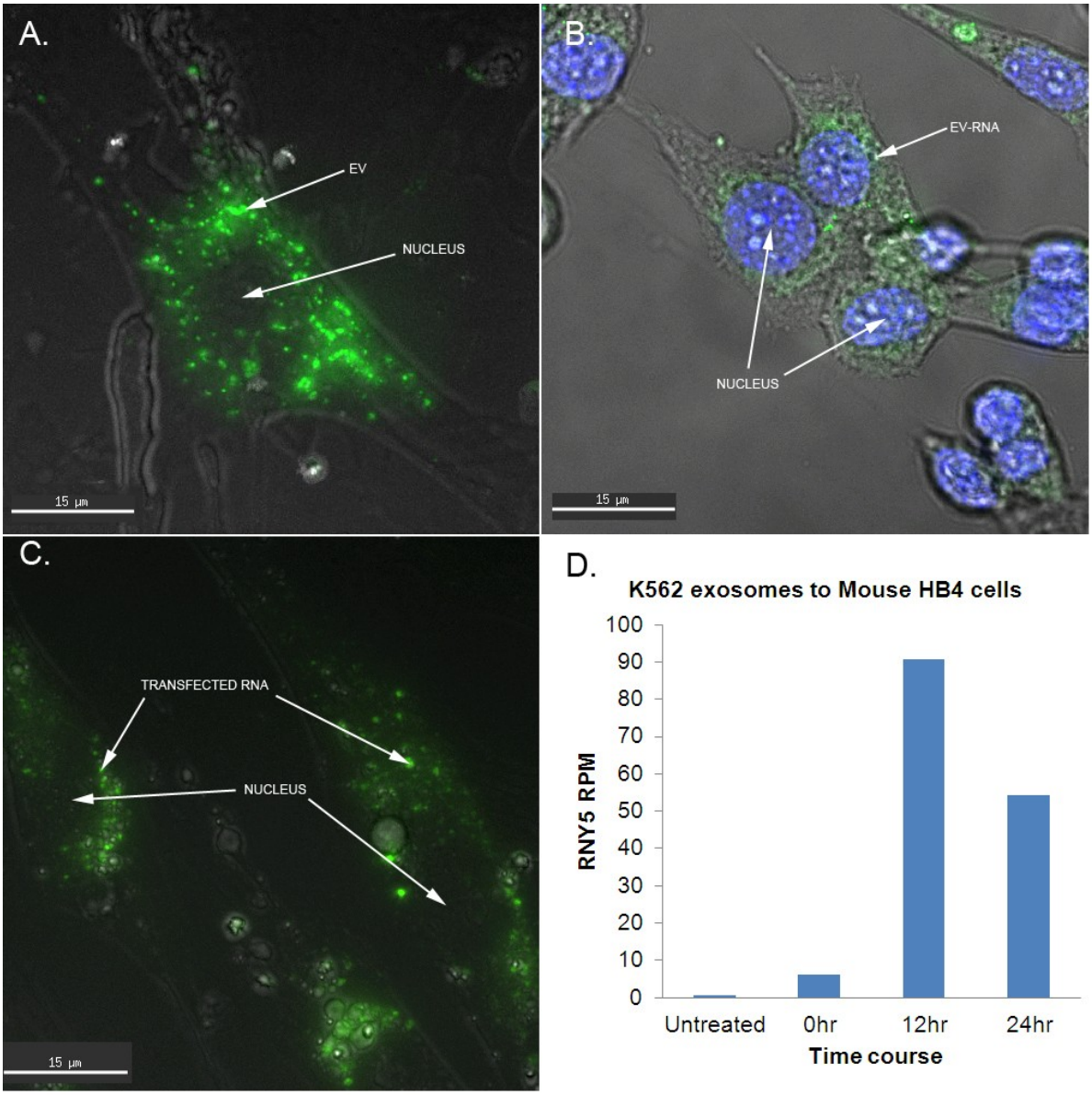

Figure 4.7: Intercellular transfer and subcellular localization of EVs and EV-RNA. (A) Transfer and subcellular localization of K562 EVs labeled with lipid dye PKH67 in BJ cells. **(B)** Transfer and subcellular localization of 5-ethynyl uridine (EU) labeled K562 EV RNA (green) in Mouse 3T3 cells treated with ActinomycinD. Nuclei are counterstained with Hoechst33342. The scale bar represents 20microns. **(C)** Subcellular localization of synthetic RNY5-31mer labeled with Alexa-488 at 3'end in BJ cells after 24 hours. Scale bar indicates 15 microns. **(D)** Time course analysis of the level of RNY5 31-mer in mouse HB4 cells when Mouse HB4 cells are incubated with K562 EVs. X-axis indicates duration of incubation (hours) while Y-axis indicates the level of RNY5 (in reads per million).

4.3.4. Biological phenotypes produced by EVs and *hY5* RNAs fragments

Based on the significant abundance of 31nt processed *RNY5* product in EVs, we took a reductionist approach to investigate the functionality of EV transferred processed RNY5 31nt product. Ectopic expression of 31nt *RNY5* product using synthetic oligonucleotides caused cell death in 4 primary cells of diverse developmental origin (BJ, HUVEC, IMR90, HFF), while cancer cells of multiple developmental lineages (K562, HeLa, MCF7,U2-Os) did not elicit a similar response (Fig 4.8A). Varying the amounts of the synthetic 31nt RNA resulted in a dose-dependent cell death phenotype for BJ cells (Figure 4.8B).

Since other forms of *RNY5* can be detected in EVs, we decided to investigate if any of them may also contribute to the phenotype. Transfection of 23nt oligonucleotide in BJ cells induced comparable levels of cell death to that seen with the 5' 31nt synthetic RNA (Figure 4.8C). However, the 83 nucleotide full length *RNY5* RNA, the synthetic version of the 3' 31nt fragment, and a double stranded version comprised of the 5' and 3' 31nt species induced substantially lower levels of cell death in BJ cells (Figure 4.8C). The levels of cell death triggered by these synthetic RNA products and observed in K562 cells were all similar and at background levels (Figure 4.8D).

We hypothesized that the inability of double stranded versions of the RNA to cause the phenotype may be related to sequestration of the 8nt motif, the importance of which was demonstrated in the processing assays. This prompted us to investigate its role in the functionality of *RNY5* processed products. We observed that the cell death phenotype in BJ cells was lost when the motif was scrambled or deleted (Figure 4.8C), further emphasizing the importance of this motif.

Next, we investigated if 5' 31nt processed RNY5 can also induce the similar response in primary cells through EVs and EV RNA. In order to recapitulate the response observed with ectopic expression of synthetic 31nt *RNY5* oligonucleotides, total RNA was isolated from K562 and BJ EV preparations from 1E8 cells. While transfection of total EV RNA obtained from K562 EVs resulted in an approximately 13% more cell death (compared with mock treatment), transfection of BJ cells with BJ EV total RNA resulted in approximately 2.5% increase in cell death compared to mock control (Figure 4.8F). K562 cells remained unaffected by the transfection of total K562 EV RNA (Figure 4.8E).

Further corroboration of the observed phenotype was made when BJ and K562 cells were treated with EVs isolated from the BJ primary fibroblasts, and four cancer (K562, HeLa, U2-OS, MCF7) cell lines. Exposure of BJ cells to BJ EVs or K562 cells to K562 EVs (Figure 4.8E, F) resulted in no observable cellular phenotype. However, exposure of primary BJ cells to EVs from each of the cancer cell lines resulted in a relatively rapid cell death phenotype (Figure 4.8F). Thus, consistent with previous results obtained by synthetic *RNY5* 31nt oligonucleotides, these results strongly suggest 31nt *RNY5* processed product as a functional RNA molecule in K562 EVs and suggest its involvement in inducing cell death response in primary cells.

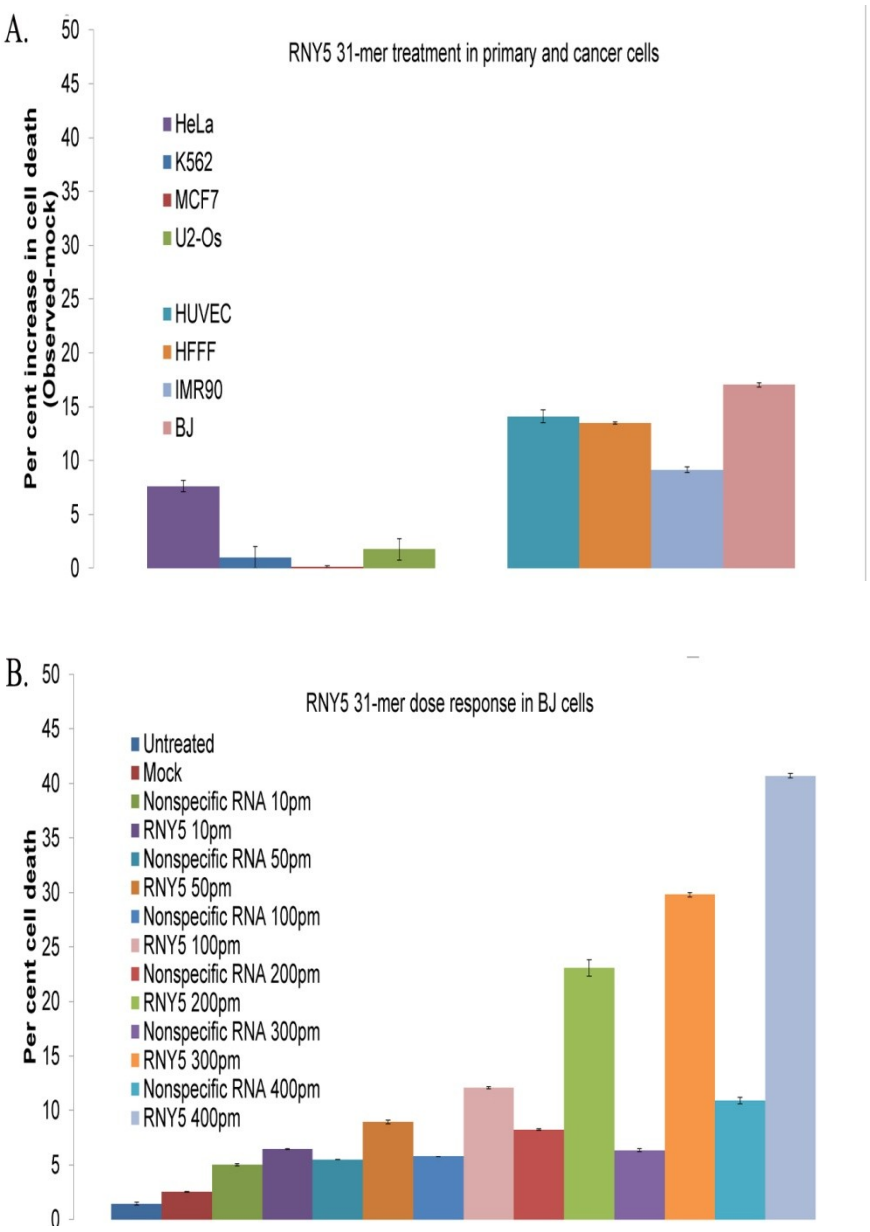

Figure 4.8: Quantification of cell death by flow cytometry. YO-PRO-1 and Hoechst33342 dyes were used for quantification of cell death. Y-axis indicates the percent of cell death indicated byYO-PRO-1 and Hoechst33342 double positive cells. **(A)** RNY5 31-mer induced cell death phenotype. Bars indicate the net increase in cell death normalized to levels of cell death from mock treatment in each cell type. 4 cancer cell lines including K562, HeLa, MCF7, U2-Os and 4 primary cells including BJ, HUVEC, IMR90 and HFFF were transfected with RNY5 31-mer. 100 pico-moles of RNY5 was used for each transfection, except HFFF where 200picomoles of RNY5 31-mer was used. (**B)** Dose response curve of RNY5 31-mer induced cell death phenotype in BJ cells. The bars represent the percent of cell death when BJ cells are treated with increasing dose (10, 50, 100, 200, 300 and 400 pico-moles) of RNY5 31-mer or nonspecific RNA. AllStars negative control RNA (Qiagen) was used as a non-specific RNA control. The levels of cell death in Untreated or Mock treated (Lipofectamine only) BJ cells are also indicated.

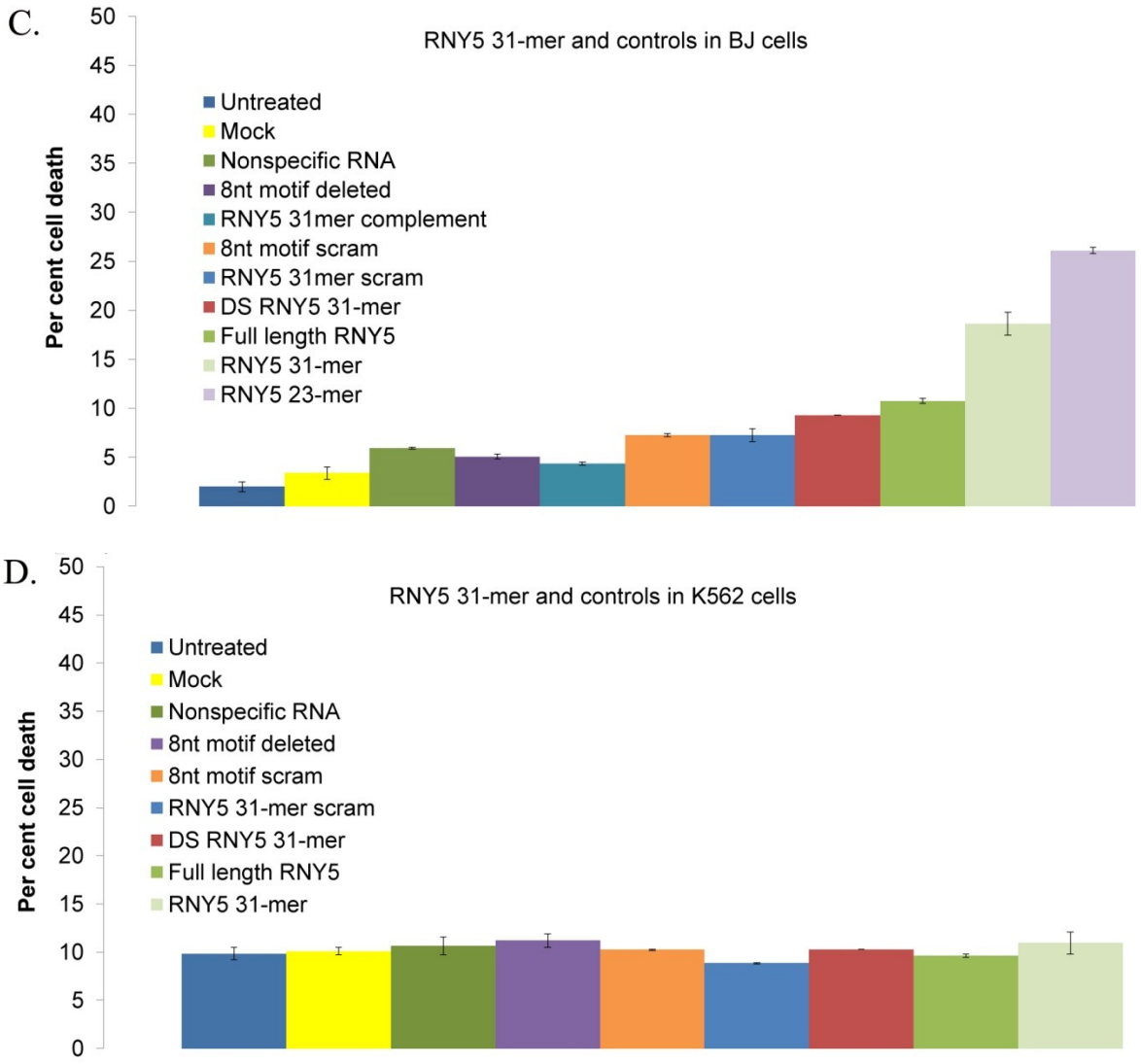

Figure 4.8 Quantification of cell death by flow cytometry. (C) Levels of cell death in BJ cells from 100 pico-moles of synthetic RNA oligonucleotides transfection. Y-axis indicates the percent cell death. The synthetic RNA oligonucleotides used for transfection are as follows: (Untreated): BJ cells without any treatment, (Mock): BJ cells with Lipofectamine treated only (no RNA), (Nonspecific RNA): Nonspecific RNA control (AllStars negative control siRNA), (8nt motif deleted): RNY5 sequence with nucleotides 14-21motif deleted, (RNY5 31-mer complement): 31nt RNY5 3' side fragment, (8nt motif scrambled): RNY5 31-mer sequence with nucleotides 14-21 scrambled, (RNY5 31-mer scram): 31nt completely scrambled sequence, (DS RNY5 31-mer): Double stranded RNY5 31-mer duplex, (Full length RNY5): RNY5 83-mer full length sequence, (RNY5 31-mer): 5' RNY5 31nt fragment, (RNY5 23-mer): 5' side RNY5 23nt fragment. **(D)** Levels of cell death observed in K562 cells from 100 pico-moles of synthetic RNA oligonucleotides transfection. Y-axis indicates percent cell death. The synthetic RNA oligonucleotides used for transfection are as follows: (Untreated): K562 cells without any treatment, (Mock): K562 cells with Lipofectamine treated only (no RNA), (Nonspecific RNA): Nonspecific RNA control (AllStars negative control siRNA), (8nt motif deleted): RNY5 sequence with nucleotides 14-21motif deleted, (8nt motif scrambled): RNY5 31-mer sequence with nucleotides 14-21 scrambled, (RNY5 31-mer scram): 31nt completely scrambled sequence, (DS RNY5): Double stranded RNY5 31-mer duplex, (Full length): RNY5 83-mer, (RNY5 31-mer): 5' RNY5 31nt fragment .

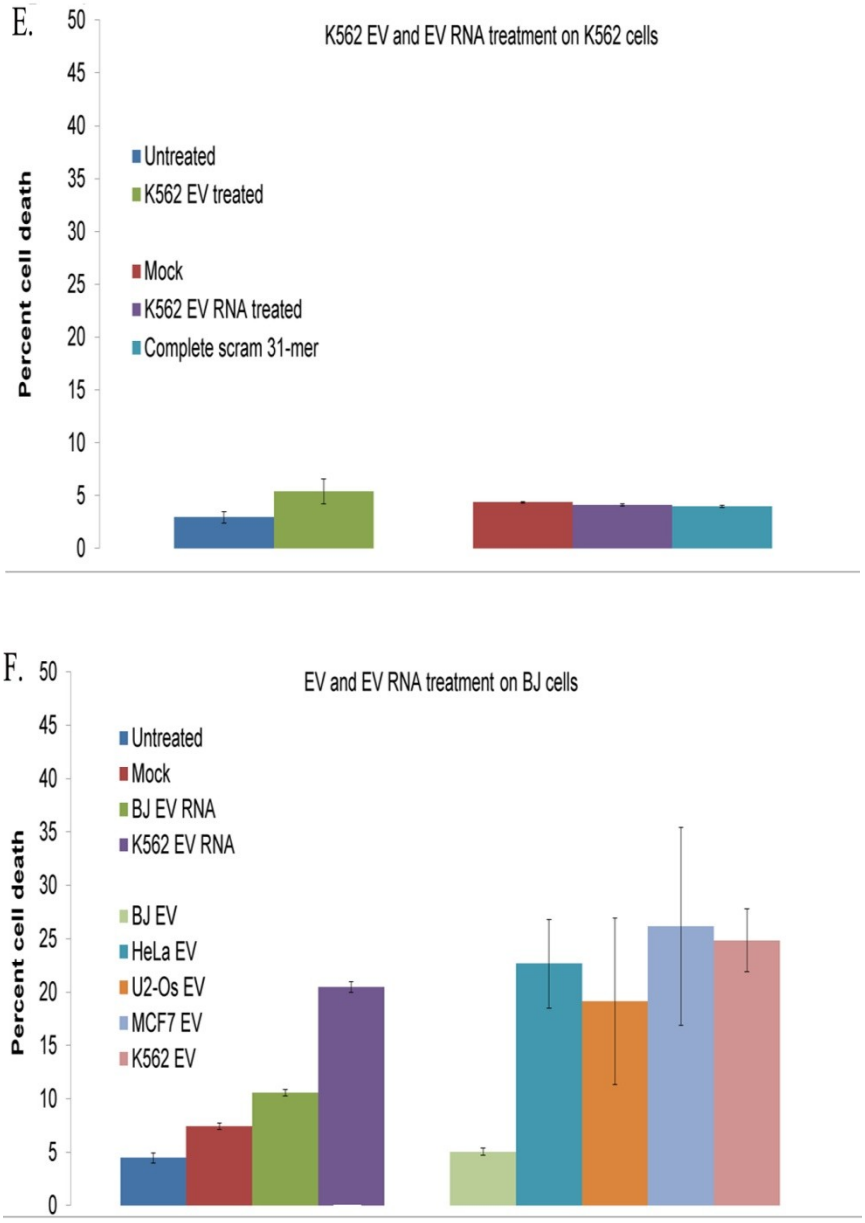

Figure 4.8 Quantification of cell death by flow cytometry. (E) Levels of cell death in K562 cells when treated with EVs and EV RNA. Y-axis indicates percent cell death observed. The following treatments are presented: (Untreated): K562 cells without any treatment, (K562 EV treated): K562 cells incubated with K562 EVs, (Mock): K562 cells with Lipofectamine treated only (no RNA), (K562 EV RNA treated): K562 cells treated with K562 EV RNA. (Complete scram 31-mer): K562 cells treated with 31nucleotide scrambled sequence. **(F)** Levels of cell death in BJ cells when treated with EVs and EV RNA. Y-axis indicates percent cell death observed. The following treatments are presented: (Untreated): BJ cells without any treatment, (Mock): BJ cells with Lipofectamine treated only (no RNA), (BJ EV RNA): BJ cells transfected with BJ EV RNA, (K562 EV RNA): BJ cells treated with K562 EV RNA, (BJ EV): BJ cells incubated with BJ EVs, (HeLa EV): BJ cells incubated with HeLa EVs, (U2-Os EV): BJ cells incubated with U2-Os EVs, (MCF7 EV): BJ cells incubated with MCF7 EVs, (K562 EV): BJ cells incubated with K562 EVs.

A. Net increase in cell death with 100 picomoles RNY5 31-mer treatment in primary and cancer cells (RNY5 treatment-Mock)

Cells	Rep1	Rep2	Mean
BJ	17.25	16.85	17.05
IMR90	8.9	9.4	9.15
HUVEC	14.7	13.5	14.1
HFFF (200picomoles RNY5 31-mer)	13.6	13.4	13.5
MCF7	0	0	0
HeLa	8.15	7.1	7.625
U2-Os	0.75	2.75	1.75
K562	0	2	1

B. Dose response (percent cell death) of RNY5 31-mer and Nonspecific RNA treatment in BJ cells

Sample	Rep1	Rep2	Mean
Untreated	1.3	1.6	1.45
Mock treated	2.6	2.5	2.55
Nonspecifiфc RNA 10picomoles	5.1	4.9	5
Nonspecific RNA 50picomoles	5.5	5.5	5.5
Nonspecific RNA 100picomoles	5.8	5.8	5.8
Nonspecific RNA 200picomoles	8.3	8.2	8.25
Nonspecific RNA 300picomoles	6.2	6.5	6.35
Nonspecific RNA 400picomoles	11.2	10.6	10.9
RNY5 31-mer10picomoles	6.4	6.5	6.45
RNY5 31-mer 50picomoles	8.8	9.1	8.95
RNY5 31-mer 100picomoles	12.2	12	12.1
RNY5 31-mer 200picomoles	23.8	22.3	23.05
RNY5 31-mer 300picomoles	30	29.6	29.8
RNY5 31-mer 400picomoles	40.9	40.5	40.7

C. Percent cell death in BJ cells with synthetic RNY5 31-mer and controls

Sample	Rep1	Rep2	Mean
Untreated	1.45	2.5	1.97
Mock treated	2.75	4	3.37
Allstar nonspecific RNA control	6	5.8	5.9
8 nucleotide motif deleted	5.3	4.8	5.05
Complementary side 32-mer	4.2	4.5	4.35
8 nucleotide motif scrambled	7.1	7.4	7.25
RNY5 completely scrambled 31-mer	6.6	7.9	7.25
Double stranded RNY5 31-mer	9.3	9.3	9.3
Full length RNY5	10.5	11	10.75
RNY5 31-mer	19.8	17.43	18.61
RNY5 23-mer	25.8	26.4	26.1

D. Percent cell death in K562 cells with synthetic RNY5 31-mer and controls

Sample	Rep1	Rep2	Mean
Untreated	9.2	10.5	9.85
Mock	9.7	10.5	10.1
8nt motif deleted	11.9	10.5	11.2
8nt motif scrambled	10.3	10.2	10.25
Allstar nonspecific RNA treated	11.6	9.7	10.65
31mer scrambled	8.9	8.8	8.85
Full length RNY5	9.8	9.5	9.65
Double stranded RNY5 31-mer	10.3	10.3	10.3
RNY5 31-mer	9.8	12.1	10.95

Table 4.3A: Levels of cell death observed with RNY5 treatment and control treatment of cells. (A) Net increase in percent cell death with 100picomoles of RNY5 31mer treatment of cancer and primary cells (RNY5 treatment - mock). **(B)** Dose response of RNY5 31mer (percent cell death) and nonspecific RNA control in BJ cells. **(C)** Percent cell death in BJ cells with synthetic RNY5 31mer and controls. **(D)** Percent cell death in K562 cells with synthetic RNY5 31mer and controls.

E. **Percent cell death observed in K562 cells when treated with K562 EVs and EV RNA**

Sample	Rep1	Rep2	Mean
Untreated	2.4	3.5	2.95
K562 EV treated	6.6	4.2	5.4
MOCK treated	4.4	4.3	4.35
K562 EV RNA treated	4.2	4	4.1
Complete scrambled 31-mer treated	3.5	4.5	4

F. **Percent cell death observed in BJ cells when treated with cancer and primary EVs and EV RNA**

Sample	Rep1	Rep2	Mean
Untreated	4	4.9	4.45
Mock treated	7.1	7.7	7.4
BJ EV RNA treated	10.3	10.9	10.6
K562 EV RNA treated	20	21	20.5
HELA EV treated	26.8	18.52	22.66
U2-OS EV treated	26.9	11.36	19.13
MCF7 EV treated	35.45	16.9	26.175
K562 EV treated	27.8	21.9	24.85
BJ EV treated	5.4	4.7	5.05

Table 4.3B: Levels of cell death observed in BJ and K562 cells with EV and EV RNA treatments. (E) Percent of cell death observed in K562 cells when treated with K562 EV and EV RNA. **(F)** Percent of cell death observed in BJ cells when treated with cancer and primary EV and EV RNA.

4.3.5. Genome-wide gene responses associated with EV and processed *RNY5*

Comparison of transcriptional profiles prior to and at 24 hours after treatment with EVs derived from K562 cells, as well as the synthetic version of the 31nt form of *RNY5* were made on two human primary cell lines (BJ and HUVEC). Of the 57,820 annotated genes in Gencode v19, we chose a two-fold cut off to characterize a gene as up or down-regulated, which put over 95% of the genes below this threshold and having a false discovery rate less than 0.05. In the case of BJ cells, 1,945 annotated genes were seen to be differentially expressed greater than two fold, 24 hours after EV treatment, while treatment with the synthetic 31nt oligonucleotide induced expression change in 1,238 genes. Interestingly, 569 genes were observed to be commonly differentially expressed both after EV or oligonucleotide treatment. Similarly, 24 hours after HUVEC cells were treated with EV or oligonucleotide, we observed 2,493 genes and 1,147 genes differentially expressed respectively, of which 385 genes were commonly differentially expressed. The large number of genes commonly differentially expressed after EV treatment and 5' 31nt treatment in both BJ and HUVEC, suggests that the 31nt *RNY5* fragment by itself was able to recapitulate a significant part of the changes caused by EVs.

Additionally, of the 1,238 genes and 1,147 genes that are differentially expressed after treatment with 5' 31nt in BJ and HUVEC cells respectively, 141 genes are commonly differentially expressed. A gene set over-representation analysis for GO pathways, with these commonly differentially expressed genes indicated significant enrichment of genes from pathways related to G2/M DNA replication checkpoints (p-value<6.51E-03), *POU5F1* (*OCT4*), *SOX2*, *NANOG* activate genes related to proliferation (p-value<1.72E-02), Activation of ATR in response to replication stress (p-value<3.17E-02) , *GRB7* events in *ERBB2* signaling (p-value<4.17x1 10^{-2}). In agreement with previous studies regarding cancer EV mediated cell death

in primary immune cells [370, 371] [372], we observed that transcriptional profiles of primary cells treated with EVs from cancer cells triggered differential expression of several genes associated with the *FAS/ TGF-β-Smad2/3* apoptotic pathway. These same genes were significantly altered both by treatment with EVs or oligonucleotides in both primary cell types tested (GO process – Signaling by TGF-beta Receptor Activating *SMADs* – EV treatment (p-value<4.4E-8, RNY5 treatment p-value<8.8E-3) (Figure 4.9). Also observable was the decrease in expression of the downstream *Ink 4b* which is a negative regulator of *cyclin E*, *cyclin A* and *CDK2,* and decreased expression of *SMAD2/3/4* re-enforcing the involvement of *RNY5* in the cell cycle (Figure 4.9). The absence of any potential cofactor accompanying the synthetic 31nt RNA, indicates that the RNA itself was sufficient to trigger the apoptotic phenotype (Figure 4.8C and Table 4.4.).

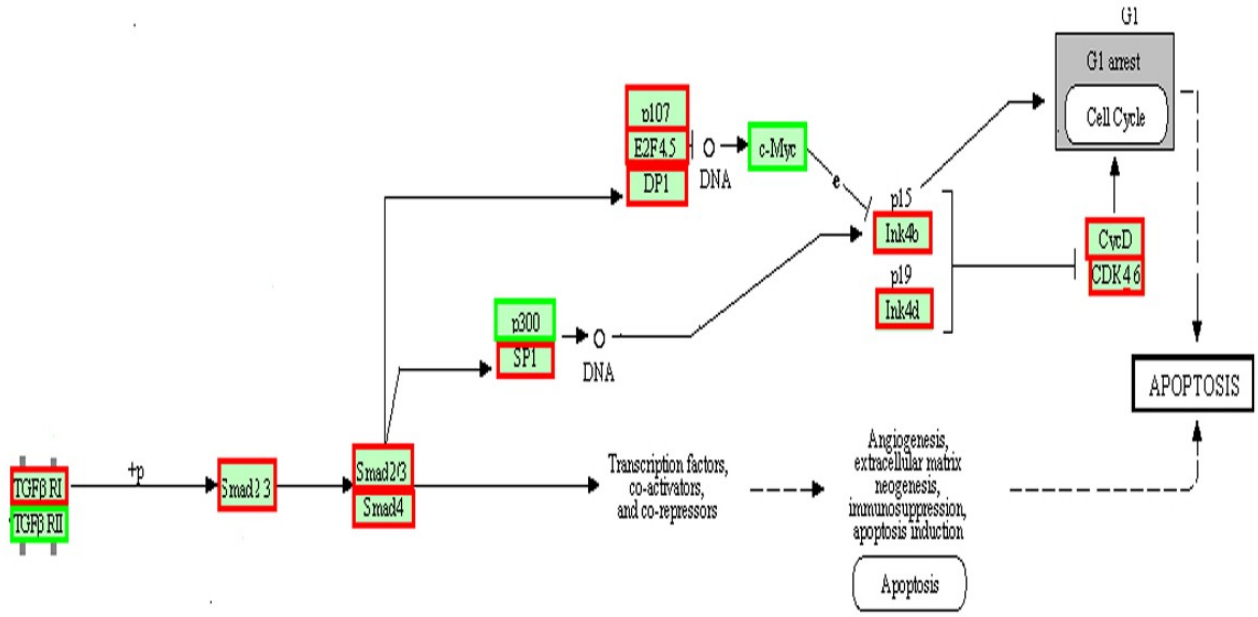

Figure 4.9: Differentially expressed genes in TGF-β pathway. The part of the TGF-β pathway depicted from KEGG pathways, where we observe similar changes in transcript levels of genes between both types of treatments (K562 EV and the 32 nucleotide synthetic RNY5 RNA) in both BJ and HUVEC cells. The schematic representation highlights a common response of transcript levels of most genes in this part of the pathway. Genes highlighted in Red box are downregulated while genes highlighted in green box is upregulated.

Fold change in genes within TGFβ pathway after treatment with K562 EV/32mer

		BJ		HUVEC	
Ensembl ID	Gene Name	EV	Y5 32mer	EV	Y5 32mer
ENSG00000011485	PP5	2.976875179	3.421057404	0.0676865	0.0084047
ENSG00000026103	FAS	4.656635422	2.048862289	0.009357006	0.563608352
ENSG00000034152	MKK3	0.09353015	0.0445025	0.0338432	0.0275619
ENSG00000060656	PTP	3.061930644	0.326981718	0.0338432	0.02029715
ENSG00000080839	p107	0	0.0171034	0	1.876965838
ENSG00000081189	MEF2C	0.117922946	1.08374729	0.583742961	0.421850359
ENSG00000099942	CRKL	0.175407565	0.31541529	4.121847102	0.442392244
ENSG00000100393	p300	3.197199574	3.231212849	0.164448822	4.850764805
ENSG00000100614	PP2CA	2.339504222	0.51617598	0.093728919	0.582309083
ENSG00000105173	CycE	0.0531801	0	0	2.380874956
ENSG00000105329	TGFB	2.058540504	1.693291308	0.131157533	0.403729161
ENSG00000105810	CDK6	4.544841922	2.544864042	0.025786698	12.85967948
ENSG00000105851	PI3K	0	0	0.00216821	0.0202628
ENSG00000106799	TGFBR1	0.191907325	0.308684282	0.217953267	1.018430748
ENSG00000108984	MKK6	0	1.743880337	0	0.01867215
ENSG00000110092	CycD	7.03248404	4.04805578	0.013477673	0.154756127
ENSG00000110395	CBL	5.852682073	1.616081412	0.021747473	0.149827381
ENSG00000111276	KIP1	0.464566725	2.858382611	0.641712284	4.832878577
ENSG00000112062	p38	3.576198214	7.138180358	0.328897645	2.043336133
ENSG00000116717	GADD45	4.831559762	0.547287857	2.056499589	1.847321473
ENSG00000117560	FASL	0	0	0	0
ENSG00000120129	MKP	0.229483538	0.390175081	0.138351762	0.297863431
ENSG00000123080	INK4C	0.613554654	1.582814268	0.152010301	2.406647683
ENSG00000123374	CDK2	6.12384958	6.836905194	0.082224316	1.471357954
ENSG00000124762	CIP1	4.745429033	3.980018471	0.132035636	3.616877976
ENSG00000125952	MAX	0.434920714	0.406949119	1.025513794	0.692645795
ENSG00000129355	INK4D	0.0198651	0.02980155	0	0.02029715
ENSG00000129757	KIP2	0.194830207	0.577973107	0.04777165	0.190159
ENSG00000132646	PCNA	0.0198651	0.059603	0	0.02029715
ENSG00000133740	E2F5	0.497752197	0.433805695	0.015289917	0.22448795
ENSG00000135446	CDK4	3.166250701	0.666385609	0.019019883	0.308141895
ENSG00000136997	c-MYC	10.50665047	5.430016103	0.059701521	2.688282508
ENSG00000141510	p53	1.98187379	3.096556868	0.0313505	0.269983647
ENSG00000141646	SMAD4	0.555839525	1.600218374	0.089552557	2.991030495
ENSG00000142208	AKT	3.356141175	1.42663778	0.018674131	0.21442243
ENSG00000145386	CycA	0.545009408	0.877365545	0.036757445	0.186117826
ENSG00000147883	INK4B	0.167797249	0.182268818	0.046117279	1.966090745
ENSG00000147889	INK4A	0.222979975	1.687551851	0.038680165	0.222069396
ENSG00000150907	FKHR	4.826340311	0.435969251	0.095522544	0.411308598
ENSG00000163513	TGFBR2	8.577095271	3.259840411	4.335404091	5.448230223
ENSG00000166949	SMAD3	0.23328192	0.299832248	0.187844567	0.32353526
ENSG00000167193	CRK	0.463050572	0.343327532	0.09405179	0.146491557
ENSG00000168229	DP1	0.0198651	0.0218838	0	0.02521415
ENSG00000175197	GADD153	1.612330178	1.296914308	0.014444114	0.231295431
ENSG00000175387	SMAD2	0.341380875	0.658706903	0.087181307	0.87631948
ENSG00000185591	SP1	0.20910152	0.244202591	0.0676865	0.03534555
ENSG00000197442	ASK1	0.290445158	2.056268419	0.08161495	0.0275619
ENSG00000204209	DAXX	6.911299992	1.936330232	0.046970451	0.251868988
ENSG00000205250	E2F4	0.287780212	0.110088552	0.016827566	0.724578517
ENSG00000253729	DNA-PK	0.273054769	0.51968317	0.163465453	2.415904373

Table 4.4: Fold change in genes within the TGF-β pathway after treatment of BJ and HUVEC cells with EV derived from K562 and the synthetic 5' 32 nucleotide fragment.

4.3.6. Evidence of primary cell targeting by cell to cell transfer

To determine if selective primary cell death caused by cancer cells present in equal numbers, co-culture of cancer and primary cells at 1:1 ratio (i.e. 2 x10^5 cells for each cell type) were carried out. Co-culture conditions were of two types, first involving cell to cell contact and second separate growth of each cell type in permeable trans-well culture conditions. Approximately four fold more cell death of primary cells (BJ) compared with untreated controls was observed in the cell to cell contact experiments (Figure 4.10). The results using a trans-well assay approach in which the primary and cancer cell populations were separated by approximately 1mm also demonstrated primary cell death, indicating that direct physical contact between cells and smaller volumes of media are not necessary for the occurrence of the phenotype.

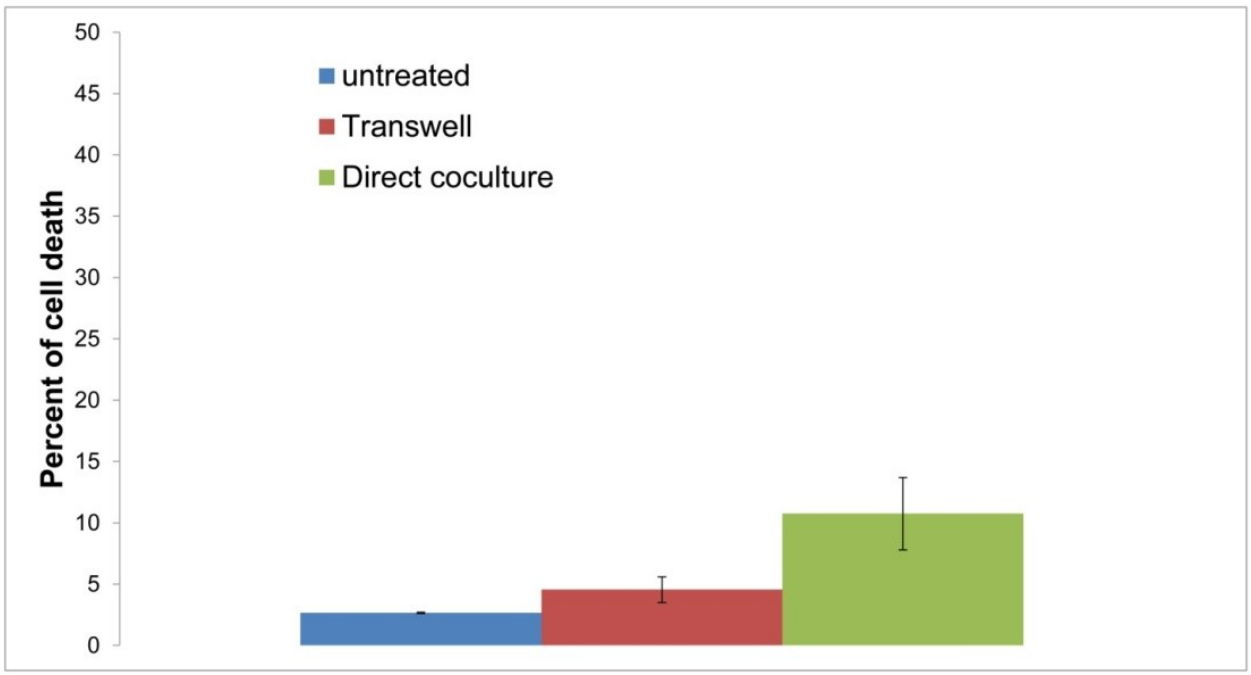

Figure 4.10: Quantification of cell death of BJ cells by co-culture with K562. Y-axis indicates the percent cell death. (Untreated): BJ cells grown without any treatment, (Transwell): Percent cell death observed in BJ cells when co-cultured with K562 cells across a Transwell membrane (1micron pore size) at 1:1 ratio, (Direct co-culture): Percent cell death observed in primary BJ cells when BJ cells are directly co-cultured in the same well with K562 cells at 1:1 ratio.

4.4. Discussion

In this study, a short non-coding RNA as component of EV cargo has been identified that can potentially play an important role in the cancer cell microenvironment. Specifically, a 31nt and 23nt processed fragments of *RNY5* has been identified as the most abundant and enriched RNA component of K562 and other cell type EVs. This processing of *RNY5* into smaller fragments likely occurs within EVs and represents the first example, in our understanding, of EV RNA processing specifically for extracellular utilization. Most importantly, using synthetic oligonucleotides based approach, we report that ectopic expression of 31nt processed fragments of RNY5 induce cell death in primary cells of multiple developmental origins in a dose dependent manner, but fail to elicit a similar response from cancer cells. Furthermore, we show that the response is mirrored when BJ cells are treated with K562 EV RNA alone as well as with K562 EVs. Finally, an eight nucleotide motif in both 31nt and a 23nt *RNY5* fragment has been identified as crucial for triggering cell death phenotype.

Single and double-stranded RNAs are well documented pathogen-associated molecular signals that are recognized by cytosolic receptors of the innate-immune system of many cell types during virus infection [373]. This recognition of exogenous RNAs can result in the activation of caspase-1 and subsequent apoptosis of affected cells [374]. Differentiation of endogenous from exogenous RNAs is partially based on the presence of 5' triphosphate or poly-uracil or adenylyl strings frequently found in RNA viral genomes [375]. The single stranded *RNY5* 31nt and 23nt processed sRNA lack these viral signals and are compartmentalized within vesicles. Interestingly, a double stranded version of the 31nt processed product triggers a substantially lower cell death phenotype, unlike that as is seen with the antiviral innate immune responses. The 83nt primary h*Y5* transcript which is reported to form a very stable hairpin

structure [376, 377] and thus likely rendering the 23nt and 31nt regions inaccessible, also triggers substantially lower cell death. Interestingly Gardiner, et al [345]and Wang et al [378] reported a double stranded version of the critical 8 nucleotides found in the *RNY5* sRNA (5'GUAGUGGG3') to be sufficient for RNY1 to support the initiation of DNA replication. However, in our studies it is clear that the *hY*5 31nt and 23nt processed products triggered cell death is attenuated in the presence of their complementary strands. Although Gardiner, et al did not report if a single-stranded version of this sequence was capable of supporting the initiation of replication, one possibility is that the single stranded 31nt and 23nt sRNAs cause inappropriate and perhaps uncontrolled DNA replication signals in primary cells, triggering cell death. Such processed *RNY5*-stimulated signals might be less effective in cancer cell lines given their characteristic loss of DNA replication controls inherent with transformed cells.

The results reported in this study prompt testable hypotheses for follow-on *in vivo* studies. While dose dependent cell death of primary cells by 5' *RNY5* 31nt fragment was observed, it is notable that not all exposed primary cells die. Different proportions of primary cells survive depending on the primary cell type and dosage used. These results appear to indicate that not all cultured cells are equally sensitive. Recent reports indicate that tumor-fibroblast interactions act in parallel to promote tumorigenicity and not all associated primary fibroblast cells may be involved in this co-operational activity [379] One testable hypothesis in future studies is to determine if the surviving primary cells after treatment with either cancer cell EVs or the 31nt processed product continue to fail to respond to the exposure of the 31nt or EVs or if they do provide support for tumor growth.

Although the 31nt and 23nt sRNAs are present in the EVs from both primary and cancer cells, exposure of EVs isolated from BJ cells did not trigger cell death in BJ cells. Increased

quantities of EVs released by cancer cells and relative abundance of processed *RNY5* transcripts in cancer cell derived EVs are likely to contribute to this differential response. An alternate possibility consistent with these results is different co-factors are associated with 31nt or 23nt *RNY5* fragments present in primary and cancer cell EVs.

Detailed understanding of the molecular mechanisms involved in 31nt *RNY5* induced cell death would be crucial in understanding the differential response by primary and cancer cells. These results also prompt us to investigate the protein binding partners of *RNY5* in cancer and primary cells as well as their respective EVs. Identification of *RNY5* binding proteins will not only provide us mechanistic insights of the observed response, but may also reveal the molecular mechanisms involved in specific sorting and processing of *RNY5* transcripts into EVs.

In the late 19th century Paget proposed the "seed and soil" hypothesis indicating that the microenvironment (soil) was key for tumor (seed) growth [380]. Increasingly, the importance of tumor microenvironment has been recognized as a key contributor for cancer progression and drug resistance [381-385]. It has been hypothesized that a component for establishing and maintaining supportive microenvironments are the contents of EVs [386]. Uncovering the functional role of processed RNY5 transcripts orchestrated through extracellular vesicles reveals an intricate competitive cell interaction mechanism, potentially involved in promoting the establishment of a microenvironment for the spread of tumor cells. While further studies are warranted to evaluate a possible *in vivo* role for the *RNY5* fragments in the tumor microenvironment, it raises an interesting possibility that *RNY5* fragment induced cell damage and lethality may also sensitize normal tissue to neoplastic cell invasion and metastasis by promoting cell removal and inducing inflammatory response.

4.5 Materials and methods

Isolation of Extracellular vesicles (EVs)

K562 cells were grown in complete RPMI1640 medium (10%FBS+1% Penicillin-Streptomycin) and BJ cells were grown in DMEM (10% FBS and 1%penicillin-streptomycin). When the cells reached approximately 70-80% confluence, the media is replaced with serum-free conditioned medium and incubated for another 24 hours. The Conditioned medium was then centrifuged at 300g for 10 minutes. The cell pellet was discarded and the supernatant was further centrifuged at 2000g for 10 minutes. The Pellet, comprising of mostly cell debris and apoptotic bodies was discarded and the supernatant was again centrifuged at 10000g for 30 minutes. The pellet, comprising of microvesicles was discarded and the supernatant was filtered at 3500g for 15 minutes using Centricon Plus70 100KD NMWL cut-off (Millipore). The filtrate was discarded and the residue, enriched with EVs and other proteins was collected. The collected residues were precipitated overnight using ExoQuick-TC (System Biosciences) at 1:5 ratio (by volume) of Exo-quick to filtration residue. Next morning, the sample was centrifuged at 1500g for 30 minutes. The supernatant was discarded and the pellet was centrifuged again at 1500g for 5 minutes. Left over supernatant, if any, was discarded and the pellet and re-suspended in 500 microliter PBS.

Electron microscopy

Negative staining of EV suspensions followed by imaging in a transmission electron microscope was used to determine vesicle shape and size distribution. Aliquots of EV suspensions were dispensed onto sheets of Parafilm in a humidified petri dish and the vesicles were adsorbed onto freshly prepared Butvar coated EM grids (glow discharged). The adsorption

was done for 5 minutes at room temperature. The petri dish containing the suspensions and EM grids was transferred to a large bucket of ice shavings and the grids were transferred to three successive drops of distilled water (30 seconds each) to remove salts, and then transferred to a drop of 1% uranyl acetate in 1% methyl cellulose for 30 seconds and then placed in a second drop of negative stain solution for 5 minutes. Excess stain was blotted off and the grids were air dried.

Immuno-gold labeling for the CD81 was done by re-suspending the EVs in primary mouse antibody to human CD81 (Abcam) diluted in PBS for 30 minutes at room temperature. Incubations were done in sterile 1.5 mL micro centrifuge tubes. The antibody labeled vesicles were pelleted by centrifugation, re-suspended in a 1:10 solution of 5nm colloidal gold conjugated to rabbit anti-mouse IgM secondary antibody (Aurion, Electron Microscopy Sciences) for 30 minutes. The gold labeled vesicles were then adsorbed to Butvar-coated grids for 5 minutes and then rinsed through 3 drops of PBS to remove unbound gold particles. Negative staining of the gold labeled vesicles was completed at described above.

Samples were imaged in the Hitachi H7000 Electron Microscope operated at 75kV. Images recorded on Kodak EM film 4489 were scanned at 2400 DPI on an Epson Perfection V750 film scanner.

Western Blot

Proteins were isolated using RIPA buffer (Pierce) using manufacturer's protocol, concentrated using Amicon Ultra 3K centrifugal filter (Millipore) and quantified using BCA protein quantification kit (Pierce). 1microgram of proteins from K562 whole cell and EVs were loaded on pre-cast 4-20% Tris-Glycine gel (Life Technologies) and transferred to PVDF

membrane. Membrane was blocked using Pierce TBST blocking buffer (Cat. no. 37571) for 1 hour at room temperature. Primary antibody incubation was performed overnight at 4deg at 1:1000 dilutions while secondary antibodies were used at 1:10000 dilutions. Membranes were developed with Amersham ECL plus western blotting development kit (GE). Anti-Fibrillarin (Abcam, cat. no. ab18380), Anti-Protein disulphide Isomerase (Abcam, cat. no. ab2792) and Anti-Prohibitin (Abcam, cat. no. ab28172) was used as nuclear, endoplasmic reticulum and mitochondrial marker, respectively. Anti-PDC6I (Abcam, cat. no. ab88743), Anti-Tsg101 (Abcam, cat. no. ab83) and Anti-Transferrin receptor (Abcam, cat. no. ab84036) were used as EV marker. Goat polyclonal to Rabbit IgG (Abcam, cat. no. ab6721) and Rabbit polyclonal to Mouse IgG (ab 6728) were used as secondary antibodies.

NTA

Quantification of the extracellular vesicles was performed by Nanoparticle Tracking Analysis (NTA) was performed using NanoSight LM10 at 25 degrees Celsius. PBS was used as a diluent and samples were run at 1:500 dilutions for K562 EVs and 1:5 dilutions for BJ EVs.

Isolation of RNA

RNA isolation was performed using Ambion's Mirvana miRNA Isolation kit (cat. no.AM1560) using manufacturer's protocol. Prior to RNA isolation, EVs were treated with Ambion RNase cocktail (cat. no.AM2286) at 37 degrees for 15 minutes. 1ml of lysis/binding buffer was immediately added to the RNAse treated EVs to deactivate the RNAse.

Detergent and RNAse treatment

To determine if the isolated RNA were true EV RNA cargo and not any artifact of purification, RNA isolate from EVs without RNase treatment was compared with RNA isolate from RNAse treated EVs and RNA isolate from detergent and RNase treated EVs. RNase treatment of EVs re-suspended in PBS was performed with Ambion RNase cocktail at 37degrees for 15 minutes. Detergent treatment was performed with RIPA buffer for 15 minutes followed by RNase treatment as described above.

Small RNA Sequencing

Small RNA was isolated with Mirvana miRNA isolation kit (Life Tech) and DNase treated with Ambion Turbo-DNase (Life Tech). Ribosomal RNA depletion was performed on Whole cell RNA using Eukaryote Ribominus kit (Life Tech) using manufacturer's protocol. Both EV and whole cell RNA was treated with Tobacco Acid Pyro-phosphatase (Epicenter) to make 5' capped and tri-phosphate RNAs amenable to adapter ligation. Libraries were constructed using Illumina TruSeq small RNA kit according to manufacturer's protocol, except reverse transcription was performed using Superscript III. Amplified libraries were run on 2% agarose gel and 20-200nts region was cut and gel-purified with Qiagen gel extraction kit. Libraries were quantified on Agilent Bio-analyzer HS-DNA chip and sequenced on Illumina HiSeq2000.

Long RNA Sequencing

Long RNA was isolated with Mirvana miRNA isolation kit and DNase treated (Ambion, cat. no.AM2238) using manufacturer's protocol. Construction of complementary-DNA libraries was performed using Illumina TruSeq stranded total RNA kit (cat. no.RS-122-2201). Libraries

were quantified using Agilent Bioanalyzer HS-DNA chip and run on Illumina Hi-Seq 2000 platform.

Bioinformatics Analyses

All data from RNA sequencing experiments in the study were mapped to Human Genome version 19 (hg19, GRCh37) obtained from the UCSC genome browser website (http://hgdownload.cse.ucsc.edu/downloads.html). RNAseq reads were aligned using the STAR v1.9 [318] software, and up to 5 mismatches per alignment were allowed. Only alignments for reads mapping to 10 or fewer loci were reported. Annotations were not utilized for mapping the data. The obtained BAM files were further processed using HTSeq [319]software in order to appropriate the number of reads originating from each annotated regions of the genome, utilizing annotations obtained from Gencode v19 [320] of the human genome, using the "Union mode" option of the software for all libraries, tRNA annotations were obtained from tRNAscan database [321]. Reads per million (rpm) values for each gene was obtained by dividing the number of reads uniquely mapping within the limits of a gene annotation, by the total number of uniquely mapping reads in the library and multiplying by a million. These rpm values were used between replicates in Supplementary figures 4.3 to establish correlation between biological replicates of EV RNA libraries. Relative abundance of RNA families in figures 4.4 was calculated using the cumulative rpm values of all genes within the Gencode defined RNA families such as miRNA, snoRNA, miscellaneous RNA (miscRNA), protein coding etc. Within each pie chart in figure 2, the group termed as "Others" includes Gencode all categories other than lincRNA, miRNA, miscRNA, rRNA, tRNA, snRNA, snoRNA and protein coding genes, (such as 3prime_overlapping_ncrna, immune-globulin genes, mitochondrial tRNA, mitochondrial rRNA, anti-sense RNA, antisense, pseudogenes, T-cell receptor genes, sense-intronic, sense-

overlapping genes etc.). Density plots in supplementary figures 4.5 were obtained by calculating the ratio of rpm within EVs to the sum of rpms within EVs and whole cell for both K562 and BJ cells. The density function for genes of each RNA family within these graphs was calculated from these ratios using the kernel density function within the R stats package.

Fragment analysis to identify the most commonly found fragments within the RNY5 gene was found by taking into account start and end positions of all reads that mapped to the RNY5 gene from chromosome 7 between position 148638580 and 148638658 in the positive strand. All reads which began at the 5' end of RNY5 gene and were greater than 29 nucleotides in length mapped uniquely to RNY5 gene. Similarly reads that began in places other than the 5' end of the RNY5 gene mapped uniquely to the genes primary location on chromosome 7. However genes which started in the 5' end of the gene and were 29 nucleotides in length or shorter were all multi-mappers and mapped with 100% identity to two other locations (chromosome 12:45581224-45581252 and chromosome 13:103472349-103472369) and 97% identity to few other locations (chromosome 12:98223788-98223816, chromosome 19:36540048-36540076, and chromosome 1:35893466-35893493), thus making it impossible to accurately establish the true origin of these reads absolutely. These locations are annotated as pseudogenes of the RNY5 gene, and to resolve this uncertainty of their origin we included them for the fragment analysis. The secondary structure of RNY5 was obtained using the online resource of the Mfold package [387], within which the most frequently occurring fragments were highlighted.

In order to identify genes which are differentially expressed (DE) between time points for the molecular phenotype section, bio-replicates from time points 2, 6 and 24 hours after treatment with EVs were compared to the untreated replicates, by using DESeq [348]on the read counts of the genes derived from the HTSeq software, filtering by false discovery rate (FDR) less

than 0.01 and by fold-change greater than or equal to 2 or less than or equal to 0.5. The fold change at the time point of maximal change was then taken into account as the maximal amplitude of change for each gene. The list of DE genes common between the two cell types on treatment with K562 EVs and the list of DE genes common between the two cell types after 5' 32mer treatment were then used for further over-representation analysis on the GO biological processes using the online resource of Panther Pathways [388], where only biological processes with a p-value less than 0.05 was taken to be significant. The list and map of genes within the FAS/TGF-β pathway was obtained from KEGG pathways [389], and those genes within out DE gene lists were overlaid on the map, where red color indicates a fold change below 0.05, and green indicates fold change greater than 2, and blue indicates no significant fold change after treatment in each cell type.

Lipid labeling of EVs & Imaging

K562 EVs were isolated as described above. 2 microliter of PKH67 (Sigma, cat. no.MINI67-1KT) was re-suspended in 500microliter diluent and added to purified EVs for 4 minutes in dark and EVs were isolated using Exoquick-TC as described above. The labelled EV pellet was re-suspended in complete medium (DMEM +10% FBS+1% Penicillin-Streptomycin) and added to BJ cells for overnight incubation. Imaging was done on Delta-vision OMX microscope and image analysis was performed with Delta-vision SoftWorx software.

Metabolic labeling of RNA & Imaging

K562 cells (2+E7) were incubated at a final concentration of 0.2milliMolar 5- Ethnyl uridine (EU) for 24 hours. EVs were isolated from the conditioned medium as described above. 3T3 cells were treated with ActinomycinD at a final concentration of 1microMolar for 1 hour to

block its endogenous transcription. The drug-treated media was replaced with fresh complete DMEM medium and the cells were incubated with EU labeled K562 EVs for 2 hours. The cells were subsequently fixed with 4% Para-formaldehyde and permeabilized with 0.5% Triton-X-100. EU incorporated EV RNA was detected using Click chemistry according to manufacturer's protocol (Life Tech, cat. no. C10329) and nuclei was counterstained using Hoechst 33342. Finally, cells were imaged on Delta-vision OMX microscope and image analysis was performed with Deltavision SoftWorx. As a negative control, 3T3 cells treated with ActinomycinD and directly incubated with EU was performed which showed no signal of EU-incorporated RNA thus confirming block of endogenous transcription (data not shown).

Subcellular localization of RNY5 31-mer:

2+E5 BJ cells were plated overnight and next morning cells were transfected with100picomoles of synthetic RNY5-31mer coupled with Alexa 488 fluorophore at its 3' end. After 6 hours, transfection medium (Opti-MEM) was replaced with complete DMEM medium and incubated for another 24 hours. Imaging was performed on Delta-Vision OMX microscope and Image processing was performed with Delta-vision SoftWorx software.

Interspecies transfer of RNA by RNA-Seq

Mouse HB4 cells (ATCC) were treated with K562 EVs for 0, 12 and 24 hours and HB4 cells untreated (Neg. control) and RNA isolation was performed using Mirvana miRNA isolation kit. Isolated RNA was ethanol-precipitated, DNase treated and size separated into long (>200 nucleotides) and short RNA (<200 nucleotides). The short RNA was ribo-depleted using Ribo-minus Eukaryote ribo-depletion kit (Life Tech) using manufacturer's protocol and ethanol precipitated. The precipitated RNA was then treated with Tobacco Acid Pyro phosphatase

(Epicenter) at 37 degrees for 1 hour to convert the 5' capped and triphosphate RNA molecules into 5' monophosphate and make them amenable for adapter ligation. RNA was then purified by phenol-chloroform treatment followed by ethanol precipitation. The Small RNA libraries were then constructed using A-tailing protocol as described in [349]. .The amplified libraries were then run on 2% agarose gel and the region between 20-200 nucleotides was cut and gel extracted with Qiagen gel extraction kit. Finally, libraries were quantified using Agilent Bioanalyzer and sequenced on Illumina MiSeq platform. Mapping was performed by STAR against combined Human and Mouse genome and reads which mapped uniquely to humans only were considered for analysis. RNY5, a human specific gene enriched in EVs was used as a marker to demonstrate inter-species transfer of human K562 EV RNA to Mouse HB4 cells.

Oligonucleotide end-labeling

Oligonucleotides (90pmol for DNA oligonucleotides and 15pmol for RNA oligonucleotides) were end-labeled in reactions containing 20 μCi of γ-^{32}P-ATP (PerkinElmer), 5 units T4 polynucleotide kinase (New England BioLabs), 70mM Tris-HCl pH 7.6, 10mM $MgCl_2$, and 5mM dithiothreitol (DTT). Labeling proceeded for 30 minutes at 37°, followed by phenol-chloroform extraction.

Northern blots

Whole cell total RNA and EV RNA from K562 and BJ cells (850 ng each) was separated on 8% acrylamide, 8 M urea gels. Thereafter, the RNA was blotted to nitrocellulose membranes (Zeta-Probe, Bio-Rad). The blots were probed with an oligonucleotide complementary to the 5' end of the RNY5 transcript (5'- CTT AAC AAT AAC CCA CAA CAC TCG GAC CAA CT -3').

***In-vitro* processing**

K562 Whole cell and EV proteins were extracted with RIPA buffer (Thermo Scientific). Cold processing reactions contained the indicated amount of protein, 10mM $MgCl_2$, 10mM DTT and 2pmol synthetic full length RNY5 RNA where indicated. After 30 minutes incubation at 37°, reactions were phenol-chloroform extracted, separated on 8% acrylamide, 8M urea gels, then blotted and probed as described for northern blots. Hot processing reactions were performed with synthetic versions of wild type RNY5 5' 31-mer, shuffled 31-mer (5'- UGG UGC GUG UUG UUU AGA UUA AGU GGU UGA C -3') or RNY5 31-mer with the 8 nt motif shuffled (GUUGUGGG→ACGUACAG). Each reaction contained 4 μg of K562 EV protein extract where indicated, 10mM $MgCl_2$ and 0.15pmol of end labeled RNA. After 2 hours incubation at 37°, samples were separated on 8% acrylamide, 8 M urea gels. Thereafter, the gels were subjected to autoradiography.

RNA Transfection

2+E5 cells were plated in 6-well plates overnight. Next day, RNA transfection was performed with Lipofectamine 2000 and Opti-MEM medium for 6 hours according to manufacturer's protocol. After 6 hours, Opti-MEM media was replaced with complete medium and cells were incubated for another 24 hours.

Flow cytometry

Quantification of cell death was performed on a BD LSR-II Cell Analyzer (BD Biosciences, San Jose, CA) using a flow cytometry kit that detects membrane permeability, chromatin condensation and dead cell apoptosis (Life Tech, cat. no.V23201). YO-PRO-1 was excited by the 488nm laser and its emission was collected with a 530/30 filter. A 405nm Violet

laser was used to excite Hoechst 33342 and emission was collected with a 440/40 filter. Unstained cells and single color control samples (YO-PRO-1 only and Hoechst33342 only) were used for setting the PMT voltages and eliminating any spectral overlap between these two fluorochromes. Only events positively labeled with Hoechst33342 were considered for quantification. Cells double-labeled with Hoechst33342 and Yo-Pro-1 were quantified as "dead cells" and cells labeled with Hoechst33342 but not with Yo-Pro-1 was quantified as "living cells".

YO-PRO1, a nucleic acid binding dye which is permeable to apoptotic and dead cells but not living cells was used for quantification of cell death. Briefly, cells were trypsinized and re-suspended in 800microliter DMEM medium. Cells were labeled with 1microliter of YO-PRO1 and Hoechst 33342 for 15 minutes at room temperature. The labeled cells were kept on ice and then passed through a cell strainer prior to running on the LSR-II.

EVs incubation with cells and cell death quantification

EVs were isolated from 1+E8 cancer (K562, HeLa, U2-Os, and MCF7) or primary (BJ) cells as explained above and incubated with BJ or K562 cells for 24 hours. After 24 hours, quantification of cell death was performed by flow cytometry as explained above.

EV RNA transfection and quantification of cell death

EV RNA was isolated from K562 and BJ EVs in duplicates with Mirvana miRNA isolation kit as explained above. RNA transfection was performed with Lipofectamine2000 and Cell death quantification was performed after 24 hours incubation by flow cytometry as described above.

Synthetic ribonucleotides transfection and cell death quantification

2+E5 BJ or K562 cells were plated overnight and next day, cells were transfected with 100Picomoles of RNY5 31-mer and 100picomoles RNY5 23-mer with 5microliter lipofectamine2000 in Opti-MEM medium. After 6 hours, Opti-MEM media was replaced with complete DMEM media (for BJ) or complete RPMI1640 medium (for K562). Untreated and Mock treatment was used as negative controls. AllStars negative control siRNA was used as non-specific RNA control. A 31nucleotide scrambled RNA oligo was used as a scrambled RNA control. Furthermore, RNA oligonucleotides with 8nt motif (nucleotides14-21) scrambled, scrambled with secondary structure intact and 8nt motif deleted oligonucleotide were used as controls for identifying the motif sequence responsible for phenotype. Finally, transfection of 83nucleotide full length RNY5 and a double stranded RNY5 31-mer shows substantially lower cell death.

Generality of the phenotype

Generality of RNY5 31-mer mediated cell death phenotype was assessed in 4 cancer (K562, HeLa, U2-Os and MCF7) and 4 primary cells (BJ, HUVEC, IMR90 and Human fetal foreskin fibroblast (HFFF)). In each case, 2+E5 cells were plated overnight. Next day, cells were transfected with100Picomoles of synthetic RNY5 31-mer (except HFFF, which was transfected with 200Picomoles of RNY5) and 5microliter Lipofectamine2000 as described above. Cell death quantification was performed after 24 hours incubation as described above.

Dose response curve of RNY5-31mer

Transfection of BJ cells was performed with RNY5 31-mer and Qiagen AllStars negative control siRNA (non-specific RNA control) in a dose dependent manner. Briefly, 2+E5 cells were

plated overnight and on the following day, cells were transfected with RNY5-31mer (10, 50,100, 200, 300 and 400Picomoles) or AllStars control (10, 50,100, 200, 300 and 400Picomoles) with 10microliter Lipofectamine in Opti-MEM medium. Both Untreated and Mock treated (Lipofectamine only) was also performed as negative controls. After 6 hours, media was replaced with complete DMEM medium and incubated for another 24 hours. Quantification of cell death was performed as described above.

Co-culture and cell death quantification:

Co-culture of K562 and BJ cells were performed both as direct co-culture as well as transwell co-culture. In direct co-culture system, 2+E5 BJ cells were plated on 6 well plates and next day, cells were labeled with Hoechst33342 for 15 minutes in dark at 37deg. Cells were washed with thrice with PBS and replaced with complete DMEM medium. 2+E5 K562 cells re-suspended in 2ml RPMI1640 medium were added to the same well and directly co-cultured with BJ cells. As negative control, BJ cells were grown alone in 2ml DMEM +2ml RPMI1640 medium. After 24 hours, both cells were harvested together but were only labeled with YO-PRO-1. Quantification of cell death was performed by flow cytometry as described above. Since K562 cells, although present in the solution were not labeled with Hoechst 33342, Hoechst33342 and YO-PRO-1double labeled cells were quantified as “dead BJ cells” while Hoechst 33342 positive but YO-PRO-1negative cells were quantified as “living BJ cells”.

In Transwell co-culture system, 2+E5 BJ cells were plated at the bottom of the well. Next day, 2+E5 K562 cells were plated in RPMI medium in the same well but across a Transwell membrane (Corning, 1micron pore size). After 24 hours, K562 cells on top of the membrane

were discarded while the BJ cells on the well were labeled with YO-PRO-1 AND Hoechst33342 and flow cytometry was performed for quantification as described above.

Synthetic RNA oligonucleotides sequences

RNY5 31-mer: 5’-rArGrU rUrGrG rUrCrC rGrArG rUrGrU rUrGrU rGrGrG rUrUrA rUrUrG rUrUrA rA-3’

RNY5 23-mer: 5’-rArGrU rUrGrG rUrCrC rGrArG rUrGrU rUrGrU rGrGrG rUrU-3’

RNY5 31nucleotide complete scrambled: 5'- rUrGrG rUrGrC rGrUrG rUrUrG rUrUrU rArGrA rUrUrA rArGrU rGrGrU rUrGrA rC -3'

RNY5 8nucleotide motif deleted: 5’-rArGrU rUrGrG rUrCrC rGrArG rUrUrU rArUrU rGrUrU rArA-3’

RNY5 31-mer with 8 nucleotide motif scrambled: 5’-rArGrU rUrGrG rUrCrC rGrArG rUrArC rGrUrA rCrArG rUrU rArUrU rGrUrU rArA-3’

RNY5 32-mer complementary (3’ side) fragment: 5’-rCrCrC rCrArC rArArC rCrGrC rGrCrU rUrGrA rCrUrA rGrCrU rUrGrC rUrGrU rUrU-3’

Full length RNY5 83-mer: 5’-rArGrU rUrGrG rUrCrC rGrArG rUrGrU rUrGrU rGrGrG rUrUrA rUrUrG rUrUrA rArGrU rUrGrA rUrUrU rArArC rArUrU rGrUrC rUrCrC rCrCrC rCrArC rArArC rCrGrC rGrCrU rUrGrA rCrUrA rGrCrU rUrGrC rUrGrU rUrU-3’

Double-stranded RNY5 31-mer:

5'-rArGrU rUrGrG rUrCrC rGrArG rUrGrU rUrGrU rGrGrG rUrUrA rUrUrG rUrUrA rArG-3'

5'-rCrCrC rCrArC rArArC rCrGrC rGrCrU rUrGrA rCrUrA rGrCrU rUrGrC rUrGrU rUrU-3'

Chapter 5

Conclusions and Significance

In this study, we examined if EV mediated transfer of RNA between cells satisfies the requirements for a medium of intercellular communication. To that end, we first developed and validated a novel and efficient method of isolation of EVs which unifies the reported advantages of multiple existing methods into one 'hybrid' method. A comparative analysis revealed that our hybrid method consistently provides higher yield of EVs and EV RNA than currently existing approaches. Importantly, our hybrid approach not only detects RNA molecules with excellent reproducibility within replicates, but is also highly consistent with existing methods of EV isolation, satisfying a crucial property for its potential future application for identification of biomarkers. Armed with this approach, we performed a comprehensive characterization of the diverse RNA cargo in EVs from nine different cell types of diverse developmental origin which revealed a non-random and cell type specific sorting of RNA messages into EVs. Our study further revealed gene family specific processed fragments of non-coding RNAs in EVs. Next, we investigated the subcellular localization and temporal kinetics of EV RNA transfer and demonstrated the transferred RNA molecules are intact and detectable up to 48 hrs. We further established the context dependent dynamicity of EV RNA cargo and its ability to elicit distinct molecular response in different cells in a cell type specific manner. While previous studies have focused on the functionality of micro-RNAs and messenger RNAs transferred through EV, we investigated the possible functionality of the 31nt processed RNY5 molecule, one of the most abundant and enriched RNA transcript in K562 and other cell type derived EVs. We observed that incubation of K562 EV as well as its de-proteinized total EV RNA, induced cell death in

primary BJ fibroblasts, but failed to elicit a similar response from K562 cells themselves. Then, we recapitulated the cell death phenotype by treating BJ cells with synthetic 31nt RNY5 alone in a dose dependent manner. Moreover, the 31nt RNY5 induced cell death phenotype was not limited to BJ cells, and was demonstrated in multiple primary cells of diverse developmental origins. Finally, we identified an 8 nucleotide motif in the 5' 31nt processed RNY5 molecule required for its functionality. These results are consistent with the suggestion that 31nucleotide processed RNY5 fragment may play a functional role through cancer cell derived EVs and in conclusion, supports the hypothesis that EVs mediated transfer of RNA between cells represents a novel medium of intercellular communication.

At least five aspects of this study reflect significant progress in the field of EV mediated communication. Firstly, our results indicate miscellaneous RNAs (especially Y RNAs) and t-RNAs are the major components of the RNA cargo encapsulated in EVs. By comparison, microRNAs and messenger RNAs fragments comprise only a small proportion of EV RNA cargo. Yet, previous studies have focused their interest in exploring the possible functionality of microRNAs and messenger RNAs because of a better understanding of their biological importance. To the best of our knowledge, 31nt RNY5 induced cell death of multiple primary cells not only represents a novel function of a processed fragment of a non-coding RNA, but represents the first evidence of possible functionality of EV RNA beyond microRNAs and messenger RNAs. Our results also indicate the abundance of various processed and full-length non-coding transcripts in EVs, the functional role of which remain as yet unexplored. The use of synthetic oligonucleotides represents a powerful approach for discovering the unknown functions of noncoding RNAs and in future, may reveal the functions of other noncoding RNAs detected within EVs.

Secondly, transfer and uptake of EVs has been reported to induce various cellular phenotypes in recipient cells, including tumor stromal interactions, induction of angiogenesis, metastasis, transfer of oncogenic activity, developmental gradient formation, antigen presentation, immune evasion and host pathogen interactions to name a few. Few of these studies have successfully identified the biomolecule in EVs responsible for the observed cellular response. These results tempt us to investigate the role of EV RNA cargo and its potential involvement in causing these cellular phenotypes in these systems.

Thirdly, transfer and functionality of processed RNY5 molecules through cancer cell derived EVs may play an important role in tumor microenvironment. Such competitive cell interactions between tumor and normal cells may remodel its microenvironment to favor the proliferation of the tumor and enrich it with nutrients required for its growth and proliferation. Transfer of 31nt RNY5 through tumor derived EVs may also induce apoptosis in immune cells present in its microenvironment. Similar to our observations, it has been reported that tumor derived EVs induce apoptosis in immune cells but not in cancer cell themselves, and the 'FasL' protein present in tumor derived EVs has been reported to be the molecule responsible for this phenotype. Our observation of RNY5 induced lethality of primary cells of distinct developmental origins, but not cancer cells, therefore has strong parallels with these previously reported observations of tumor EVs mediated apoptosis of immune cells and may represent yet another mechanism of immune evasion employed by tumor cells. These results also raise an interesting possibility that RNY5 processed fragment induced cell damage and lethality may sensitize normal tissue to neoplastic cell invasion and metastasis by promoting cell removal and induce inflammatory response. While further studies are necessary to evaluate a possible *in vivo* role for the RNY5 fragments in the tumor microenvironment, targeted knock out experiments of

RNY5 gene with CRISPR-CAS technology in future may provide more definitive evidence and reveal the extent of RNY5 functionality through EVs. Nevertheless, our study underscores the importance of EV RNA in a tumor's interactions with its microenvironment and prompt us to investigate the role of other RNAs enriched in cancer cell derived EVs in the context of tumor microenvironments.

Fourthly, the identification of unique and cell type specific RNA signature in EVs forms the basis of their proposed application as biomarkers. In future, similar identification of RNA signatures in EVs from patient derived body fluids using our hybrid approach may allow us to identify novel and minimally invasive biomarkers for various patho-physiological conditions, including cancer.

Finally, these results encourage us to investigate the molecular mechanisms underlying the specific sorting and enrichment of RNA molecules to EVs which may allow us to target our RNA of interest into EVs, a crucial requirement for its potential application in therapeutics and drug delivery. Further studies focused on uncovering the molecular mechanisms underlying the processing of various classes of non-coding RNA may reveal previously unknown layers of regulation of non-coding RNA and EV biology.

Chapter 6

Bibliography

1. Nakanishi, S., *Molecular mechanisms of intercellular communication in the hormonal and neural systems.* IUBMB Life, 2006. **58**(5-6): p. 349-57.
2. Pankov, Y.A., *Hormones as life regulators in the current molecular endocrinology.* Biochemistry (Mosc), 1998. **63**(12): p. 1361-73.
3. Goodenough, D.A. and D.L. Paul, *Gap junctions.* Cold Spring Harb Perspect Biol, 2009. **1**(1): p. a002576.
4. Herve, J.C. and M. Derangeon, *Gap-junction-mediated cell-to-cell communication.* Cell Tissue Res, 2013. **352**(1): p. 21-31.
5. Gyorgy, B., et al., *Membrane vesicles, current state-of-the-art: emerging role of extracellular vesicles.* Cell Mol Life Sci, 2011. **68**(16): p. 2667-88.
6. Turturici, G., et al., *Extracellular membrane vesicles as a mechanism of cell-to-cell communication: advantages and disadvantages.* Am J Physiol Cell Physiol, 2014. **306**(7): p. C621-33.
7. Colombo, M., G. Raposo, and C. Thery, *Biogenesis, secretion, and intercellular interactions of exosomes and other extracellular vesicles.* Annu Rev Cell Dev Biol, 2014. **30**: p. 255-89.
8. Chargaff, E. and R. West, *The biological significance of the thromboplastic protein of blood.* J Biol Chem, 1946. **166**(1): p. 189-97.
9. Wolf, P., *The nature and significance of platelet products in human plasma.* Br J Haematol, 1967. **13**(3): p. 269-88.
10. Kim, D.K., et al., *EVpedia: a community web portal for extracellular vesicles research.* Bioinformatics, 2015. **31**(6): p. 933-9.
11. Kalra, H., et al., *Vesiclepedia: a compendium for extracellular vesicles with continuous community annotation.* PLoS Biol, 2012. **10**(12): p. e1001450.
12. Caby, M.P., et al., *Exosomal-like vesicles are present in human blood plasma.* Int Immunol, 2005. **17**(7): p. 879-87.
13. Keller, S., et al., *Body fluid derived exosomes as a novel template for clinical diagnostics.* J Transl Med, 2011. **9**: p. 86.

14. Pisitkun, T., R.F. Shen, and M.A. Knepper, *Identification and proteomic profiling of exosomes in human urine.* Proc Natl Acad Sci U S A, 2004. **101**(36): p. 13368-73.
15. Street, J.M., et al., *Identification and proteomic profiling of exosomes in human cerebrospinal fluid.* J Transl Med, 2012. **10**: p. 5.
16. Marzesco, A.M., et al., *Release of extracellular membrane particles carrying the stem cell marker prominin-1 (CD133) from neural progenitors and other epithelial cells.* J Cell Sci, 2005. **118**(Pt 13): p. 2849-58.
17. Keller, S., et al., *CD24 is a marker of exosomes secreted into urine and amniotic fluid.* Kidney Int, 2007. **72**(9): p. 1095-102.
18. Gyorgy, B., et al., *Improved flow cytometric assessment reveals distinct microvesicle (cell-derived microparticle) signatures in joint diseases.* PLoS One, 2012. **7**(11): p. e49726.
19. Skriner, K., et al., *Association of citrullinated proteins with synovial exosomes.* Arthritis Rheum, 2006. **54**(12): p. 3809-14.
20. Gould, S.J. and G. Raposo, *As we wait: coping with an imperfect nomenclature for extracellular vesicles.* J Extracell Vesicles, 2013. **2**.
21. Thery, C., M. Ostrowski, and E. Segura, *Membrane vesicles as conveyors of immune responses.* Nat Rev Immunol, 2009. **9**(8): p. 581-93.
22. Thery, C., L. Zitvogel, and S. Amigorena, *Exosomes: composition, biogenesis and function.* Nat Rev Immunol, 2002. **2**(8): p. 569-79.
23. Harding, C., J. Heuser, and P. Stahl, *Endocytosis and intracellular processing of transferrin and colloidal gold-transferrin in rat reticulocytes: demonstration of a pathway for receptor shedding.* Eur J Cell Biol, 1984. **35**(2): p. 256-63.
24. Pan, B.T. and R.M. Johnstone, *Fate of the transferrin receptor during maturation of sheep reticulocytes in vitro: selective externalization of the receptor.* Cell, 1983. **33**(3): p. 967-78.
25. Johnstone, R.M., et al., *Vesicle formation during reticulocyte maturation. Association of plasma membrane activities with released vesicles (exosomes).* J Biol Chem, 1987. **262**(19): p. 9412-20.
26. Akers, J.C., et al., *Biogenesis of extracellular vesicles (EV): exosomes, microvesicles, retrovirus-like vesicles, and apoptotic bodies.* J Neurooncol, 2013. **113**(1): p. 1-11.
27. Crescitelli, R., et al., *Distinct RNA profiles in subpopulations of extracellular vesicles: apoptotic bodies, microvesicles and exosomes.* J Extracell Vesicles, 2013. **2**.
28. Lazaro-Ibanez, E., et al., *Different gDNA content in the subpopulations of prostate cancer extracellular vesicles: apoptotic bodies, microvesicles, and exosomes.* Prostate, 2014. **74**(14): p. 1379-90.

29. Antonyak, M.A. and R.A. Cerione, *Emerging picture of the distinct traits and functions of microvesicles and exosomes.* Proc Natl Acad Sci U S A, 2015. **112**(12): p. 3589-90.
30. Osteikoetxea, X., et al., *Improved characterization of EV preparations based on protein to lipid ratio and lipid properties.* PLoS One, 2015. **10**(3): p. e0121184.
31. Kalra, H., et al., *Comparative proteomics evaluation of plasma exosome isolation techniques and assessment of the stability of exosomes in normal human blood plasma.* Proteomics, 2013. **13**(22): p. 3354-64.
32. Tauro, B.J., et al., *Comparison of ultracentrifugation, density gradient separation, and immunoaffinity capture methods for isolating human colon cancer cell line LIM1863-derived exosomes.* Methods, 2012. **56**(2): p. 293-304.
33. Mack, M., et al., *Transfer of the chemokine receptor CCR5 between cells by membrane-derived microparticles: a mechanism for cellular human immunodeficiency virus 1 infection.* Nat Med, 2000. **6**(7): p. 769-75.
34. Al-Nedawi, K., et al., *Intercellular transfer of the oncogenic receptor EGFRvIII by microvesicles derived from tumour cells.* Nat Cell Biol, 2008. **10**(5): p. 619-24.
35. Peinado, H., et al., *Melanoma exosomes educate bone marrow progenitor cells toward a pro-metastatic phenotype through MET.* Nat Med, 2012. **18**(6): p. 883-91.
36. Saunderson, S.C., et al., *CD169 mediates the capture of exosomes in spleen and lymph node.* Blood, 2014. **123**(2): p. 208-16.
37. Barres, C., et al., *Galectin-5 is bound onto the surface of rat reticulocyte exosomes and modulates vesicle uptake by macrophages.* Blood, 2010. **115**(3): p. 696-705.
38. Fitzner, D., et al., *Selective transfer of exosomes from oligodendrocytes to microglia by macropinocytosis.* J Cell Sci, 2011. **124**(Pt 3): p. 447-58.
39. Parolini, I., et al., *Microenvironmental pH is a key factor for exosome traffic in tumor cells.* J Biol Chem, 2009. **284**(49): p. 34211-22.
40. Morelli, A.E., et al., *Endocytosis, intracellular sorting, and processing of exosomes by dendritic cells.* Blood, 2004. **104**(10): p. 3257-66.
41. Christianson, H.C., et al., *Cancer cell exosomes depend on cell-surface heparan sulfate proteoglycans for their internalization and functional activity.* Proc Natl Acad Sci U S A, 2013. **110**(43): p. 17380-5.
42. Feng, D., et al., *Cellular internalization of exosomes occurs through phagocytosis.* Traffic, 2010. **11**(5): p. 675-87.
43. Yanez-Mo, M., et al., *Biological properties of extracellular vesicles and their physiological functions.* J Extracell Vesicles, 2015. **4**: p. 27066.

44. Rand, M.L., et al., *Rapid clearance of procoagulant platelet-derived microparticles from the circulation of rabbits.* J Thromb Haemost, 2006. **4**(7): p. 1621-3.
45. Willekens, F.L., et al., *Liver Kupffer cells rapidly remove red blood cell-derived vesicles from the circulation by scavenger receptors.* Blood, 2005. **105**(5): p. 2141-5.
46. Takahashi, Y., et al., *Visualization and in vivo tracking of the exosomes of murine melanoma B16-BL6 cells in mice after intravenous injection.* J Biotechnol, 2013. **165**(2): p. 77-84.
47. Gonzales, P.A., et al., *Large-scale proteomics and phosphoproteomics of urinary exosomes.* J Am Soc Nephrol, 2009. **20**(2): p. 363-79.
48. Jeppesen, D.K., et al., *Quantitative proteomics of fractionated membrane and lumen exosome proteins from isogenic metastatic and nonmetastatic bladder cancer cells reveal differential expression of EMT factors.* Proteomics, 2014. **14**(6): p. 699-712.
49. Ostergaard, O., et al., *Quantitative proteome profiling of normal human circulating microparticles.* J Proteome Res, 2012. **11**(4): p. 2154-63.
50. Tauro, B.J., et al., *Two distinct populations of exosomes are released from LIM1863 colon carcinoma cell-derived organoids.* Mol Cell Proteomics, 2013. **12**(3): p. 587-98.
51. Pallet, N., et al., *A comprehensive characterization of membrane vesicles released by autophagic human endothelial cells.* Proteomics, 2013. **13**(7): p. 1108-20.
52. Aatonen, M.T., et al., *Isolation and characterization of platelet-derived extracellular vesicles.* J Extracell Vesicles, 2014. **3**.
53. Krishnamoorthy, L., et al., *HIV-1 and microvesicles from T cells share a common glycome, arguing for a common origin.* Nat Chem Biol, 2009. **5**(4): p. 244-50.
54. Batista, B.S., et al., *Identification of a conserved glycan signature for microvesicles.* J Proteome Res, 2011. **10**(10): p. 4624-33.
55. Escrevente, C., et al., *Interaction and uptake of exosomes by ovarian cancer cells.* BMC Cancer, 2011. **11**: p. 108.
56. Wollert, T., et al., *Membrane scission by the ESCRT-III complex.* Nature, 2009. **458**(7235): p. 172-7.
57. Fyfe, I., et al., *Association of the endosomal sorting complex ESCRT-II with the Vps20 subunit of ESCRT-III generates a curvature-sensitive complex capable of nucleating ESCRT-III filaments.* J Biol Chem, 2011. **286**(39): p. 34262-70.

58. Metcalf, D. and A.M. Isaacs, *The role of ESCRT proteins in fusion events involving lysosomes, endosomes and autophagosomes.* Biochem Soc Trans, 2010. **38**(6): p. 1469-73.
59. Hanson, P.I., S. Shim, and S.A. Merrill, *Cell biology of the ESCRT machinery.* Curr Opin Cell Biol, 2009. **21**(4): p. 568-74.
60. Perez-Hernandez, D., et al., *The intracellular interactome of tetraspanin-enriched microdomains reveals their function as sorting machineries toward exosomes.* J Biol Chem, 2013. **288**(17): p. 11649-61.
61. Nazarenko, I., et al., *Cell surface tetraspanin Tspan8 contributes to molecular pathways of exosome-induced endothelial cell activation.* Cancer Res, 2010. **70**(4): p. 1668-78.
62. Capraro, B.R., et al., *Curvature sensing by the epsin N-terminal homology domain measured on cylindrical lipid membrane tethers.* J Am Chem Soc, 2010. **132**(4): p. 1200-1.
63. Hsieh, W.T., et al., *Curvature sorting of peripheral proteins on solid-supported wavy membranes.* Langmuir, 2012. **28**(35): p. 12838-43.
64. Choi, D.S., et al., *Proteomics, transcriptomics and lipidomics of exosomes and ectosomes.* Proteomics, 2013. **13**(10-11): p. 1554-71.
65. Kooijmans, S.A., et al., *Exosome mimetics: a novel class of drug delivery systems.* Int J Nanomedicine, 2012. **7**: p. 1525-41.
66. Record, M., et al., *Exosomes as new vesicular lipid transporters involved in cell-cell communication and various pathophysiologies.* Biochim Biophys Acta, 2014. **1841**(1): p. 108-20.
67. Baig, S., et al., *Lipidomic analysis of human placental syncytiotrophoblast microvesicles in adverse pregnancy outcomes.* Placenta, 2013. **34**(5): p. 436-42.
68. Smyth, T.J., et al., *Examination of the specificity of tumor cell derived exosomes with tumor cells in vitro.* Biochim Biophys Acta, 2014. **1838**(11): p. 2954-65.
69. Trajkovic, K., et al., *Ceramide triggers budding of exosome vesicles into multivesicular endosomes.* Science, 2008. **319**(5867): p. 1244-7.
70. Del Conde, I., et al., *Tissue-factor-bearing microvesicles arise from lipid rafts and fuse with activated platelets to initiate coagulation.* Blood, 2005. **106**(5): p. 1604-11.
71. Llorente, A., B. van Deurs, and K. Sandvig, *Cholesterol regulates prostasome release from secretory lysosomes in PC-3 human prostate cancer cells.* Eur J Cell Biol, 2007. **86**(7): p. 405-15.
72. Pilzer, D., et al., *Emission of membrane vesicles: roles in complement resistance, immunity and cancer.* Springer Semin Immunopathol, 2005. **27**(3): p. 375-87.

73. Matsuo, H., et al., *Role of LBPA and Alix in multivesicular liposome formation and endosome organization.* Science, 2004. **303**(5657): p. 531-4.
74. Biro, E., et al., *The phospholipid composition and cholesterol content of platelet-derived microparticles: a comparison with platelet membrane fractions.* J Thromb Haemost, 2005. **3**(12): p. 2754-63.
75. Simons, K. and J.L. Sampaio, *Membrane organization and lipid rafts.* Cold Spring Harb Perspect Biol, 2011. **3**(10): p. a004697.
76. Valadi, H., et al., *Exosome-mediated transfer of mRNAs and microRNAs is a novel mechanism of genetic exchange between cells.* Nat Cell Biol, 2007. **9**(6): p. 654-9.
77. Balaj, L., et al., *Tumour microvesicles contain retrotransposon elements and amplified oncogene sequences.* Nat Commun, 2011. **2**: p. 180.
78. Guescini, M., et al., *Astrocytes and Glioblastoma cells release exosomes carrying mtDNA.* J Neural Transm, 2010. **117**(1): p. 1-4.
79. Thakur, B.K., et al., *Double-stranded DNA in exosomes: a novel biomarker in cancer detection.* Cell Res, 2014. **24**(6): p. 766-9.
80. Waldenstrom, A., et al., *Cardiomyocyte microvesicles contain DNA/RNA and convey biological messages to target cells.* PLoS One, 2012. **7**(4): p. e34653.
81. Lee, T.H., et al., *Oncogenic ras-driven cancer cell vesiculation leads to emission of double-stranded DNA capable of interacting with target cells.* Biochem Biophys Res Commun, 2014. **451**(2): p. 295-301.
82. Ratajczak, J., et al., *Embryonic stem cell-derived microvesicles reprogram hematopoietic progenitors: evidence for horizontal transfer of mRNA and protein delivery.* Leukemia, 2006. **20**(5): p. 847-56.
83. Valadi, H., et al., *Exosome-mediated transfer of mRNAs and microRNAs is a novel mechanism of genetic exchange between cells.* Nature cell biology, 2007. **9**(6): p. 654-9.
84. Skog, J., et al., *Glioblastoma microvesicles transport RNA and proteins that promote tumour growth and provide diagnostic biomarkers.* Nat Cell Biol, 2008. **10**(12): p. 1470-6.
85. Chen, T.S., et al., *Mesenchymal stem cell secretes microparticles enriched in pre-microRNAs.* Nucleic Acids Res, 2010. **38**(1): p. 215-24.
86. Batagov, A.O. and I.V. Kurochkin, *Exosomes secreted by human cells transport largely mRNA fragments that are enriched in the 3'-untranslated regions.* Biol Direct, 2013. **8**: p. 12.
87. Pigati, L., et al., *Selective release of microRNA species from normal and malignant mammary epithelial cells.* PLoS One, 2010. **5**(10): p. e13515.

88. Mittelbrunn, M., et al., *Unidirectional transfer of microRNA-loaded exosomes from T cells to antigen-presenting cells.* Nat Commun, 2011. **2**: p. 282.
89. Cheng, L., et al., *Exosomes provide a protective and enriched source of miRNA for biomarker profiling compared to intracellular and cell-free blood.* J Extracell Vesicles, 2014. **3**.
90. Baj-Krzyworzeka, M., et al., *Tumour-derived microvesicles carry several surface determinants and mRNA of tumour cells and transfer some of these determinants to monocytes.* Cancer Immunol Immunother, 2006. **55**(7): p. 808-18.
91. Bruno, S., et al., *Microvesicles derived from mesenchymal stem cells enhance survival in a lethal model of acute kidney injury.* PLoS One, 2012. **7**(3): p. e33115.
92. Deregibus, M.C., et al., *Endothelial progenitor cell derived microvesicles activate an angiogenic program in endothelial cells by a horizontal transfer of mRNA.* Blood, 2007. **110**(7): p. 2440-8.
93. Kogure, T., et al., *Extracellular Vesicle-Mediated Transfer of a Novel Long Noncoding RNA TUC339: A Mechanism of Intercellular Signaling in Human Hepatocellular Cancer.* Genes Cancer, 2013. **4**(7-8): p. 261-72.
94. Huang, X., et al., *Characterization of human plasma-derived exosomal RNAs by deep sequencing.* BMC Genomics, 2013. **14**: p. 319.
95. Miranda, K.C., et al., *Massively parallel sequencing of human urinary exosome/microvesicle RNA reveals a predominance of non-coding RNA.* PLoS One, 2014. **9**(5): p. e96094.
96. Dhahbi, J.M., et al., *Deep Sequencing of Serum Small RNAs Identifies Patterns of 5' tRNA Half and YRNA Fragment Expression Associated with Breast Cancer.* Biomark Cancer, 2014. **6**: p. 37-47.
97. Dhahbi, J.M., et al., *5'-YRNA fragments derived by processing of transcripts from specific YRNA genes and pseudogenes are abundant in human serum and plasma.* Physiological genomics, 2013. **45**(21): p. 990-8.
98. Nolte-'t Hoen, E.N., et al., *Deep sequencing of RNA from immune cell-derived vesicles uncovers the selective incorporation of small non-coding RNA biotypes with potential regulatory functions.* Nucleic Acids Res, 2012. **40**(18): p. 9272-85.
99. Bellingham, S.A., B.M. Coleman, and A.F. Hill, *Small RNA deep sequencing reveals a distinct miRNA signature released in exosomes from prion-infected neuronal cells.* Nucleic Acids Res, 2012. **40**(21): p. 10937-49.
100. Villarroya-Beltri, C., et al., *Sorting it out: regulation of exosome loading.* Semin Cancer Biol, 2014. **28**: p. 3-13.

101. Hadi Valadi, K.E., Apostolos Bossios, Margareta Sjöstrand, James J Lee & Jan O Lötvall, *Exosome-mediated transfer of mRNAs and microRNAs is a novel mechanism of genetic exchange between cells*. 2007.
102. Batagov, A.O., V.A. Kuznetsov, and I.V. Kurochkin, *Identification of nucleotide patterns enriched in secreted RNAs as putative cis-acting elements targeting them to exosome nano-vesicles.* BMC Genomics, 2011. **12 Suppl 3**: p. S18.
103. Bolukbasi, M.F., et al., *miR-1289 and "Zipcode"-like Sequence Enrich mRNAs in Microvesicles.* Mol Ther Nucleic Acids, 2012. **1**: p. e10.
104. Koppers-Lalic, D., et al., *Nontemplated nucleotide additions distinguish the small RNA composition in cells from exosomes.* Cell Rep, 2014. **8**(6): p. 1649-58.
105. Villarroya-Beltri, C., et al., *Sumoylated hnRNPA2B1 controls the sorting of miRNAs into exosomes through binding to specific motifs.* Nat Commun, 2013. **4**: p. 2980.
106. Greco, V., M. Hannus, and S. Eaton, *Argosomes: a potential vehicle for the spread of morphogens through epithelia.* Cell, 2001. **106**(5): p. 633-45.
107. Erickson, J.L., *Formation and maintenance of morphogen gradients: an essential role for the endomembrane system in Drosophila melanogaster wing development.* Fly (Austin), 2011. **5**(3): p. 266-71.
108. Gross, J.C., et al., *Active Wnt proteins are secreted on exosomes.* Nat Cell Biol, 2012. **14**(10): p. 1036-45.
109. Matusek, T., et al., *The ESCRT machinery regulates the secretion and long-range activity of Hedgehog.* Nature, 2014. **516**(7529): p. 99-103.
110. Gradilla, A.C., et al., *Exosomes as Hedgehog carriers in cytoneme-mediated transport and secretion.* Nat Commun, 2014. **5**: p. 5649.
111. Lakkaraju, A. and E. Rodriguez-Boulan, *Itinerant exosomes: emerging roles in cell and tissue polarity.* Trends Cell Biol, 2008. **18**(5): p. 199-209.
112. Kriebel, P.W., et al., *Collective cell migration requires vesicular trafficking for chemoattractant delivery at the trailing edge.* J Cell Biol, 2008. **183**(5): p. 949-61.
113. Oreshkova, T., R. Dimitrov, and M. Mourdjeva, *A cross-talk of decidual stromal cells, trophoblast, and immune cells: a prerequisite for the success of pregnancy.* Am J Reprod Immunol, 2012. **68**(5): p. 366-73.
114. Arck, P.C. and K. Hecher, *Fetomaternal immune cross-talk and its consequences for maternal and offspring's health.* Nat Med, 2013. **19**(5): p. 548-56.
115. Redman, C.W. and I.L. Sargent, *Placental debris, oxidative stress and pre-eclampsia.* Placenta, 2000. **21**(7): p. 597-602.

116. Gercel-Taylor, C., et al., *Shed membrane fragment modulation of CD3-zeta during pregnancy: link with induction of apoptosis.* J Reprod Immunol, 2002. **56**(1-2): p. 29-44.
117. Stenqvist, A.C., et al., *Exosomes secreted by human placenta carry functional Fas ligand and TRAIL molecules and convey apoptosis in activated immune cells, suggesting exosome-mediated immune privilege of the fetus.* J Immunol, 2013. **191**(11): p. 5515-23.
118. Hedlund, M., et al., *Human placenta expresses and secretes NKG2D ligands via exosomes that down-modulate the cognate receptor expression: evidence for immunosuppressive function.* J Immunol, 2009. **183**(1): p. 340-51.
119. Korkut, C., et al., *Trans-synaptic transmission of vesicular Wnt signals through Evi/Wntless.* Cell, 2009. **139**(2): p. 393-404.
120. Korkut, C., et al., *Regulation of postsynaptic retrograde signaling by presynaptic exosome release.* Neuron, 2013. **77**(6): p. 1039-46.
121. Gabrielli, M., et al., *Active endocannabinoids are secreted on extracellular membrane vesicles.* EMBO Rep, 2015. **16**(2): p. 213-20.
122. Prada, I., et al., *Classical and unconventional pathways of vesicular release in microglia.* Glia, 2013. **61**(7): p. 1003-17.
123. Antonucci, F., et al., *Microvesicles released from microglia stimulate synaptic activity via enhanced sphingolipid metabolism.* EMBO J, 2012. **31**(5): p. 1231-40.
124. Verderio, C., et al., *Myeloid microvesicles are a marker and therapeutic target for neuroinflammation.* Ann Neurol, 2012. **72**(4): p. 610-24.
125. Frohlich, D., et al., *Multifaceted effects of oligodendroglial exosomes on neurons: impact on neuronal firing rate, signal transduction and gene regulation.* Philos Trans R Soc Lond B Biol Sci, 2014. **369**(1652).
126. Lopez-Verrilli, M.A., F. Picou, and F.A. Court, *Schwann cell-derived exosomes enhance axonal regeneration in the peripheral nervous system.* Glia, 2013. **61**(11): p. 1795-806.
127. Wang, J.G., et al., *Monocytic microparticles activate endothelial cells in an IL-1beta-dependent manner.* Blood, 2011. **118**(8): p. 2366-74.
128. Oehmcke, S., et al., *Stimulation of blood mononuclear cells with bacterial virulence factors leads to the release of pro-coagulant and pro-inflammatory microparticles.* Cell Microbiol, 2012. **14**(1): p. 107-19.
129. Mastronardi, M.L., et al., *Circulating microparticles from septic shock patients exert differential tissue expression of enzymes related to inflammation and oxidative stress.* Crit Care Med, 2011. **39**(7): p. 1739-48.
130. Prakash, P.S., et al., *Human microparticles generated during sepsis in patients with critical illness are neutrophil-derived and modulate the*

immune response. J Trauma Acute Care Surg, 2012. **73**(2): p. 401-6; discussion 406-7.
131. Boilard, E., et al., *Platelets amplify inflammation in arthritis via collagen-dependent microparticle production.* Science, 2010. **327**(5965): p. 580-3.
132. Cloutier, N., et al., *The exposure of autoantigens by microparticles underlies the formation of potent inflammatory components: the microparticle-associated immune complexes.* EMBO Mol Med, 2013. **5**(2): p. 235-49.
133. Hoyer, F.F., et al., *Monocytic microparticles promote atherogenesis by modulating inflammatory cells in mice.* J Cell Mol Med, 2012. **16**(11): p. 2777-88.
134. Holder, B.S., et al., *Heightened pro-inflammatory effect of preeclamptic placental microvesicles on peripheral blood immune cells in humans.* Biol Reprod, 2012. **86**(4): p. 103.
135. Gasser, O. and J.A. Schifferli, *Activated polymorphonuclear neutrophils disseminate anti-inflammatory microparticles by ectocytosis.* Blood, 2004. **104**(8): p. 2543-8.
136. Eken, C., et al., *Polymorphonuclear neutrophil-derived ectosomes interfere with the maturation of monocyte-derived dendritic cells.* J Immunol, 2008. **180**(2): p. 817-24.
137. Montecalvo, A., et al., *Exosomes as a short-range mechanism to spread alloantigen between dendritic cells during T cell allorecognition.* J Immunol, 2008. **180**(5): p. 3081-90.
138. Mallegol, J., et al., *T84-intestinal epithelial exosomes bear MHC class II/peptide complexes potentiating antigen presentation by dendritic cells.* Gastroenterology, 2007. **132**(5): p. 1866-76.
139. Aline, F., et al., *Toxoplasma gondii antigen-pulsed-dendritic cell-derived exosomes induce a protective immune response against T. gondii infection.* Infect Immun, 2004. **72**(7): p. 4127-37.
140. Thery, C., et al., *Indirect activation of naive CD4+ T cells by dendritic cell-derived exosomes.* Nat Immunol, 2002. **3**(12): p. 1156-62.
141. Raposo, G., et al., *B lymphocytes secrete antigen-presenting vesicles.* J Exp Med, 1996. **183**(3): p. 1161-72.
142. Rialland, P., et al., *BCR-bound antigen is targeted to exosomes in human follicular lymphoma B-cells.* Biol Cell, 2006. **98**(8): p. 491-501.
143. Giri, P.K. and J.S. Schorey, *Exosomes derived from M. Bovis BCG infected macrophages activate antigen-specific CD4+ and CD8+ T cells in vitro and in vivo.* PLoS One, 2008. **3**(6): p. e2461.
144. Skokos, D., et al., *Mast cell-derived exosomes induce phenotypic and functional maturation of dendritic cells and elicit specific immune responses in vivo.* J Immunol, 2003. **170**(6): p. 3037-45.

145. Schnitzer, J.K., et al., *Fragments of antigen-loaded dendritic cells (DC) and DC-derived exosomes induce protective immunity against Leishmania major.* Vaccine, 2010. **28**(36): p. 5785-93.
146. Ramachandra, L., et al., *Mycobacterium tuberculosis synergizes with ATP to induce release of microvesicles and exosomes containing major histocompatibility complex class II molecules capable of antigen presentation.* Infect Immun, 2010. **78**(12): p. 5116-25.
147. Admyre, C., et al., *B cell-derived exosomes can present allergen peptides and activate allergen-specific T cells to proliferate and produce TH2-like cytokines.* J Allergy Clin Immunol, 2007. **120**(6): p. 1418-24.
148. Peche, H., et al., *Presentation of donor major histocompatibility complex antigens by bone marrow dendritic cell-derived exosomes modulates allograft rejection.* Transplantation, 2003. **76**(10): p. 1503-10.
149. Kim, S.H., et al., *Effective treatment of inflammatory disease models with exosomes derived from dendritic cells genetically modified to express IL-4.* J Immunol, 2007. **179**(4): p. 2242-9.
150. Kim, S.H., et al., *Exosomes derived from IL-10-treated dendritic cells can suppress inflammation and collagen-induced arthritis.* J Immunol, 2005. **174**(10): p. 6440-8.
151. Ali, S.Y., S.W. Sajdera, and H.C. Anderson, *Isolation and characterization of calcifying matrix vesicles from epiphyseal cartilage.* Proc Natl Acad Sci U S A, 1970. **67**(3): p. 1513-20.
152. Nahar, N.N., et al., *Matrix vesicles are carriers of bone morphogenetic proteins (BMPs), vascular endothelial growth factor (VEGF), and noncollagenous matrix proteins.* J Bone Miner Metab, 2008. **26**(5): p. 514-9.
153. Aalberts, M., T.A. Stout, and W. Stoorvogel, *Prostasomes: extracellular vesicles from the prostate.* Reproduction, 2014. **147**(1): p. R1-14.
154. Mayorga, L.S., C.N. Tomes, and S.A. Belmonte, *Acrosomal exocytosis, a special type of regulated secretion.* IUBMB Life, 2007. **59**(4-5): p. 286-92.
155. Bailey, J.L., *Factors regulating sperm capacitation.* Syst Biol Reprod Med, 2010. **56**(5): p. 334-48.
156. Kelly, R.W., *Immunosuppressive mechanisms in semen: implications for contraception.* Hum Reprod, 1995. **10**(7): p. 1686-93.
157. Ronquist, G., *Prostasomes are mediators of intercellular communication: from basic research to clinical implications.* J Intern Med, 2012. **271**(4): p. 400-13.
158. Skibinski, G., et al., *Immunosuppression by human seminal plasma--extracellular organelles (prostasomes) modulate activity of phagocytic cells.* Am J Reprod Immunol, 1992. **28**(2): p. 97-103.

159. He, J., et al., *Bone marrow stem cells-derived microvesicles protect against renal injury in the mouse remnant kidney model.* Nephrology (Carlton), 2012. **17**(5): p. 493-500.
160. Lai, R.C., et al., *Exosome secreted by MSC reduces myocardial ischemia/reperfusion injury.* Stem Cell Res, 2010. **4**(3): p. 214-22.
161. Aliotta, J.M., et al., *Alteration of marrow cell gene expression, protein production, and engraftment into lung by lung-derived microvesicles: a novel mechanism for phenotype modulation.* Stem Cells, 2007. **25**(9): p. 2245-56.
162. Herrera, M.B., et al., *Human liver stem cell-derived microvesicles accelerate hepatic regeneration in hepatectomized rats.* J Cell Mol Med, 2010. **14**(6B): p. 1605-18.
163. Royo, F., et al., *Transcriptome of extracellular vesicles released by hepatocytes.* PLoS One, 2013. **8**(7): p. e68693.
164. Owens, A.P., 3rd and N. Mackman, *Microparticles in hemostasis and thrombosis.* Circ Res, 2011. **108**(10): p. 1284-97.
165. Toti, F., et al., *Scott syndrome, characterized by impaired transmembrane migration of procoagulant phosphatidylserine and hemorrhagic complications, is an inherited disorder.* Blood, 1996. **87**(4): p. 1409-15.
166. Harding, C., J. Heuser, and P. Stahl, *Receptor-mediated endocytosis of transferrin and recycling of the transferrin receptor in rat reticulocytes.* J Cell Biol, 1983. **97**(2): p. 329-39.
167. Vidal, M., *Exosomes in erythropoiesis.* Transfus Clin Biol, 2010. **17**(3): p. 131-7.
168. Rhee, J.S., et al., *The functional role of blood platelet components in angiogenesis.* Thromb Haemost, 2004. **92**(2): p. 394-402.
169. Salomon, C., et al., *Exosomal signaling during hypoxia mediates microvascular endothelial cell migration and vasculogenesis.* PLoS One, 2013. **8**(7): p. e68451.
170. Sheldon, H., et al., *New mechanism for Notch signaling to endothelium at a distance by Delta-like 4 incorporation into exosomes.* Blood, 2010. **116**(13): p. 2385-94.
171. Umezu, T., et al., *Exosomal miR-135b shed from hypoxic multiple myeloma cells enhances angiogenesis by targeting factor-inhibiting HIF-1.* Blood, 2014. **124**(25): p. 3748-57.
172. An, K., et al., *Exosomes neutralize synaptic-plasticity-disrupting activity of Abeta assemblies in vivo.* Mol Brain, 2013. **6**: p. 47.
173. Al-Dossary, A.A., E.E. Strehler, and P.A. Martin-Deleon, *Expression and secretion of plasma membrane Ca2+-ATPase 4a (PMCA4a) during murine*

estrus: association with oviductal exosomes and uptake in sperm. PLoS One, 2013. **8**(11): p. e80181.
174. Griffiths, G.S., et al., *Investigating the role of murine epididymosomes and uterosomes in GPI-linked protein transfer to sperm using SPAM1 as a model.* Mol Reprod Dev, 2008. **75**(11): p. 1627-36.
175. Kumamoto, K., et al., *CD52 expression is induced in the mouse uterus at the time of embryo implantation.* J Reprod Immunol, 2009. **82**(1): p. 32-9.
176. Kabir-Salmani, M., et al., *Secretory role for human uterodomes (pinopods): secretion of LIF.* Mol Hum Reprod, 2005. **11**(8): p. 553-9.
177. Aghajanova, L., et al., *Disturbances in the LIF pathway in the endometrium among women with unexplained infertility.* Fertil Steril, 2009. **91**(6): p. 2602-10.
178. Asea, A., et al., *Heat shock protein-containing exosomes in mid-trimester amniotic fluids.* J Reprod Immunol, 2008. **79**(1): p. 12-7.
179. Jean-Pierre, C., et al., *Extracellular 70-kd heat shock protein in mid-trimester amniotic fluid and its effect on cytokine production by ex vivo-cultured amniotic fluid cells.* Am J Obstet Gynecol, 2006. **194**(3): p. 694-8.
180. Bretz, N.P., et al., *Body fluid exosomes promote secretion of inflammatory cytokines in monocytic cells via Toll-like receptor signaling.* J Biol Chem, 2013. **288**(51): p. 36691-702.
181. Zhu, M., et al., *Exosomes as extrapulmonary signaling conveyors for nanoparticle-induced systemic immune activation.* Small, 2012. **8**(3): p. 404-12.
182. Bhatnagar, S., et al., *Exosomes released from macrophages infected with intracellular pathogens stimulate a proinflammatory response in vitro and in vivo.* Blood, 2007. **110**(9): p. 3234-44.
183. Almqvist, N., et al., *Serum-derived exosomes from antigen-fed mice prevent allergic sensitization in a model of allergic asthma.* Immunology, 2008. **125**(1): p. 21-7.
184. Shin, T.S., et al., *Extracellular vesicles are key intercellular mediators in the development of immune dysfunction to allergens in the airways.* Allergy, 2010. **65**(10): p. 1256-65.
185. Villalba, M., R. Rodriguez, and E. Batanero, *The spectrum of olive pollen allergens. From structures to diagnosis and treatment.* Methods, 2014. **66**(1): p. 44-54.
186. Kosaka, N., et al., *microRNA as a new immune-regulatory agent in breast milk.* Silence, 2010. **1**(1): p. 7.
187. Zhou, Q., et al., *Immune-related microRNAs are abundant in breast milk exosomes.* International journal of biological sciences, 2012. **8**(1): p. 118-23.

188. Admyre, C., et al., *Exosomes with immune modulatory features are present in human breast milk.* J Immunol, 2007. **179**(3): p. 1969-78.
189. Gu, Y., et al., *Lactation-related microRNA expression profiles of porcine breast milk exosomes.* PLoS One, 2012. **7**(8): p. e43691.
190. Melnik, B.C., S.M. John, and G. Schmitz, *Milk is not just food but most likely a genetic transfection system activating mTORC1 signaling for postnatal growth.* Nutr J, 2013. **12**: p. 103.
191. Izumi, H., et al., *Purification of RNA from milk whey.* Methods Mol Biol, 2013. **1024**: p. 191-201.
192. Berckmans, R.J., et al., *Cell-derived vesicles exposing coagulant tissue factor in saliva.* Blood, 2011. **117**(11): p. 3172-80.
193. Ogawa, Y., et al., *Proteomic analysis of two types of exosomes in human whole saliva.* Biol Pharm Bull, 2011. **34**(1): p. 13-23.
194. Hiemstra, T.F., et al., *Human urinary exosomes as innate immune effectors.* J Am Soc Nephrol, 2014. **25**(9): p. 2017-27.
195. Kleinjan, A., et al., *Microparticles in vascular disorders: how tissue factor-exposing vesicles contribute to pathology and physiology.* Thromb Res, 2012. **130 Suppl 1**: p. S71-3.
196. Knepper, M.A. and T. Pisitkun, *Exosomes in urine: who would have thought...?* Kidney Int, 2007. **72**(9): p. 1043-5.
197. van Balkom, B.W., et al., *Exosomes and the kidney: prospects for diagnosis and therapy of renal diseases.* Kidney Int, 2011. **80**(11): p. 1138-45.
198. Masyuk, A.I., et al., *Ciliary subcellular localization of TGR5 determines the cholangiocyte functional response to bile acid signaling.* Am J Physiol Gastrointest Liver Physiol, 2013. **304**(11): p. G1013-24.
199. Masyuk, A.I., et al., *Biliary exosomes influence cholangiocyte regulatory mechanisms and proliferation through interaction with primary cilia.* Am J Physiol Gastrointest Liver Physiol, 2010. **299**(4): p. G990-9.
200. Kang, C.S., et al., *Extracellular vesicles derived from gut microbiota, especially Akkermansia muciniphila, protect the progression of dextran sulfate sodium-induced colitis.* PLoS One, 2013. **8**(10): p. e76520.
201. Andre, F., et al., *Malignant effusions and immunogenic tumour-derived exosomes.* Lancet, 2002. **360**(9329): p. 295-305.
202. Chaput, N., et al., *Exosomes as potent cell-free peptide-based vaccine. II. Exosomes in CpG adjuvants efficiently prime naive Tc1 lymphocytes leading to tumor rejection.* J Immunol, 2004. **172**(4): p. 2137-46.
203. Wolfers, J., et al., *Tumor-derived exosomes are a source of shared tumor rejection antigens for CTL cross-priming.* Nat Med, 2001. **7**(3): p. 297-303.

204. Lamparski, H.G., et al., *Production and characterization of clinical grade exosomes derived from dendritic cells.* J Immunol Methods, 2002. **270**(2): p. 211-26.
205. Morse, M.A., et al., *A phase I study of dexosome immunotherapy in patients with advanced non-small cell lung cancer.* J Transl Med, 2005. **3**(1): p. 9.
206. Andreola, G., et al., *Induction of lymphocyte apoptosis by tumor cell secretion of FasL-bearing microvesicles.* J Exp Med, 2002. **195**(10): p. 1303-16.
207. Huber, V., et al., *Human colorectal cancer cells induce T-cell death through release of proapoptotic microvesicles: role in immune escape.* Gastroenterology, 2005. **128**(7): p. 1796-804.
208. Klibi, J., et al., *Blood diffusion and Th1-suppressive effects of galectin-9-containing exosomes released by Epstein-Barr virus-infected nasopharyngeal carcinoma cells.* Blood, 2009. **113**(9): p. 1957-66.
209. Taylor, D.D., et al., *T-cell apoptosis and suppression of T-cell receptor/CD3-zeta by Fas ligand-containing membrane vesicles shed from ovarian tumors.* Clin Cancer Res, 2003. **9**(14): p. 5113-9.
210. Clayton, A., et al., *Human tumor-derived exosomes down-modulate NKG2D expression.* J Immunol, 2008. **180**(11): p. 7249-58.
211. Clayton, A., et al., *Human tumor-derived exosomes selectively impair lymphocyte responses to interleukin-2.* Cancer Res, 2007. **67**(15): p. 7458-66.
212. Szajnik, M., et al., *Tumor-derived microvesicles induce, expand and up-regulate biological activities of human regulatory T cells (Treg).* PLoS One, 2010. **5**(7): p. e11469.
213. Wieckowski, E.U., et al., *Tumor-derived microvesicles promote regulatory T cell expansion and induce apoptosis in tumor-reactive activated CD8+ T lymphocytes.* J Immunol, 2009. **183**(6): p. 3720-30.
214. Wada, J., et al., *Surface-bound TGF-beta1 on effusion-derived exosomes participates in maintenance of number and suppressive function of regulatory T-cells in malignant effusions.* Anticancer Res, 2010. **30**(9): p. 3747-57.
215. Valenti, R., et al., *Human tumor-released microvesicles promote the differentiation of myeloid cells with transforming growth factor-beta-mediated suppressive activity on T lymphocytes.* Cancer Res, 2006. **66**(18): p. 9290-8.
216. Yu, S., et al., *Tumor exosomes inhibit differentiation of bone marrow dendritic cells.* J Immunol, 2007. **178**(11): p. 6867-75.

217. Liu, Y., et al., *Contribution of MyD88 to the tumor exosome-mediated induction of myeloid derived suppressor cells.* Am J Pathol, 2010. **176**(5): p. 2490-9.
218. Gesierich, S., et al., *Systemic induction of the angiogenesis switch by the tetraspanin D6.1A/CO-029.* Cancer Res, 2006. **66**(14): p. 7083-94.
219. Jubb, A.M., et al., *Expression of delta-like ligand 4 (Dll4) and markers of hypoxia in colon cancer.* Br J Cancer, 2009. **101**(10): p. 1749-57.
220. Markiewicz, M., et al., *Impact of endothelial microparticles on coagulation, inflammation, and angiogenesis in age-related vascular diseases.* J Aging Res, 2013. **2013**: p. 734509.
221. Webber, J., et al., *Cancer exosomes trigger fibroblast to myofibroblast differentiation.* Cancer Res, 2010. **70**(23): p. 9621-30.
222. Webber, J.P., et al., *Differentiation of tumour-promoting stromal myofibroblasts by cancer exosomes.* Oncogene, 2015. **34**(3): p. 290-302.
223. Webber, J., V. Yeung, and A. Clayton, *Extracellular vesicles as modulators of the cancer microenvironment.* Semin Cell Dev Biol, 2015. **40**: p. 27-34.
224. Atay, S., et al., *Oncogenic KIT-containing exosomes increase gastrointestinal stromal tumor cell invasion.* Proc Natl Acad Sci U S A, 2014. **111**(2): p. 711-6.
225. Hood, J.L., R.S. San, and S.A. Wickline, *Exosomes released by melanoma cells prepare sentinel lymph nodes for tumor metastasis.* Cancer Res, 2011. **71**(11): p. 3792-801.
226. Joyce, J.A. and J.W. Pollard, *Microenvironmental regulation of metastasis.* Nat Rev Cancer, 2009. **9**(4): p. 239-52.
227. Mashburn, L.M. and M. Whiteley, *Membrane vesicles traffic signals and facilitate group activities in a prokaryote.* Nature, 2005. **437**(7057): p. 422-5.
228. Mashburn-Warren, L., R.J. McLean, and M. Whiteley, *Gram-negative outer membrane vesicles: beyond the cell surface.* Geobiology, 2008. **6**(3): p. 214-9.
229. Mashburn-Warren, L.M. and M. Whiteley, *Special delivery: vesicle trafficking in prokaryotes.* Mol Microbiol, 2006. **61**(4): p. 839-46.
230. Ciofu, O., et al., *Chromosomal beta-lactamase is packaged into membrane vesicles and secreted from Pseudomonas aeruginosa.* J Antimicrob Chemother, 2000. **45**(1): p. 9-13.
231. Rivera, J., et al., *Bacillus anthracis produces membrane-derived vesicles containing biologically active toxins.* Proc Natl Acad Sci U S A, 2010. **107**(44): p. 19002-7.
232. Zhang, G., et al., *Effects of Helicobacter suis gamma-glutamyl transpeptidase on lymphocytes: modulation by glutamine and glutathione*

supplementation and outer membrane vesicles as a putative delivery route of the enzyme. PLoS One, 2013. **8**(10): p. e77966.
233. McBroom, A.J. and M.J. Kuehn, *Release of outer membrane vesicles by Gram-negative bacteria is a novel envelope stress response.* Mol Microbiol, 2007. **63**(2): p. 545-58.
234. Baumgarten, T., et al., *Membrane vesicle formation as a multiple-stress response mechanism enhances Pseudomonas putida DOT-T1E cell surface hydrophobicity and biofilm formation.* Appl Environ Microbiol, 2012. **78**(17): p. 6217-24.
235. Schooling, S.R. and T.J. Beveridge, *Membrane vesicles: an overlooked component of the matrices of biofilms.* J Bacteriol, 2006. **188**(16): p. 5945-57.
236. Schooling, S.R., A. Hubley, and T.J. Beveridge, *Interactions of DNA with biofilm-derived membrane vesicles.* J Bacteriol, 2009. **191**(13): p. 4097-102.
237. Yonezawa, H., et al., *Outer membrane vesicles of Helicobacter pylori TK1402 are involved in biofilm formation.* BMC Microbiol, 2009. **9**: p. 197.
238. Yu, Q., et al., *In vitro evaluation of tobramycin and aztreonam versus Pseudomonas aeruginosa biofilms on cystic fibrosis-derived human airway epithelial cells.* J Antimicrob Chemother, 2012. **67**(11): p. 2673-81.
239. Bayer-Santos, E., et al., *Proteomic analysis of Trypanosoma cruzi secretome: characterization of two populations of extracellular vesicles and soluble proteins.* J Proteome Res, 2013. **12**(2): p. 883-97.
240. Cestari, I., et al., *Trypanosoma cruzi immune evasion mediated by host cell-derived microvesicles.* J Immunol, 2012. **188**(4): p. 1942-52.
241. Goncalves, M.F., et al., *Trypanosoma cruzi: shedding of surface antigens as membrane vesicles.* Exp Parasitol, 1991. **72**(1): p. 43-53.
242. Halle, M., et al., *The Leishmania surface protease GP63 cleaves multiple intracellular proteins and actively participates in p38 mitogen-activated protein kinase inactivation.* J Biol Chem, 2009. **284**(11): p. 6893-908.
243. Jaramillo, M., et al., *Leishmania repression of host translation through mTOR cleavage is required for parasite survival and infection.* Cell Host Microbe, 2011. **9**(4): p. 331-41.
244. Santarem, N., et al., *Exoproteome dynamics in Leishmania infantum.* J Proteomics, 2013. **84**: p. 106-18.
245. Silverman, J.M., et al., *An exosome-based secretion pathway is responsible for protein export from Leishmania and communication with macrophages.* J Cell Sci, 2010. **123**(Pt 6): p. 842-52.
246. Silverman, J.M., et al., *Leishmania exosomes modulate innate and adaptive immune responses through effects on monocytes and dendritic cells.* J Immunol, 2010. **185**(9): p. 5011-22.

247. Nantakomol, D., et al., *Circulating red cell-derived microparticles in human malaria.* J Infect Dis, 2011. **203**(5): p. 700-6.
248. Regev-Rudzki, N., et al., *Cell-cell communication between malaria-infected red blood cells via exosome-like vesicles.* Cell, 2013. **153**(5): p. 1120-33.
249. Couper, K.N., et al., *Parasite-derived plasma microparticles contribute significantly to malaria infection-induced inflammation through potent macrophage stimulation.* PLoS Pathog, 2010. **6**(1): p. e1000744.
250. Campos, F.M., et al., *Augmented plasma microparticles during acute Plasmodium vivax infection.* Malar J, 2010. **9**: p. 327.
251. Calzolari, A., et al., *TfR2 localizes in lipid raft domains and is released in exosomes to activate signal transduction along the MAPK pathway.* J Cell Sci, 2006. **119**(Pt 21): p. 4486-98.
252. Simons, M. and G. Raposo, *Exosomes--vesicular carriers for intercellular communication.* Curr Opin Cell Biol, 2009. **21**(4): p. 575-81.
253. Fevrier, B., et al., *Cells release prions in association with exosomes.* Proc Natl Acad Sci U S A, 2004. **101**(26): p. 9683-8.
254. Katzmann, D.J., G. Odorizzi, and S.D. Emr, *Receptor downregulation and multivesicular-body sorting.* Nat Rev Mol Cell Biol, 2002. **3**(12): p. 893-905.
255. Keller, S., et al., *Exosomes: from biogenesis and secretion to biological function.* Immunol Lett, 2006. **107**(2): p. 102-8.
256. Raiborg, C., T.E. Rusten, and H. Stenmark, *Protein sorting into multivesicular endosomes.* Curr Opin Cell Biol, 2003. **15**(4): p. 446-55.
257. Stoorvogel, W., et al., *The biogenesis and functions of exosomes.* Traffic, 2002. **3**(5): p. 321-30.
258. Clayton, A., et al., *Adhesion and signaling by B cell-derived exosomes: the role of integrins.* FASEB J, 2004. **18**(9): p. 977-9.
259. Viaud, S., et al., *Dendritic cell-derived exosomes promote natural killer cell activation and proliferation: a role for NKG2D ligands and IL-15Ralpha.* PLoS One, 2009. **4**(3): p. e4942.
260. Pizzirani, C., et al., *Stimulation of P2 receptors causes release of IL-1beta-loaded microvesicles from human dendritic cells.* Blood, 2007. **109**(9): p. 3856-64.
261. Gulinelli, S., et al., *IL-18 associates to microvesicles shed from human macrophages by a LPS/TLR-4 independent mechanism in response to P2X receptor stimulation.* Eur J Immunol, 2012. **42**(12): p. 3334-45.
262. Hasegawa, H., et al., *Native IL-32 is released from intestinal epithelial cells via a non-classical secretory pathway as a membrane-associated protein.* Cytokine, 2011. **53**(1): p. 74-83.

263. Kandere-Grzybowska, K., et al., *IL-1 induces vesicular secretion of IL-6 without degranulation from human mast cells.* J Immunol, 2003. **171**(9): p. 4830-6.
264. Sullivan, R., et al., *Role of exosomes in sperm maturation during the transit along the male reproductive tract.* Blood Cells Mol Dis, 2005. **35**(1): p. 1-10.
265. Kim, H.K., et al., *Platelet microparticles induce angiogenesis in vitro.* Br J Haematol, 2004. **124**(3): p. 376-84.
266. Zhang, H.G., et al., *A membrane form of TNF-alpha presented by exosomes delays T cell activation-induced cell death.* J Immunol, 2006. **176**(12): p. 7385-93.
267. Sarkar, A., et al., *Monocyte derived microvesicles deliver a cell death message via encapsulated caspase-1.* PLoS One, 2009. **4**(9): p. e7140.
268. Alonso, R., et al., *Diacylglycerol kinase alpha regulates the formation and polarisation of mature multivesicular bodies involved in the secretion of Fas ligand-containing exosomes in T lymphocytes.* Cell Death Differ, 2011. **18**(7): p. 1161-73.
269. Hedlund, M., et al., *Thermal- and oxidative stress causes enhanced release of NKG2D ligand-bearing immunosuppressive exosomes in leukemia/lymphoma T and B cells.* PLoS One, 2011. **6**(2): p. e16899.
270. Busch, A., et al., *Transfer of T cell surface molecules to dendritic cells upon CD4+ T cell priming involves two distinct mechanisms.* J Immunol, 2008. **181**(6): p. 3965-73.
271. Monleon, I., et al., *Differential secretion of Fas ligand- or APO2 ligand/TNF-related apoptosis-inducing ligand-carrying microvesicles during activation-induced death of human T cells.* J Immunol, 2001. **167**(12): p. 6736-44.
272. Xie, Y., et al., *Dendritic cells recruit T cell exosomes via exosomal LFA-1 leading to inhibition of CD8+ CTL responses through downregulation of peptide/MHC class I and Fas ligand-mediated cytotoxicity.* J Immunol, 2010. **185**(9): p. 5268-78.
273. Subra, C., et al., *Exosomes account for vesicle-mediated transcellular transport of activatable phospholipases and prostaglandins.* J Lipid Res, 2010. **51**(8): p. 2105-20.
274. Beloribi, S., et al., *Exosomal lipids impact notch signaling and induce death of human pancreatic tumoral SOJ-6 cells.* PLoS One, 2012. **7**(10): p. e47480.
275. Kim, C.W., et al., *Extracellular membrane vesicles from tumor cells promote angiogenesis via sphingomyelin.* Cancer Res, 2002. **62**(21): p. 6312-7.

276. Palmerini, C.A., et al., *Role of cholesterol, DOTAP, and DPPC in prostasome/spermatozoa interaction and fusion.* J Membr Biol, 2006. **211**(3): p. 185-90.
277. Sullivan, R. and F. Saez, *Epididymosomes, prostasomes, and liposomes: their roles in mammalian male reproductive physiology.* Reproduction, 2013. **146**(1): p. R21-35.
278. Bruno, S., et al., *Mesenchymal stem cell-derived microvesicles protect against acute tubular injury.* J Am Soc Nephrol, 2009. **20**(5): p. 1053-67.
279. Kanada, M., et al., *Differential fates of biomolecules delivered to target cells via extracellular vesicles.* Proc Natl Acad Sci U S A, 2015. **112**(12): p. E1433-42.
280. Morel, L., et al., *Neuronal exosomal miRNA-dependent translational regulation of astroglial glutamate transporter GLT1.* J Biol Chem, 2013. **288**(10): p. 7105-16.
281. Forterre, A., et al., *Myotube-derived exosomal miRNAs downregulate Sirtuin1 in myoblasts during muscle cell differentiation.* Cell Cycle, 2014. **13**(1): p. 78-89.
282. Xu, J.F., et al., *Altered microRNA expression profile in exosomes during osteogenic differentiation of human bone marrow-derived mesenchymal stem cells.* PLoS One, 2014. **9**(12): p. e114627.
283. Santonocito, M., et al., *Molecular characterization of exosomes and their microRNA cargo in human follicular fluid: bioinformatic analysis reveals that exosomal microRNAs control pathways involved in follicular maturation.* Fertil Steril, 2014. **102**(6): p. 1751-61 e1.
284. Pegtel, D.M., et al., *Functional delivery of viral miRNAs via exosomes.* Proc Natl Acad Sci U S A, 2010. **107**(14): p. 6328-33.
285. Ostenfeld, M.S., et al., *Cellular disposal of miR23b by RAB27-dependent exosome release is linked to acquisition of metastatic properties.* Cancer Res, 2014. **74**(20): p. 5758-71.
286. Gibbings, D.J., et al., *Multivesicular bodies associate with components of miRNA effector complexes and modulate miRNA activity.* Nat Cell Biol, 2009. **11**(9): p. 1143-9.
287. Okoye, I.S., et al., *MicroRNA-containing T-regulatory-cell-derived exosomes suppress pathogenic T helper 1 cells.* Immunity, 2014. **41**(1): p. 89-103.
288. Ekstrom, K., et al., *Characterization of mRNA and microRNA in human mast cell-derived exosomes and their transfer to other mast cells and blood CD34 progenitor cells.* J Extracell Vesicles, 2012. **1**.

289. Cantaluppi, V., et al., *Microvesicles derived from endothelial progenitor cells enhance neoangiogenesis of human pancreatic islets.* Cell Transplant, 2012. **21**(6): p. 1305-20.
290. Zhang, Y., et al., *Secreted monocytic miR-150 enhances targeted endothelial cell migration.* Mol Cell, 2010. **39**(1): p. 133-44.
291. Hergenreider, E., et al., *Atheroprotective communication between endothelial cells and smooth muscle cells through miRNAs.* Nat Cell Biol, 2012. **14**(3): p. 249-56.
292. Arroyo, J.D., et al., *Argonaute2 complexes carry a population of circulating microRNAs independent of vesicles in human plasma.* Proc Natl Acad Sci U S A, 2011. **108**(12): p. 5003-8.
293. Li, L., et al., *Argonaute 2 complexes selectively protect the circulating microRNAs in cell-secreted microvesicles.* PLoS One, 2012. **7**(10): p. e46957.
294. Turchinovich, A., et al., *Characterization of extracellular circulating microRNA.* Nucleic Acids Res, 2011. **39**(16): p. 7223-33.
295. Vickers, K.C., et al., *MicroRNAs are transported in plasma and delivered to recipient cells by high-density lipoproteins.* Nat Cell Biol, 2011. **13**(4): p. 423-33.
296. Santana, S.M., et al., *Microfluidic isolation of cancer-cell-derived microvesicles from hetergeneous extracellular shed vesicle populations.* Biomed Microdevices, 2014. **16**(6): p. 869-77.
297. Lee, K., et al., *Acoustic purification of extracellular microvesicles.* ACS Nano, 2015. **9**(3): p. 2321-7.
298. Boing, A.N., et al., *Single-step isolation of extracellular vesicles by size-exclusion chromatography.* J Extracell Vesicles, 2014. **3**.
299. Oksvold, M.P., A. Neurauter, and K.W. Pedersen, *Magnetic bead-based isolation of exosomes.* Methods Mol Biol, 2015. **1218**: p. 465-81.
300. Thery, C., et al., *Isolation and characterization of exosomes from cell culture supernatants and biological fluids.* Current protocols in cell biology / editorial board, Juan S. Bonifacino ... [et al.], 2006. **Chapter 3**: p. Unit 3 22.
301. Taylor, D.D. and S. Shah, *Methods of isolating extracellular vesicles impact down-stream analyses of their cargoes.* Methods, 2015.
302. Li, M., et al., *An optimized procedure for exosome isolation and analysis using serum samples: Application to cancer biomarker discovery.* Methods, 2015.
303. Cheruvanky, A., et al., *Rapid isolation of urinary exosomal biomarkers using a nanomembrane ultrafiltration concentrator.* Am J Physiol Renal Physiol, 2007. **292**(5): p. F1657-61.

304. Nordin, J.Z., et al., *Ultrafiltration with size-exclusion liquid chromatography for high yield isolation of extracellular vesicles preserving intact biophysical and functional properties.* Nanomedicine, 2015. **11**(4): p. 879-83.
305. Grant, R., et al., *A filtration-based protocol to isolate human plasma membrane-derived vesicles and exosomes from blood plasma.* J Immunol Methods, 2011. **371**(1-2): p. 143-51.
306. Heinemann, M.L., et al., *Benchtop isolation and characterization of functional exosomes by sequential filtration.* J Chromatogr A, 2014. **1371C**: p. 125-135.
307. Rana, S., et al., *Toward tailored exosomes: the exosomal tetraspanin web contributes to target cell selection.* Int J Biochem Cell Biol, 2012. **44**(9): p. 1574-84.
308. Yamada, T., et al., *Comparison of methods for isolating exosomes from bovine milk.* J Vet Med Sci, 2012. **74**(11): p. 1523-5.
309. Van Deun, J., et al., *The impact of disparate isolation methods for extracellular vesicles on downstream RNA profiling.* J Extracell Vesicles, 2014. **3**.
310. Lane, R.E., et al., *Analysis of exosome purification methods using a model liposome system and tunable-resistive pulse sensing.* Sci Rep, 2015. **5**: p. 7639.
311. Taylor, D.D., W. Zacharias, and C. Gercel-Taylor, *Exosome isolation for proteomic analyses and RNA profiling.* Methods Mol Biol, 2011. **728**: p. 235-46.
312. Rood, I.M., et al., *Comparison of three methods for isolation of urinary microvesicles to identify biomarkers of nephrotic syndrome.* Kidney Int, 2010. **78**(8): p. 810-6.
313. Momen-Heravi, F., et al., *Current methods for the isolation of extracellular vesicles.* Biol Chem, 2013. **394**(10): p. 1253-62.
314. Momen-Heravi, F., et al., *Impact of biofluid viscosity on size and sedimentation efficiency of the isolated microvesicles.* Front Physiol, 2012. **3**: p. 162.
315. Cvjetkovic, A., J. Lotvall, and C. Lasser, *The influence of rotor type and centrifugation time on the yield and purity of extracellular vesicles.* J Extracell Vesicles, 2014. **3**.
316. Witwer, K.W., et al., *Standardization of sample collection, isolation and analysis methods in extracellular vesicle research.* J Extracell Vesicles, 2013. **2**.
317. Mathivanan, S., et al., *Proteomics analysis of A33 immunoaffinity-purified exosomes released from the human colon tumor cell line LIM1215 reveals a*

tissue-specific protein signature. Mol Cell Proteomics, 2010. **9**(2): p. 197-208.
318. Dobin, A., et al., *STAR: ultrafast universal RNA-seq aligner.* Bioinformatics, 2013. **29**(1): p. 15-21.
319. Anders, S., P.T. Pyl, and W. Huber, *HTSeq--a Python framework to work with high-throughput sequencing data.* Bioinformatics, 2015. **31**(2): p. 166-9.
320. Harrow, J., et al., *GENCODE: the reference human genome annotation for The ENCODE Project.* Genome Res, 2012. **22**(9): p. 1760-74.
321. Schattner, P., A.N. Brooks, and T.M. Lowe, *The tRNAscan-SE, snoscan and snoGPS web servers for the detection of tRNAs and snoRNAs.* Nucleic Acids Res, 2005. **33**(Web Server issue): p. W686-9.
322. Gorkin, D.U., D. Leung, and B. Ren, *The 3D genome in transcriptional regulation and pluripotency.* Cell Stem Cell, 2014. **14**(6): p. 762-75.
323. Wendt, K.S. and F.G. Grosveld, *Transcription in the context of the 3D nucleus.* Curr Opin Genet Dev, 2014. **25**: p. 62-7.
324. de Laat, W., et al., *Three-dimensional organization of gene expression in erythroid cells.* Curr Top Dev Biol, 2008. **82**: p. 117-39.
325. Kim, S., N.K. Yu, and B.K. Kaang, *CTCF as a multifunctional protein in genome regulation and gene expression.* Exp Mol Med, 2015. **47**: p. e166.
326. Bernstein, E. and C.D. Allis, *RNA meets chromatin.* Genes Dev, 2005. **19**(14): p. 1635-55.
327. Rinn, J.L., et al., *Functional demarcation of active and silent chromatin domains in human HOX loci by noncoding RNAs.* Cell, 2007. **129**(7): p. 1311-23.
328. Schubeler, D., *Function and information content of DNA methylation.* Nature, 2015. **517**(7534): p. 321-6.
329. Lev Maor, G., A. Yearim, and G. Ast, *The alternative role of DNA methylation in splicing regulation.* Trends Genet, 2015. **31**(5): p. 274-80.
330. Meng, H., et al., *DNA methylation, its mediators and genome integrity.* Int J Biol Sci, 2015. **11**(5): p. 604-17.
331. Kishore, S. and S. Stamm, *The snoRNA HBII-52 regulates alternative splicing of the serotonin receptor 2C.* Science, 2006. **311**(5758): p. 230-2.
332. He, L. and G.J. Hannon, *MicroRNAs: small RNAs with a big role in gene regulation.* Nat Rev Genet, 2004. **5**(7): p. 522-31.
333. Bartel, D.P., *MicroRNAs: genomics, biogenesis, mechanism, and function.* Cell, 2004. **116**(2): p. 281-97.
334. Eberle, A.B. and N. Visa, *Quality control of mRNP biogenesis: networking at the transcription site.* Semin Cell Dev Biol, 2014. **32**: p. 37-46.

335. Braun, K.A. and E.T. Young, *Coupling mRNA synthesis and decay.* Mol Cell Biol, 2014. **34**(22): p. 4078-87.
336. Dinger, M.E., T.R. Mercer, and J.S. Mattick, *RNAs as extracellular signaling molecules.* J Mol Endocrinol, 2008. **40**(4): p. 151-9.
337. Simon Anders, W.H., *Differential expression analysis for sequence count data.* Genome Biology, 2010. **11**(10): p. R106.
338. Dhahbi, J.M., et al., *5'-YRNA fragments derived by processing of transcripts from specific YRNA genes and pseudogenes are abundant in human serum and plasma.* Physiol Genomics, 2013. **45**(21): p. 990-8.
339. Dhahbi, J.M., et al., *5' tRNA halves are present as abundant complexes in serum, concentrated in blood cells, and modulated by aging and calorie restriction.* BMC Genomics, 2013. **14**: p. 298.
340. Yong Sun Lee, Y.S., Ankit Malhotra, and Anindya Dutta, *A novel class of small RNAs: tRNA-derived RNA fragments (tRFs).* Genes and Development, 2009. **23**(22): p. 2639-2649.
341. Ivanov, P., et al., *Angiogenin-induced tRNA fragments inhibit translation initiation.* Mol Cell, 2011. **43**(4): p. 613-23.
342. Sobala, A. and G. Hutvagner, *Small RNAs derived from the 5' end of tRNA can inhibit protein translation in human cells.* RNA Biol, 2013. **10**(4): p. 553-63.
343. Raina, M. and M. Ibba, *tRNAs as regulators of biological processes.* Front Genet, 2014. **5**: p. 171.
344. Christov, C.P., et al., *Functional requirement of noncoding Y RNAs for human chromosomal DNA replication.* Molecular and cellular biology, 2006. **26**(18): p. 6993-7004.
345. Gardiner, T.J., et al., *A conserved motif of vertebrate Y RNAs essential for chromosomal DNA replication.* RNA, 2009. **15**(7): p. 1375-85.
346. Krude, T., et al., *Y RNA functions at the initiation step of mammalian chromosomal DNA replication.* J Cell Sci, 2009. **122**(Pt 16): p. 2836-45.
347. Zhang, A.T., et al., *Dynamic interaction of Y RNAs with chromatin and initiation proteins during human DNA replication.* J Cell Sci, 2011. **124**(Pt 12): p. 2058-69.
348. Anders, S. and W. Huber, *Differential expression analysis for sequence count data.* Genome Biol, 2010. **11**(10): p. R106.
349. Djebali, S., et al., *Landscape of transcription in human cells.* Nature, 2012. **489**(7414): p. 101-8.
350. Ratajczak, J., et al., *Membrane-derived microvesicles: important and underappreciated mediators of cell-to-cell communication.* Leukemia, 2006. **20**(9): p. 1487-95.

351. Skog, J., et al., *Glioblastoma microvesicles transport RNA and proteins that promote tumour growth and provide diagnostic biomarkers.* Nature cell biology, 2008. **10**(12): p. 1470-6.
352. Koh, W., et al., *Analysis of deep sequencing microRNA expression profile from human embryonic stem cells derived mesenchymal stem cells reveals possible role of let-7 microRNA family in downstream targeting of hepatic nuclear factor 4 alpha.* BMC genomics, 2010. **11 Suppl 1**: p. S6.
353. Luo, S.S., et al., *Human villous trophoblasts express and secrete placenta-specific microRNAs into maternal circulation via exosomes.* Biology of reproduction, 2009. **81**(4): p. 717-29.
354. Nolte-'t Hoen, E.N., et al., *Deep sequencing of RNA from immune cell-derived vesicles uncovers the selective incorporation of small non-coding RNA biotypes with potential regulatory functions.* Nucleic acids research, 2012. **40**(18): p. 9272-85.
355. Tuck, A.C. and D. Tollervey, *RNA in pieces.* Trends in genetics : TIG, 2011. **27**(10): p. 422-32.
356. Vojtech, L., et al., *Exosomes in human semen carry a distinctive repertoire of small non-coding RNAs with potential regulatory functions.* Nucleic acids research, 2014. **42**(11): p. 7290-304.
357. Hendrick, J.P., et al., *Ro small cytoplasmic ribonucleoproteins are a subclass of La ribonucleoproteins: further characterization of the Ro and La small ribonucleoproteins from uninfected mammalian cells.* Molecular and cellular biology, 1981. **1**(12): p. 1138-49.
358. O'Brien, C.A. and J.B. Harley, *A subset of hY RNAs is associated with erythrocyte Ro ribonucleoproteins.* The EMBO journal, 1990. **9**(11): p. 3683-9.
359. Wolin, S.L. and J.A. Steitz, *Genes for two small cytoplasmic Ro RNAs are adjacent and appear to be single-copy in the human genome.* Cell, 1983. **32**(3): p. 735-44.
360. Sim, S. and S.L. Wolin, *Emerging roles for the Ro 60-kDa autoantigen in noncoding RNA metabolism.* Wiley interdisciplinary reviews. RNA, 2011. **2**(5): p. 686-99.
361. Perreault, J., et al., *Retropseudogenes derived from the human Ro/SS-A autoantigen-associated hY RNAs.* Nucleic acids research, 2005. **33**(6): p. 2032-41.
362. Perreault, J., J.P. Perreault, and G. Boire, *Ro-associated Y RNAs in metazoans: evolution and diversification.* Molecular biology and evolution, 2007. **24**(8): p. 1678-89.

363. Lerner, M.R., et al., *Two novel classes of small ribonucleoproteins detected by antibodies associated with lupus erythematosus.* Science, 1981. **211**(4480): p. 400-2.
364. Sim, S., et al., *The subcellular distribution of an RNA quality control protein, the Ro autoantigen, is regulated by noncoding Y RNA binding.* Molecular biology of the cell, 2009. **20**(5): p. 1555-64.
365. Chen, X., et al., *The Ro autoantigen binds misfolded U2 small nuclear RNAs and assists mammalian cell survival after UV irradiation.* Current biology : CB, 2003. **13**(24): p. 2206-11.
366. Hogg, J.R. and K. Collins, *Human Y5 RNA specializes a Ro ribonucleoprotein for 5S ribosomal RNA quality control.* Genes & development, 2007. **21**(23): p. 3067-72.
367. Langley, A.R., et al., *Ribonucleoprotein particles containing non-coding Y RNAs, Ro60, La and nucleolin are not required for Y RNA function in DNA replication.* PloS one, 2010. **5**(10): p. e13673.
368. Nicolas, F.E., et al., *Biogenesis of Y RNA-derived small RNAs is independent of the microRNA pathway.* FEBS letters, 2012. **586**(8): p. 1226-30.
369. Lee, Y., S. El Andaloussi, and M.J. Wood, *Exosomes and microvesicles: extracellular vesicles for genetic information transfer and gene therapy.* Human molecular genetics, 2012. **21**(R1): p. R125-34.
370. Taylor, D.D., et al., *T-cell apoptosis and suppression of T-cell receptor/CD3-zeta by Fas ligand-containing membrane vesicles shed from ovarian tumors.* Clinical cancer research : an official journal of the American Association for Cancer Research, 2003. **9**(14): p. 5113-9.
371. Kim, J.W., et al., *Fas ligand-positive membranous vesicles isolated from sera of patients with oral cancer induce apoptosis of activated T lymphocytes.* Clinical cancer research : an official journal of the American Association for Cancer Research, 2005. **11**(3): p. 1010-20.
372. Abusamra, A.J., et al., *Tumor exosomes expressing Fas ligand mediate CD8+ T-cell apoptosis.* Blood cells, molecules & diseases, 2005. **35**(2): p. 169-73.
373. Saito, T. and M. Gale, Jr., *Differential recognition of double-stranded RNA by RIG-I-like receptors in antiviral immunity.* The Journal of experimental medicine, 2008. **205**(7): p. 1523-7.
374. Mogensen, T.H., *Pathogen recognition and inflammatory signaling in innate immune defenses.* Clinical microbiology reviews, 2009. **22**(2): p. 240-73, Table of Contents.
375. Takeuchi, O. and S. Akira, *Innate immunity to virus infection.* Immunological reviews, 2009. **227**(1): p. 75-86.

376. Maraia, R., et al., *Gene encoding human Ro-associated autoantigen Y5 RNA.* Nucleic acids research, 1996. **24**(18): p. 3552-9.
377. van Gelder, C.W., et al., *Common structural features of the Ro RNP associated hY1 and hY5 RNAs.* Nucleic acids research, 1994. **22**(13): p. 2498-506.
378. Wang, I., et al., *Nucleotide contributions to the structural integrity and DNA replication initiation activity of noncoding y RNA.* Biochemistry, 2014. **53**(37): p. 5848-63.
379. Rajaram, M., et al., *System-wide analysis reveals a complex network of tumor-fibroblast interactions involved in tumorigenicity.* PLoS genetics, 2013. **9**(9): p. e1003789.
380. Paget, S., *The distribution of secondary growths in cancer of the breast.* Cancer and Metastasis Reviews, 1889. **8**: p. 98-101.
381. Heinrich, E.L., et al., *The inflammatory tumor microenvironment, epithelial mesenchymal transition and lung carcinogenesis.* Cancer microenvironment : official journal of the International Cancer Microenvironment Society, 2012. **5**(1): p. 5-18.
382. Mendoza, M. and C. Khanna, *Revisiting the seed and soil in cancer metastasis.* The international journal of biochemistry & cell biology, 2009. **41**(7): p. 1452-62.
383. Peinado, H., S. Lavotshkin, and D. Lyden, *The secreted factors responsible for pre-metastatic niche formation: old sayings and new thoughts.* Seminars in cancer biology, 2011. **21**(2): p. 139-46.
384. Bidard, F.C., et al., *A "class action" against the microenvironment: do cancer cells cooperate in metastasis?* Cancer metastasis reviews, 2008. **27**(1): p. 5-10.
385. Kaplan, R.N., S. Rafii, and D. Lyden, *Preparing the "soil": the premetastatic niche.* Cancer research, 2006. **66**(23): p. 11089-93.
386. Hood, J.L., R.S. San, and S.A. Wickline, *Exosomes released by melanoma cells prepare sentinel lymph nodes for tumor metastasis.* Cancer research, 2011. **71**(11): p. 3792-801.
387. Zuker, M., *Mfold web server for nucleic acid folding and hybridization prediction.* Nucleic Acids Res, 2003. **31**(13): p. 3406-15.
388. Mi, H., et al., *The PANTHER database of protein families, subfamilies, functions and pathways.* Nucleic Acids Res, 2005. **33**(Database issue): p. D284-8.
389. Kanehisa, M. and S. Goto, *KEGG: kyoto encyclopedia of genes and genomes.* Nucleic Acids Res, 2000. **28**(1): p. 27-30.